# Application of Passivity-Based Control to Series-Parallel Connected DC-DC Converters and their Circuit Characteristics

**Yuma Murakawa**

**2023**

# Application of Passivity-Based Control to Series-Parallel Connected DC-DC Converters and their Circuit Characteristics

A Dissertation

Presented to the Graduate School of Engineering

of Kyoto University

in Partial Fulfillment of the Requirements for the Degree of

Doctor of Philosophy

by

Yuma Murakawa

March 2023

# Abstract

The series-parallel connection of power converters has been widely used in various fields of power electronics based on several advantages over a single high-power centralized converter, such as lower component stress, higher reliability, easier maintenance, improved thermal management, and so on. Due to these advantages, the series-parallel connection is being adopted in the fields of high power converters, photovoltaic systems, hybrid power systems, distributed power generation, and more. The series-parallel design of power converters is clearly an essential technique for high-power converters and combined use of distributed power sources.

Passivity-based control is a class of nonlinear control schemes that aims to achieve asymptotic stability of passive systems by adding some damping to the system's storage function. A system composed of passive subsystems is a passive system. A dc-dc converter is also a passive system in the sense that the switches do not provide any additional energy to the system. Therefore, the series-parallel converters form a passive system from the fact that each dc-dc converter is a passive subsystem. Then, from an energy point of view, the series-parallel converters are expected to be asymptotically stable by applying passivity-based control to each converter.

This dissertation studies the application of passivity-based control to the series-parallel connection of dc-dc converters. The asymptotic stability of series-parallel connected dc-dc converters regulated by passivity-based control is theoretically demonstrated. Then, this theoretical result is confirmed in numerical simulation and experiment. The agreement between the simulated and experimental waveforms is also verified. In addition, the steady-state and transient characteristics of passivity-based control are numerically analyzed. These transient features are utilized for cooperative power management in series-paralleled converter systems. The contents of this dissertation are explained below.

Firstly, the basic concepts of this study, such as passivity, port-controlled Hamiltonian systems, and Lyapunov stability, are explained. Then, the passivity-based control law is

derived for three types of dc-dc converters, boost, buck, and buck-boost. Adaptive and decoupling passivity-based control are also derived for advanced transient feature. The characteristics of these control methods are analyzed numerically.

Secondly, passivity-based control of output series-parallel connected dc-dc converters is discussed from a theoretical viewpoint. It is shown that output series-parallel connected dc-dc converters are asymptotically stable when independent passivity-based control is applied to each converter. An external input is added to the port-controlled Hamiltonian system which represents the interconnection of the converters. By assigning circuit constraints to these external inputs, they are able to represent the series-parallel connection. It follows that the arbitrary series-parallel connection of power converters is represented as a port-controlled Hamiltonian system, and asymptotic stabilization can be achieved by applying passivity-based control to each converter. Finally, the theory is numerically confirmed by the simulation of series-paralleled boost, buck, and buck-boost converters.

Thirdly, passivity-based control of boost and buck converters connected in parallel is numerically and experimentally examined. The parallel connected boost and buck converters are modeled as a port-controlled Hamiltonian system, and the asymptotic stability is obtained by individual passivity-based control. Numerical simulations are performed reflecting the circuit and control setup used in the experiments. Steady-state characteristics such as error and ripple and transient characteristics such as settling time are analyzed to determine the feedback gains. The waveforms obtained from experiments and numerical simulations are compared to confirm the correspondence of asymptotic stability and transient characteristics.

Fourthly, we discuss a power management method using passivity-based control for a system with multiple power converters connected in series-parallel. Power management refers to the control of the power supply ratio among series-paralleled converters in response to changes in load and target conditions. The control methods, adaptive and decoupling passivity-based control, are used for the system to respond to load fluctuations and changes in desired states. The construction of the experimental setup is also explained.

Finally, the studies mentioned above are summarized, and the future directions of this study are mentioned. The most important result of this dissertation is that the passivity-based control of series-parallel connected dc-dc converters was shown theoretically to asymptotically stabilize the system. This results was confirmed numerically and

experimentally. The study must be extended in several ways, such as additional experimental considerations, increasing the diversity of the system, and integration of power converters.

# Acknowledgments

First and foremost, I would like to express my most sincere gratitude to Professor Takashi Hikihara for introducing me to the academic world. He has given me constant support, encouragement, positivity, invaluable discussions and guidance throughout my doctoral course. His comments, supported by his broad insight, helped the construction of my research theme. Moreover, he provided me many precious opportunities to grow up as a researcher.

I would also like to thank my co-supervisor Professor Hirotsugu Kojima and Associate Professor Yoshihiko Susuki for numerous discussions and valuable comments about my research as well as giving me constant encouragement. In addition, I would like to thank my former co-supervisor Associate Professor Masayuki Kimura of Setsunan University for his invaluable discussions and comments for my research. I would like to thank Professor Shinji Doi for participating in the review of my doctoral dissertation.

I would also like to extend my gratitude to Professor Tsuyoshi Funaki, who kindly accepted me to study in his laboratory for the field practice program. I would like to appreciate Assistant Professor Shuhei Fukunaga for his guidance and discussions throughout the field practice program.

I would like to acknowledge Professor Alberto Castellazzi in Kyoto University of Advanced Science for the suggestions and comments he has given for me in the weekly meetings. He also provided me an opportunity to meet and have conversation with foreign researchers. I would also like to thank Professor Giampaolo Buticchi in University of Nottingham for the discussions, comments, and evaluation he has given for my research.

I would also like to take this opportunity to thank all the former and current members of Advanced Electrical Systems Theory Laboratory, Kyoto University, for providing me with fine research environment. In particular, Assistant Professor Takafumi Okuda (currently in Iwate Fukushima SiC Applied Engineering Inc), a former staff of the laboratory, offered insightful comments in the regular meeting of the laboratory, as well as daily

encouragement. I would like to thank Ms. Yoshiko Deguchi for all the assistance and encouragement she has provided to me during my doctoral course. I would like to thank all the former and current students of the laboratory. Especially, I had fruitful research discussions with Associate Professor Ryo Takahashi, Assistant Professor Shiu Mochiyama, Dr. Manuel Antonio Sanchez Tejada, Dr. Toko Mannari, Dr. Rutvika Manohar Nandan, Dr. Kazuki Hashimoto, Dr. Baek Seong Cheol, Mr. Naomitsu Yoshida, Dr. Shinji Katayama, Mr. Ryosuke Maeda, Mr. Yasushi Okutsu, Ms. Nodoka Asayama, Mr. Hirotaka Araki, Mr. Kai Katakami, Mr. Shota Inagaki, Mr. Takumi Yamamoto, Mr. Singh Satyam, Mr. Hajime Takayama, and Ms. Yanran Wang.

Last but not least, I sincerely wish to thank my family and all of my friends for their understanding, support, and heartfelt encouragement.

This work was partially supported by the Super Cluster Program from Japan Science and Technology Agency, the Program on Open Innovation Platform with Enterprises, Research Institute and Academia of Japan Science and Technology Agency, the Doctoral Program for World-leading Innovative and Smart Education, Ministry of Education, Culture, Sports, Science and Technology, the Cross-ministerial Strategic Innovation Promotion Program No. 18088028 of Japan Science and Technology Agency, the JSPS KAKENHI under Grant Number JP20234533, and the JST SPRING under Grant Number JPMJSP2110. The author was supported by Nissin Electric Group Foundation for Social Contribution.

# Contents

# Notations and Symbols

## Notations

| Notation | Usage | Meaning |
|---|---|---|
| $\mathbb{R}$ | | Set of real numbers |
| $\mathbb{N}$ | | Set of natural numbers |
| e | | Napier's constant |
| $\frac{\mathrm{d}y}{\mathrm{d}x}$ | | Derivative of $y$ with respect to $x$ |
| $\frac{\partial y}{\partial x}$ | | Partial derivative of $y$ with respect to $x$ |
| $\dot{}$ | $\dot{\boldsymbol{x}}$ | Time derivative of $\boldsymbol{x}$ |
| $\|\| \cdot \|\|$ | $\|\|\boldsymbol{x}\|\|$ | Norm of $\boldsymbol{x}$ |
| $\in$ | $a \in A$ | $a$ is an element of $A$ |
| $\subset$ | $A \subset B$ | $A$ is a subset of $B$ |
| T | $\boldsymbol{x}^{\mathrm{T}}$, $\boldsymbol{A}^{\mathrm{T}}$ | Transpose of a vector $\boldsymbol{x}$ or matrix $\boldsymbol{A}$ |

# Symbols

| Symbol | Unit | Meaning |
|---|---|---|
| $k$ | - | Feedback gain |
| $i$ | A | Current |
| $j$ | A | Current due to interaction |
| $t$ | s | Time |
| $v$ | V | Voltage |
| $w$ | V | Voltage due to interaction |
| $E$ | V | Input source voltage |
| $R$ | Ω | Resistance |
| $L$ | H | Inductance |
| $C$ | F | Capacitance |

# Acronyms

| | |
|---|---|
| **AC** | Alternating Current |
| **APBC** | Adaptive Passivity-Based Control |
| **DC** | Direct Current |
| **DPBC** | Decoupled Passivity-Based Control |
| **FPGA** | Field Programmable Gate Array |
| **GaN** | Gallium Nitride |
| **HPS** | Hybrid Power System |
| **PBC** | Passivity-Based Control |
| **PCHS** | Port-Controlled Hamiltonian System |
| **PV** | Photovoltaic |
| **PWM** | Pulse Width Modulation |
| **MOSFET** | Metal-Oxide-Semiconductor Field-Effect Transistor |
| **Si** | Silicon |
| **SiC** | Silicon Carbide |

# Chapter 1

# Introduction

## 1.1 Series-parallel connection of power converters

Series-parallel connection of multiple power converters is utilized in diverse fields of electrical engineering for improved power conversion [1–36]. It provides advantages over single, high-power, centralized power converters such as higher efficiency, increased reliability, ease of maintenance, lower component stresses, improved thermal management, and more [1–10]. Previous researches have reported the load-sharing design of high-power converters [1–9], the achievement of higher efficiency in photovoltaic (PV) systems [10–16], the construction of hybrid power systems (HPS) [17–30], and distributed generation [31–36] by the adoption of series-parallel connection of power converters. The series-paralleling technique of power converters is crucial for high-power conversion and the combined use of power sources.

The series-parallel connection refers to a different circuit structure depending on the research field. In the most common case, it represents multiple power converters connected in series or parallel at both of their inputs and outputs as shown in Fig. 1.1 [1–9]. In this case, the power converters have identical circuit configurations and parameters. Moreover, they are explicitly controlled to obtain equal load-sharing. References [1, 2] have classified the load-sharing methods for the input-output paralleled converters. Similarly, input-output series-paralleled converters were investigated and generalized in [5–8]. Though these considerations have strongly contributed to the load-sharing of high-power converters, it must be noted that the diversity of converter types and operations is not adequately examined. The lack of scalability of the method has been also pointed out.

The series-parallel connection of power converters is also considered in the research

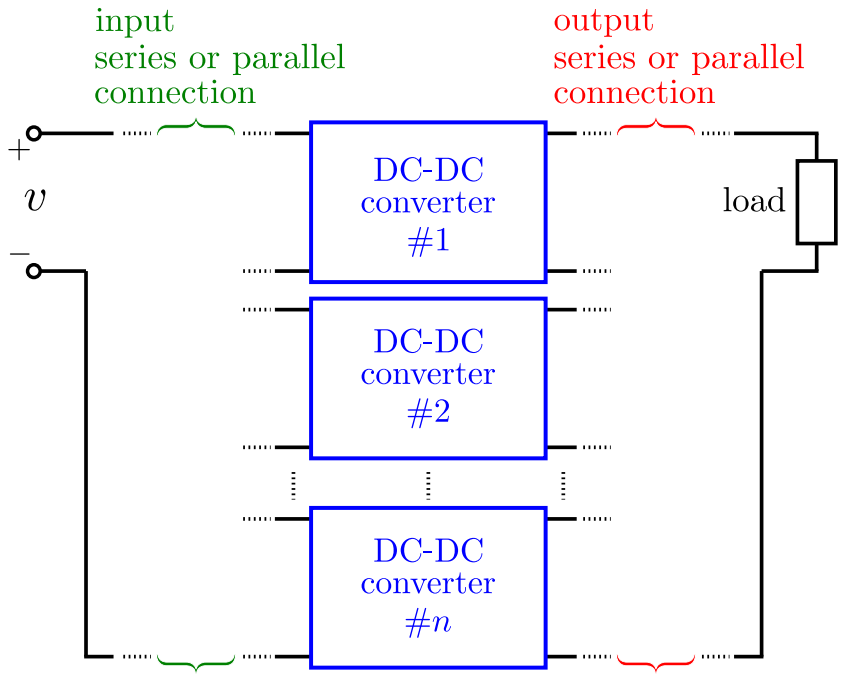


Figure 1.1: DC-DC converters connected in series-parallel at input and output.

fields of PV systems [10–16], HPS [17–30], and distributed generation [31–36]. In these considerations, the series-parallel connection of power converters appears at their output as shown in Fig. 1.2, because the power sources are distributed rather than concentrated. This circuit design aims to achieve the cooperative use of distributed power sources by controlling the power converters. Moreover, the system typically has diverse operating modes depending on the power flow of each converter. In these cases, the control strategies for the converters must be designed to cover a wide range of efficient operations. For example, the bifurcations and instabilities of a PV-battery HPS are analyzed in [19].

In summary, the circuit configurations shown in Fig. 1.1 and Fig. 1.2 have completely different applications and requirements for control. Thus, their research domain has not been discussed in the same context. Rather, they have often been addressed as a method to satisfy the demand in specific applications. The general discussions on the series-parallel connection of power converters have been lacking, apart from the fact that they have diversity and scalability issues in common. It is necessary to construct a control scheme that widely covers the circuit topologies and the operating range of power converters for the diverse and scalable series-parallel connection.

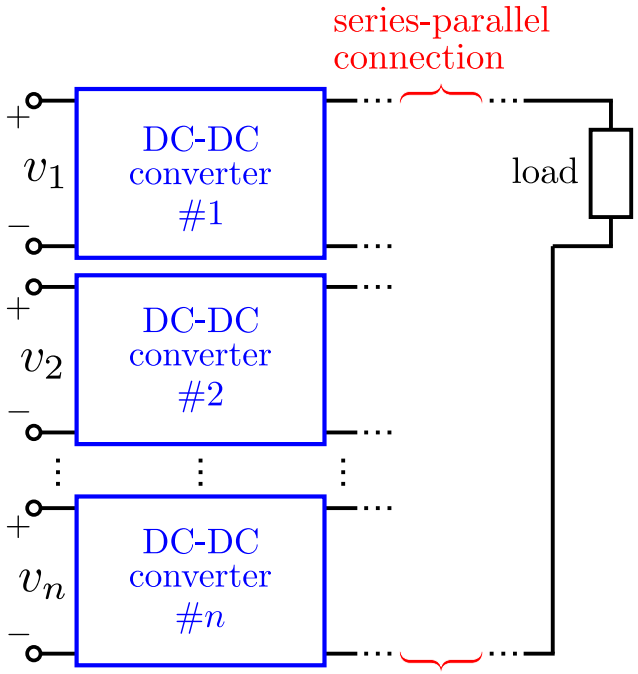


Figure 1.2: DC-DC converters connected in series-parallel at output.

## 1.2 Passivity-based control of series-parallel connected power converters

The control methods of power converters can be categorized into either linear or nonlinear control. Previous research on series-parallel connected converters, including the above-mentioned references, has mainly been based on linear control, though the switched power converters are inherently nonlinear systems [37–40]. Moreover, the series-paralleled converters have mutual interactions in contrast to single dc-dc converters. Therefore, linear controllers are unlikely to give robust solutions and optimum performance for the series-parallel connected converters [41]. Eigenvalue and time-delay analyses [42] can reveal the local linearized properties, but due to the nonlinearity and the connection of the converters, the performance for the overall operating region of the series-paralleled converters may not be illustrated. This is the biggest reason for the lack of scalability in series-parallel connected converters. The characteristics and features of linear control are not guaranteed to be maintained as the number of series-paralleled converters increases.

In this study, we adopt passivity-based control (PBC) [43,44,46–48] for the regulation of series-parallel connected converters. This control method is a class of nonlinear control schemes, which aims to achieve the asymptotic stability of passive systems by adding some

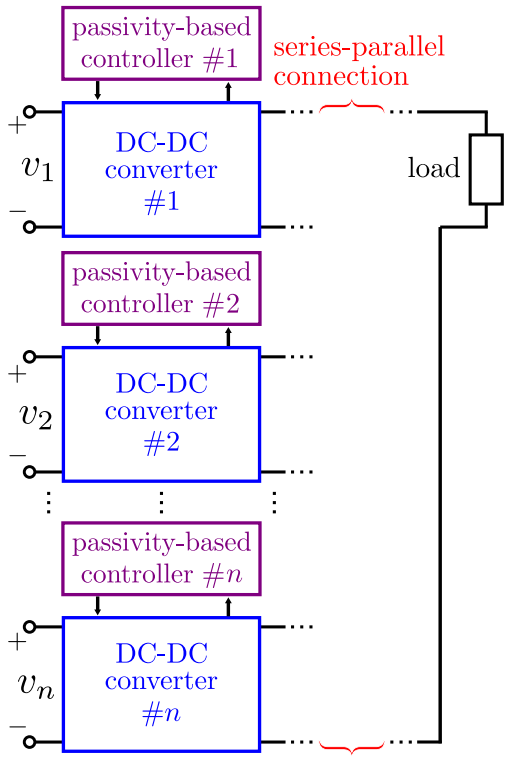


Figure 1.3: Series-parallel connection of dc-dc converters regulated by PBC.

damping to the system's storage function. Since PBC is based on the physical properties of the system, it gives simple and robust control laws [43, 44, 46]. The schematics of this system configuration are shown in Fig. 1.3.

The control system design based on passivity was initiated in [49], whose objective was to render the closed loop passive for the adaptive control of robot manipulators. Later, similar works have been proposed in [50,51], which studied the PBC of mechanical systems as a new adaptive control. Furthermore, it was proposed that this control system design can be applied not only to mechanical systems but also to dc-dc converters [43]. The performance of PBC for dc-dc converters was tested experimentally in [52]. Then, PBC was generalized for Euler-Lagrange systems in [44]. Recently, the application of PBC to power converters is considered in [53–59], where the excellent performance of PBC has been shown in terms of stability, robustness, and transient features.

The interconnection of passive subsystems compose a passive system [60]. A dc-dc converter can be modeled as a passive system, in the sense that the internal switches do not supply any energy to the system [43, 44]. Rather, they serve to intermittently switch the connection structure of the passive components [61, 62]. Thus, the series-parallel

connected converters constitute a passive system, since the dc-dc converters are passive subsystems. It is expected from the perspective of energy that the series-parallel connected converters are asymptotically stable by the application of PBC to each converter. Previous research has considered the PBC of series-paralleled converters based on this viewpoint. The regulation of Ćuk converters connected in parallel by PBC is discussed in [63]. The PBC of ring-coupled boost converters is considered in [64,65]. The application of PBC to HPS is considered numerically and experimentally in [26–30]. Yet, these considerations are limited to specific circuit configurations and control. General discussions on the properties for the series-parallel converters regulated PBC have not yet been presented.

From the above background, this dissertation discusses the application of PBC to the series-paralleled dc-dc converters from theoretical, numerical, and experimental viewpoints. PBC is able to develop general discussions for the series-paralleled converters, guaranteeing the diversity and scalability of the system. The basic concepts related to this study are first explained. Then, the asymptotic stability of output series-paralleled dc-dc converters regulated by PBC is shown in rigor mathematical manner. The system is analyzed in terms of transient characteristics by numerical simulations. Experimental consideration will also be provided to verify the theoretical and numerical results.

## 1.3 Overview of dissertation

The main contribution of this dissertation is that we have proved the asymptotic stability of the output series-paralleled converters regulated by PBC. The asymptotic stability is rigorously shown from the perspectives of stored energy and Lyapunov stability theory. We focus on the general converter model of the port-controlled Hamiltonian system (PCHS) and its connection structures, in contrast to the studies which consider specific circuit configurations. Hence, the results provided in this dissertation are general and are able to support the numerical and experimental results of the previous studies. In addition, our theoretical aspects justify the further extension of the series-paralleled converters due to generality and scalability. In order to verify these features, the numerical simulations of the series-paralleled converters are also provided.

The thesis is organized as follows. In Chapter 2, we introduce the basic concepts related to this research. Passivity and Lyapunov stability theory are first explained, and then the generalized derivation process of PBC for PCHS is presented. The PBC laws for

three types of dc-dc converters, boost, buck, and buck-boost converters, are derived. In addition, adaptive passivity-based control (APBC) and decoupling passivity-based control (DPBC) are introduced as more advanced control methods. A numerical analysis of the control performance for the above control methods is also presented.

In Chapter 3, the PBC of output series-parallel connected dc-dc converters is discussed from a theoretical viewpoint. It is shown theoretically that each power converter is asymptotically stable when regulated by PBC. First, an external input variable is added to PCHS representing a single dc-dc converter. By assigning circuit constraints to these variables they are able to represent the series-parallel connection. It follows that the series-parallel connection of arbitrary power converters is represented as PCHS, and asymptotic stabilization is achieved by applying PBC to each converter. Finally, it is numerically confirmed by the simulation of boost, buck, and buck-boost converter connected in series-parallel.

In Chapter 4, the PBC of boost and buck converters connected in parallel is numerically and experimentally investigated. The parallel connected boost and buck converters are modeled as PCHS, and their asymptotic stability is shown to be obtained by PBC. Numerical simulations are also performed reflecting the circuit and control setup used in the experiments. Steady-state characteristics such as error and ripple in the steady-state, and transient characteristics such as settling time are analyzed to determine the feedback gains for PBC. Finally, the waveforms obtained from the experiment and the simulation are compared to confirm the asymptotic stability and control performance.

In Chapter 5, we discuss the power management method for multiple converters connected in series-parallel using PBC. Power management refers to the control of the power supply ratio among the series-paralleled converters in response to changes in load and target conditions. APBC and DPBC introduced in Chapter 2 are adopted to respond to the load fluctuations and changes of the desired states. The construction of the experimental setup is also explained.

In Chapter 6, the conclusions and future work of this research are presented. In this dissertation, the PBC of series-parallel connected dc-dc converters is investigated from the viewpoints of asymptotic stability and control performance. The results of this dissertation are concluded that it contributes to providing more diversity and scalability in the series-parallel connection of power converters. As for future directions, the following three viewpoints are addressed; experiment, expansion, and integration.

# Chapter 2

# Passivity-based control of dc-dc converters

PBC is a control method which asymptotically stabilizes the desired equilibrium by shaping the energy characteristics of the system, and then adding some damping [43, 44, 46–48]. Energy shaping implies the design of a new desired storage function with a minimum at the desired equilibrium, which becomes the candidate of a Lyapunov function. Then, appropriate damping is added to the system to guarantee asymptotic stability. For electronic systems consisting of semiconductor devices such as diodes and switches, the Lagrangian formulation may be difficult or impossible to implement since the Euler-Lagrange parameters are modified by the state of these elements [44]. On the other hand, the Hamiltonian model of the switched power converter has the same state variables, Hamiltonian, and dissipation function for all operating modes of the converter [45]. Given these constraints, instead of Euler-Lagrange modelling, PCHS is often used to achieve better results with PBC [46–48].

In this chapter, the basic concepts of this study are introduced. Passivity, PCHS, and Lyapunov stability theory are first explained in detail. Then, averaged models of boost, buck, and buck-boost converters are represented as PCHS. Lastly, the derivation process of PBC law for each of these converters is shown. APBC and DPBC will also be introduced for the advanced transient features in the series-parallel connection. Moreover, the characteristics of the control methods are numerically analyzed.

## 2.1 Passivity

Passivity is a fundamental property of dynamical systems, closely related to the concept of energy. It was first introduced in [66] in the context of electrical circuits. The rate at which energy is stored in a passive system is always less than or equal to the energy supplied to it [44]. This fact implies the dissipative property of a passive system that it cannot store more energy than it is supplied with. The dissipated energy is given by the difference between the supplied and the stored energy. In order to mathematically define the property of passivity, two functions must be introduced; the storage function and the supply rate. The storage function represents the amount of energy stored inside the system. The supply rate is implies the energy flow into the system from outside.

Consider a system

$$\begin{cases} \dot{\boldsymbol{x}} = f(\boldsymbol{x}, \boldsymbol{u}), \ \boldsymbol{x}(0) = \boldsymbol{x}_0 \in \mathbb{R}^n, \\ \boldsymbol{y} = h(\boldsymbol{x}, \boldsymbol{u}), \end{cases} \tag{2.1}$$

where $\boldsymbol{x} \in \mathbb{R}^n$, $\boldsymbol{u} \in \mathbb{R}^m$, and $\boldsymbol{y} \in \mathbb{R}^m$ are state, input, and output, respectively. The dot $(\dot{})$ stands for time differentiation. The system (2.1) is dissipative [44, 67] if and only if there exists a non-negative real function $\mathcal{H}(\boldsymbol{x}) : \mathbb{R}^n \to \mathbb{R}_{\geq 0}$, called the storage function, such that

$$\mathcal{H}(\boldsymbol{x}(T)) - \mathcal{H}(\boldsymbol{x}(0)) \leq \int_0^T w(\boldsymbol{u}, \boldsymbol{y}) \mathrm{d}t, \tag{2.2}$$

for all $\boldsymbol{u}$ and $T > 0$. Here, $w(\boldsymbol{u}, \boldsymbol{y}) : \mathbb{R}^m \times \mathbb{R}^m \to \mathbb{R}$ is the supply rate. It is clear from (2.2) that the energy stored inside a dissipative system is always less than the energy supplied to it.

The system (2.1) is passive [44, 66] if it is dissipative with respect to the supply rate

$$w(\boldsymbol{u}, \boldsymbol{y}) = \boldsymbol{u}^{\mathrm{T}} \boldsymbol{y}. \tag{2.3}$$

Then the variables $\boldsymbol{u}$ and $\boldsymbol{y}$ are conjugated in the sense that their product has the units of power, assuming that the storage function $\mathcal{H}(\boldsymbol{x})$ of the system has the unit of energy. For instance, the variables $\boldsymbol{u}$ and $\boldsymbol{y}$ would imply currents and voltages in an electrical circuit or forces and velocities in a mechanical system [46].

Table 2.1: List of Symbols.

| Symbol | Definition | Property |
|---|---|---|
| $\mathcal{A} \in \mathbb{R}^{n\times n}$ | Circuit parameter | Positive definite |
| $\mathcal{J} \in \mathbb{R}^{n\times n}$ | Internal structure | Skew-symmetric |
| $\mathcal{R} \in \mathbb{R}^{n\times n}$ | Dissipation | Positive semi-definite |
| $\boldsymbol{g} \in \mathbb{R}^{n\times m}$ | Input structure | |
| $\boldsymbol{x} \in \mathbb{R}^{n}$ | State variables | |
| $\boldsymbol{u} \in \mathbb{R}^{m}$ | Input | |
| $\boldsymbol{s} \in [0,1]^{l}$ | Duty ratios | |

## 2.2 Port-controlled Hamiltonian system

As a general model for the dc-dc converters, we assume

$$\mathcal{A}\dot{\boldsymbol{x}} = \{\mathcal{J}(\boldsymbol{s}) - \mathcal{R}\}\boldsymbol{x} + \boldsymbol{g}(\boldsymbol{s})\boldsymbol{u}. \tag{2.4}$$

The symbols in (2.4) are explained in Table 2.1, where $n, m, l \in \mathbb{N}$ are natural numbers. This model is a PCHS [68, 69] with modifications to represent a switched power converter [48]. Moreover, (2.4) is an averaged model [70–72] based on the assumption that the switches have sufficiently fast switching operation compared to the circuit parameters. Thus, the model is approximated to be a continuous system controlled by the duty ratios $\boldsymbol{s} \in [0,1]^l$. It is confirmed in detail that (2.4) describes a variety of dc-dc converters in [44, 48].

The storage function of (2.4) is given by

$$\mathcal{H} = \frac{1}{2}\boldsymbol{x}^{\mathrm{T}}\mathcal{A}\boldsymbol{x}. \tag{2.5}$$

Then, the time derivative of the storage function is obtained as

$$\dot{\mathcal{H}} = \boldsymbol{x}^{\mathrm{T}}\mathcal{A}\dot{\boldsymbol{x}} = -\boldsymbol{x}^{\mathrm{T}}\mathcal{R}\boldsymbol{x} + \boldsymbol{x}^{\mathrm{T}}\boldsymbol{g}(\boldsymbol{s})\boldsymbol{u}. \tag{2.6}$$

Here, the first term on the right-hand side $-\boldsymbol{x}^{\mathrm{T}}\mathcal{R}\boldsymbol{x}$ is the dissipation of the system, which is negative at $\boldsymbol{x} \neq 0$. The second term $\boldsymbol{x}^{\mathrm{T}}\boldsymbol{g}(\boldsymbol{s})\boldsymbol{u}$ is the power supplied from outside to the system. It follows that (2.6) satisfies the conditions of passivity represented in (2.2) and (2.3). Therefore, we have confirmed that any system modeled as PCHS satisfies the property of passivity.

## 2.3 Lyapunov stability theory

The stability of the solutions for differential equations can be analyzed by the Lyapunov stability theory [73]. This theory has been the basic concept in the research domain of PBC to confirm its stability aspect. In this section, the Lyapunov stability theory is explained according to [74]. Detailed definitions of stability and asymptotic stability are also given based on [74].

Stability, asymptotic stability, and instability are defined as follows. Consider the system

$$\dot{\boldsymbol{x}} = f(\boldsymbol{x}), \tag{2.7}$$

where $f : D \to \mathbb{R}^n$ is a locally Lipschitz map from a domain $D \subset \mathbb{R}^n$ into $\mathbb{R}^n$. Suppose that the domain $D$ contains $\boldsymbol{x} = 0$ as an equilibrium point of (2.7). The equilibrium point $\boldsymbol{x} = 0$ of (2.7) is stable if, for each $\epsilon > 0$, there is $\delta = \delta(\epsilon) > 0$ such that

$$||\boldsymbol{x}(0)|| < \delta \;\Rightarrow\; ||\boldsymbol{x}(t)|| < \epsilon, \quad \forall\, t \geq 0. \tag{2.8}$$

It is asymptotically stable if it is stable and $\delta$ can be chosen such that

$$||\boldsymbol{x}(0)|| < \delta \;\Rightarrow\; \lim_{t\to\infty} \boldsymbol{x}(t) = 0. \tag{2.9}$$

The equilibrium point is unstable if not stable.

Accordingly, the Lyapunov stability theory is given as follows. Let $V : D \to \mathbb{R}$ be a continuously differentiable function, such that

$$\begin{cases} V(0) = 0 \;\text{ and }\; V(\boldsymbol{x}) > 0 \text{ in } D - \{0\}, \\ \dot{V}(\boldsymbol{x}) \leq 0 \text{ in } D. \end{cases} \tag{2.10}$$

Then, $\boldsymbol{x} = 0$ is stable. Moreover, if

$$\dot{V}(\boldsymbol{x}) < 0 \text{ in } D - \{0\}, \tag{2.11}$$

then $\boldsymbol{x} = 0$ is asymptotically stable. Here, $D - \{0\}$ implies the domain $D$ excluding the origin.

Note that the Lyapunov stability theory determines the local stability due to the domain $D$. For global stability, the property of radial unboundedness has to be satisfied. The domain $D$ corresponds to the operating region of the power converter, limited by the

specifications of its components. This is the reason we are not able to state the global asymptotic stability of PBC for power converters. The function $V(\boldsymbol{x})$ is called a Lyapunov function and it is analogous to the energy of the system. Therefore, the energy function of the system is often adopted as the Lyapunov function to test its stability, though the Lyapunov function does not necessarily have to represent the system's energy [75].

## 2.4 Passivity-based control

In this section, general explanation of PBC is provided. The explanation of PBC is provided in three steps; error dynamics, asymptotic stabilization, and application to power converters. The discussions below are based on premises such as Lyapunov stability theory and PCHS, shown in previous sections. For more advanced discussions of PBC, see [44, 46–48]

### 2.4.1 Error dynamics

First, the error dynamics of PCHS is introduced for the simplicity of the discussion. The steady-state equation i.e. the null dynamics of (2.4) is obtained as

$$\{\mathcal{J}(\boldsymbol{s}) - \mathcal{R}\}\boldsymbol{x} + \boldsymbol{g}(\boldsymbol{s})\boldsymbol{u} = 0 \tag{2.12}$$

by setting the differential terms to zero. The desired state $\boldsymbol{x} = \boldsymbol{x}_{\mathrm{d}}$ and the corresponding duty ratios $\boldsymbol{s} = \boldsymbol{s}_{\mathrm{d}}$ are determined as the constants to satisfy (2.12). Hereafter, the subscript 'd' indicates the desired value. The control aims to achieve the asymptotic stability at $\boldsymbol{x} = \boldsymbol{x}_{\mathrm{d}}$ by modifying the duty ratios $\boldsymbol{s}$ at the transient state.

The error $\tilde{\boldsymbol{x}} = \boldsymbol{x} - \boldsymbol{x}_{\mathrm{d}}$ satisfies

$$\mathcal{A}\dot{\tilde{\boldsymbol{x}}} = \{\mathcal{J}(\boldsymbol{s}) - \mathcal{R}\}\tilde{\boldsymbol{x}} + \tilde{\boldsymbol{g}}(\boldsymbol{s})\tilde{\boldsymbol{u}} \tag{2.13}$$

from (2.4) and (2.12). The input structure $\tilde{\boldsymbol{g}}$ and input $\tilde{\boldsymbol{u}}$ are defined as

$$\tilde{\boldsymbol{g}}(\boldsymbol{s}) = [\mathcal{J}(\boldsymbol{s}) - \mathcal{R}\ \boldsymbol{g}(\boldsymbol{s})],\ \tilde{\boldsymbol{u}} = \begin{bmatrix} \boldsymbol{x}_{\mathrm{d}} \\ \boldsymbol{u} \end{bmatrix}. \tag{2.14}$$

Then, the system is interpreted as a port network shown in Fig. 2.1. The system description of (2.13) simplifies the control task to achieving the asymptotic stability at $\tilde{\boldsymbol{x}} = 0$. Thus, we consider PBC in the following discussions by (2.13).

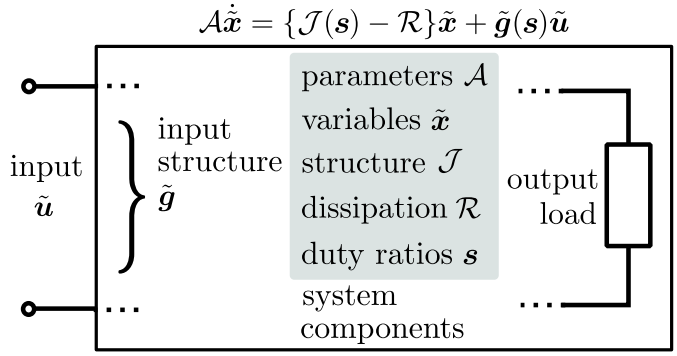


Figure 2.1: Diagrammatical interpretation of dc-dc converters as port network. Output load is considered as internal element. © 2021 IEEE

### 2.4.2 Asymptotic stabilization

The storage function of (2.13) is defined as

$$\mathcal{H} = \frac{1}{2}\tilde{\boldsymbol{x}}^{\mathrm{T}}\mathcal{A}\tilde{\boldsymbol{x}}. \tag{2.15}$$

(2.15) has its minimum at $\tilde{\boldsymbol{x}} = 0$. The time derivative of the storage function (2.15) is

$$\dot{\mathcal{H}} = \tilde{\boldsymbol{x}}^{\mathrm{T}}\mathcal{A}\dot{\tilde{\boldsymbol{x}}} = -\tilde{\boldsymbol{x}}^{\mathrm{T}}\mathcal{R}\tilde{\boldsymbol{x}} + \tilde{\boldsymbol{x}}^{\mathrm{T}}\tilde{\boldsymbol{g}}(\boldsymbol{s})\tilde{\boldsymbol{u}}. \tag{2.16}$$

Here, we assume $\dot{\boldsymbol{x}}_{\mathrm{d}} = 0$, since we are considering a dc system with constant voltage output. This assumption yields simpler discussions and control compared to [43, 44, 48]. The first term on the right-hand side $-\tilde{\boldsymbol{x}}^{\mathrm{T}}\mathcal{R}\tilde{\boldsymbol{x}}$ is the dissipation of the system, which is negative at $\tilde{\boldsymbol{x}} \neq 0$. The second term $\tilde{\boldsymbol{x}}^{\mathrm{T}}\tilde{\boldsymbol{g}}(\boldsymbol{s})\tilde{\boldsymbol{u}}$ corresponds to the power supplied from the externals.

Therefore, when the externally supplied power satisfies

$$\tilde{\boldsymbol{x}}^{\mathrm{T}}\tilde{\boldsymbol{g}}(\boldsymbol{s})\tilde{\boldsymbol{u}} < 0,\ \tilde{\boldsymbol{x}} \neq 0, \tag{2.17}$$

the remaining energy dissipation guarantees

$$\dot{\mathcal{H}} = -\tilde{\boldsymbol{x}}^{\mathrm{T}}\mathcal{R}\tilde{\boldsymbol{x}} + \tilde{\boldsymbol{x}}^{\mathrm{T}}\tilde{\boldsymbol{g}}(\boldsymbol{s})\tilde{\boldsymbol{u}} < 0,\ \tilde{\boldsymbol{x}} \neq 0. \tag{2.18}$$

The storage function $\mathcal{H}$ plays the role of a Lyapunov function of (2.13) and ensures the asymptotic stability at $\tilde{\boldsymbol{x}} = 0$. To summarize, PBC for the dc-dc converters prepares a control rule for the duty ratios $\boldsymbol{s}$ given to satisfy the condition (2.17).

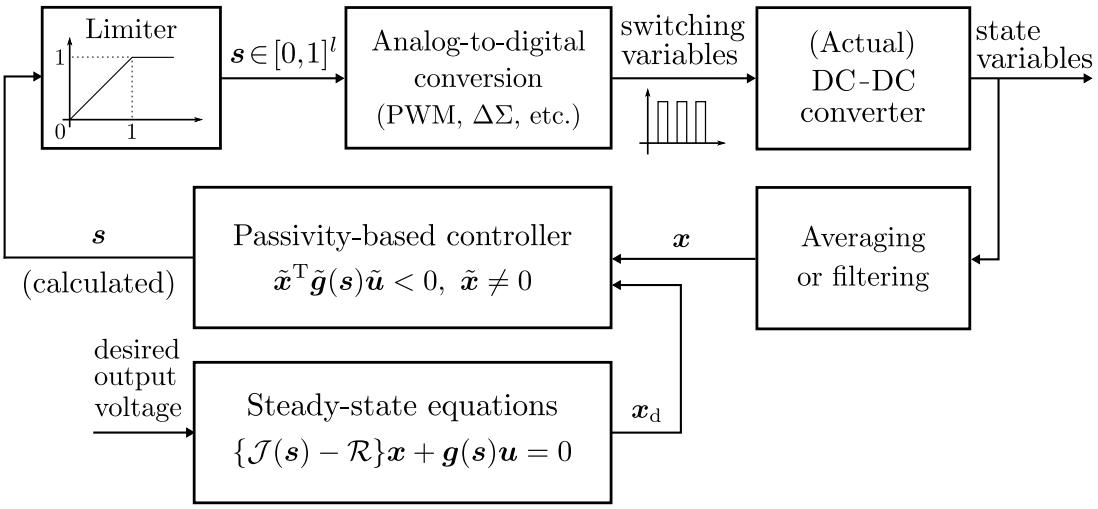


Figure 2.2: Feedback control scheme for the PBC of dc-dc converters. © 2021 IEEE

### 2.4.3 Application to switched power converters

The schematic diagram of the feedback control scheme for the PBC of dc-dc converters is shown in Fig. 2.2. The actual dc-dc converter is regulated by a discrete switching variable. Thus, the duty ratio must be processed through analog-to-digital conversion, such as pulse-width modulation (PWM) or ΔΣ modulation [48, 76]. A hard limiter is implemented to ensure the duty ratio is in the closed interval [0,1]. Regardless, the feedback gain should be determined for the duty ratios to not saturate in the converter's operating range. Averaging or filtering of the state variables is also necessary, since the feedback control is based on the averaged system. The actual state variables have small high-frequency ripples, due to the switching operation. This process is accomplished by the low-pass filtering nature of the passive elements and the design of noise reduction filters for the analog sensors. The The desired state $\boldsymbol{x}_{\mathrm{d}}$ is uniquely determined by (2.12). The feedback control implemented in the later chapters operates as shown in Fig. 2.2 both in simulation and experiment.

## 2.5 Derivation process of passivity-based control laws for dc-dc converters

In this section, the actual control law for boost, buck, and buck-boost converters are derived. The detailed process is first shown for the boost converter. For the buck and

buck-boost converter, the process is abbreviated since it proceeds the exact same way as the boost converter. The obtained PBC laws are numerically analyzed for an optimal feedback gain setting.

### 2.5.1 Boost converter

Fig. 2.3(a) shows the circuit schematic of a boost converter. According to the Kirchhoff's laws, the dynamics of a boost converter is formulated as

$$\begin{bmatrix} L & 0 \\ 0 & C \end{bmatrix} \begin{bmatrix} \dot{i} \\ \dot{v} \end{bmatrix} = \begin{bmatrix} 0 & -(1-u) \\ (1-u) & -1/R \end{bmatrix} \begin{bmatrix} i \\ v \end{bmatrix} + \begin{bmatrix} 1 \\ 0 \end{bmatrix} E, \tag{2.19}$$

where $u \in \{0, 1\}$ is the discrete switching variable. Assuming a sufficiently high frequency switching operation, the averaged model [70–72] of a boost converter is obtained as

$$\begin{bmatrix} L & 0 \\ 0 & C \end{bmatrix} \begin{bmatrix} \dot{i} \\ \dot{v} \end{bmatrix} = \begin{bmatrix} 0 & -(1-\mu) \\ (1-\mu) & -1/R \end{bmatrix} \begin{bmatrix} i \\ v \end{bmatrix} + \begin{bmatrix} 1 \\ 0 \end{bmatrix} E, \tag{2.20}$$

where the switching variable $u$ is replaced with the duty ratio $\mu \in [0, 1]$. By averaging, the state variables are also averaged in the sense that they no longer show ripples caused by the switching operation. Then, the steady-state equations are obtained as

$$\begin{cases} \mu = 1 - \dfrac{E}{v}, \\ Ei = \dfrac{v^2}{R}. \end{cases} \tag{2.21}$$

The desired state $[i\, v]^{\mathrm{T}} = [i_{\mathrm{d}}\, v_{\mathrm{d}}]^{\mathrm{T}}$ and the desired duty ratio $\mu_{\mathrm{d}} \in [0, 1]$ are determined as constants to satisfy (2.21).

Putting $\tilde{\boldsymbol{x}} = [i - i_{\mathrm{d}}\, v - v_{\mathrm{d}}]^{\mathrm{T}}$ gives the storage function of

$$\begin{aligned} \mathcal{H} =& \frac{1}{2}\tilde{\boldsymbol{x}}^{\mathrm{T}}\mathcal{A}\tilde{\boldsymbol{x}} = \frac{1}{2}\begin{bmatrix} i - i_{\mathrm{d}} \\ v - v_{\mathrm{d}} \end{bmatrix}^{\mathrm{T}} \begin{bmatrix} L & 0 \\ 0 & C \end{bmatrix} \begin{bmatrix} i - i_{\mathrm{d}} \\ v - v_{\mathrm{d}} \end{bmatrix} \\ =& \frac{1}{2}L(i - i_{\mathrm{d}})^2 + \frac{1}{2}C(v - v_{\mathrm{d}})^2. \end{aligned} \tag{2.22}$$

In order to form (2.22) as a Lyapunov function,

$$\begin{aligned} \tilde{\boldsymbol{x}}^{\mathrm{T}}\tilde{\boldsymbol{g}}(\mu)\tilde{\boldsymbol{u}} &= \begin{bmatrix} i - i_{\mathrm{d}} \\ v - v_{\mathrm{d}} \end{bmatrix}^{\mathrm{T}} \begin{bmatrix} 0 & -(1-\mu) & 1 \\ (1-\mu) & -1/R & 0 \end{bmatrix} \begin{bmatrix} i_{\mathrm{d}} \\ v_{\mathrm{d}} \\ E \end{bmatrix} \\ &= (\mu - \mu_{\mathrm{d}})(iv_{\mathrm{d}} - i_{\mathrm{d}}v) < 0,\ \tilde{\boldsymbol{x}} \neq 0 \end{aligned} \tag{2.23}$$

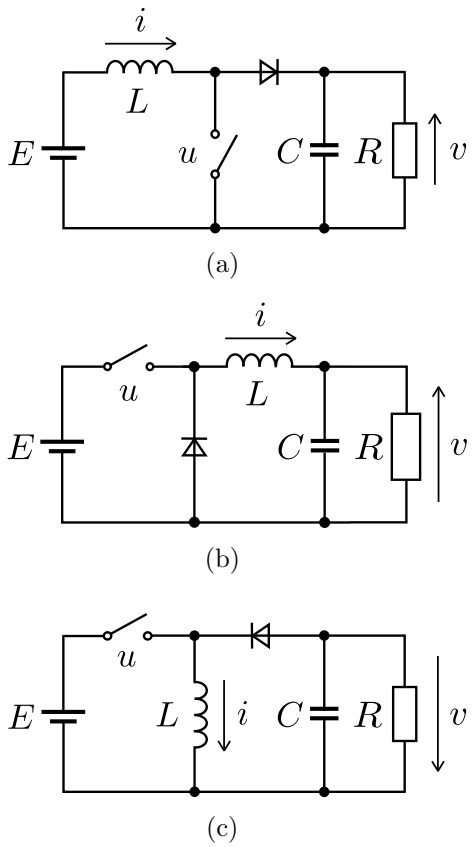


Figure 2.3: Example circuit schematics of dc-dc converters. (a) Boost converter. (b) Buck converter. (c) Buck-boost converter.

has to be satisfied according to (2.17). The condition (2.23) is fulfilled by controlling the duty ratio $\mu$ as

$$\mu = \mu_{\mathrm{d}} - k(iv_{\mathrm{d}} - i_{\mathrm{d}}v),\ k > 0, \tag{2.24}$$

where $k$ is a positive feedback gain. Therefore, PBC for the boost converter is obtained as (2.24).

The transient characteristics of the PBC law for boost converter are shown in Fig. 2.4. The transient feature is evaluated in regards to overshoot and settling time. The initial state and circuit parameters are determined based on the settings in Chapter 4. The parameters are set as $L = 470\,\mu\mathrm{H}$, $C = 10\,\mu\mathrm{F}$, $E = 9\,\mathrm{V}$, $R = 65.8\,\Omega$, $v_{\mathrm{d}} = 18\,\mathrm{V}$, $i_{\mathrm{d}} = 0.548\,\mathrm{A}$. As the feedback gain $k$ is set higher, the overshoot converges to zero. However, settling time has a peak. Fig. 2.5 shows the actual waveforms obtained for specific feedback gain settings. These characteristics greatly depend on the circuit parameters and initial

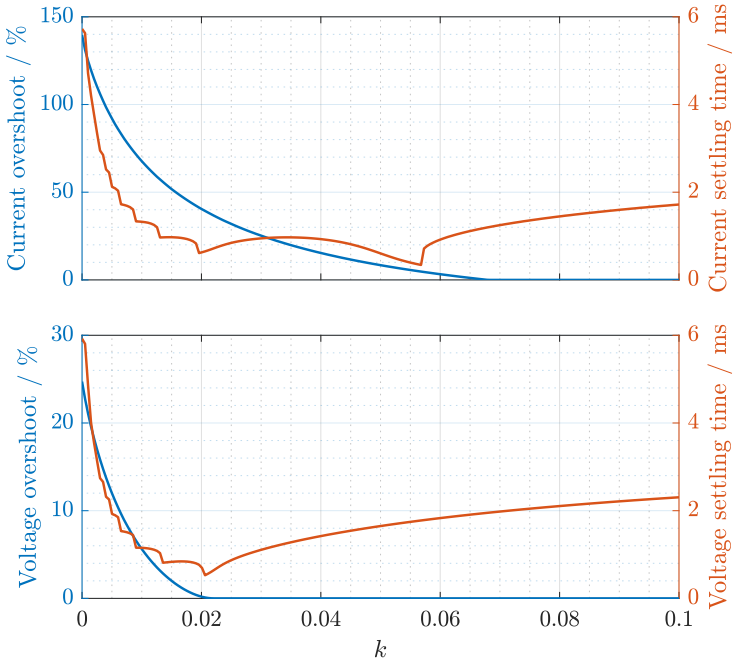


Figure 2.4: Transient characteristics of passivity-based control for boost converter.

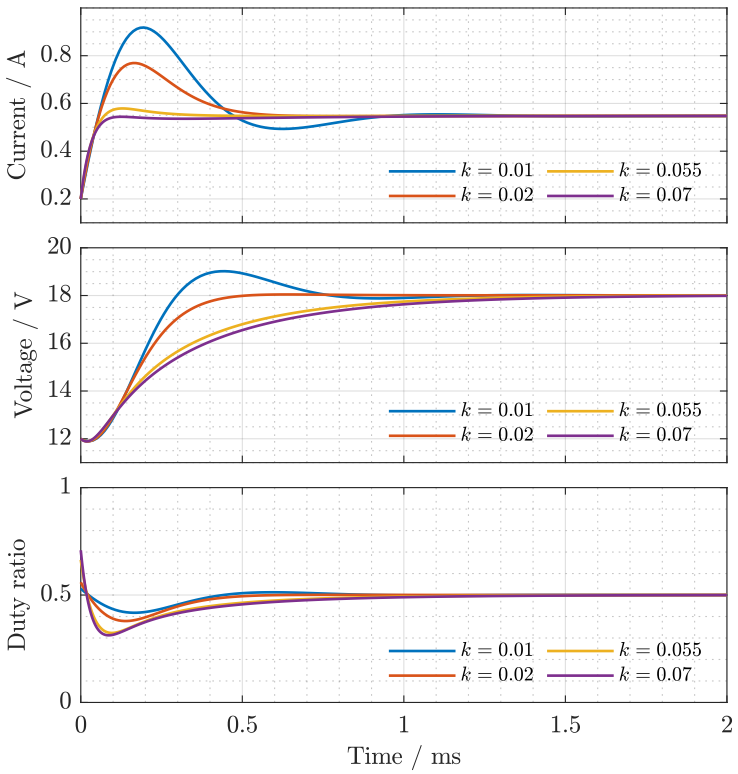


Figure 2.5: Waveforms of passivity-based control for boost converter with specific feedback gain settings.

states. Therefore, the feedback gain must be analyzed widely throughout the region of operation.

### 2.5.2 Buck converter

PBC for the buck converter follows the same derivation process as the boost converter. The averaged model of the buck converter shown in Fig. 2.3(b) is

$$\begin{bmatrix} L & 0 \\ 0 & C \end{bmatrix} \begin{bmatrix} \dot{i} \\ \dot{v} \end{bmatrix} = \begin{bmatrix} 0 & -1 \\ 1 & -1/R \end{bmatrix} \begin{bmatrix} i \\ v \end{bmatrix} + \begin{bmatrix} \mu \\ 0 \end{bmatrix} E, \tag{2.25}$$

which is clearly in the form of PCHS. The steady-state equations for the buck converter are obtained as

$$\begin{cases} \mu = \dfrac{v}{E}, \\ i = \dfrac{v}{R}, \end{cases} \tag{2.26}$$

by setting the left hand side of (2.25) to zero. Similarly to the boost converter, the desired state $[i\, v]^{\mathrm{T}} = [i_{\mathrm{d}}\, v_{\mathrm{d}}]^{\mathrm{T}}$ and the desired duty ratio $\mu_{\mathrm{d}} \in [0, 1]$ are determined to satisfy (2.26). Then, the condition for the asymptotic stability is

$$\begin{aligned} \tilde{\boldsymbol{x}}^{\mathrm{T}} \tilde{\boldsymbol{g}}(\mu) \tilde{\boldsymbol{u}} &= \begin{bmatrix} i - i_{\mathrm{d}} \\ v - v_{\mathrm{d}} \end{bmatrix}^{\mathrm{T}} \begin{bmatrix} 0 & -1 & \mu \\ 1 & -1/R & 0 \end{bmatrix} \begin{bmatrix} i_{\mathrm{d}} \\ v_{\mathrm{d}} \\ E \end{bmatrix} \\ &= (\mu - \mu_{\mathrm{d}})(i - i_{\mathrm{d}})E < 0, \ \tilde{\boldsymbol{x}} \neq 0, \end{aligned} \tag{2.27}$$

from (2.17). This condition is satisfied by

$$\mu = \mu_{\mathrm{d}} - k(i - i_{\mathrm{d}}), \ k > 0. \tag{2.28}$$

Thus, (2.28) is obtained as the PBC law for the buck converter.

The transient characteristics of the PBC law for buck converter are shown in Fig. 2.6. The parameters are $L = 630\,\mu\mathrm{H}$, $C = 4.7\,\mu\mathrm{F}$, $E = 36\,\mathrm{V}$, $R = 162\,\Omega$, $v_{\mathrm{d}} = 18\,\mathrm{V}$, $i_{\mathrm{d}} = 0.108\,\mathrm{A}$. Note that the current overshoot does not converge to zero in this setting, unlike the boost converter. This is due to the eigenvalues of this equilibrium point. Fig. 2.7 shows the actual waveforms obtained for specific feedback gain settings. Here, we are able to confirm that the current overshoot remains in all feedback gain settings. The overshoot and the settling time are a trade-off in this case.

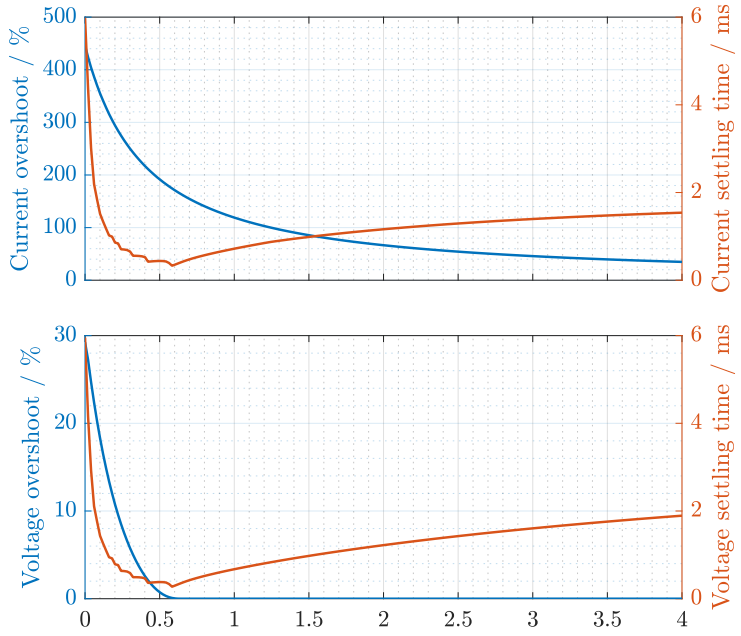


Figure 2.6: Transient characteristics of passivity-based control for buck converter.

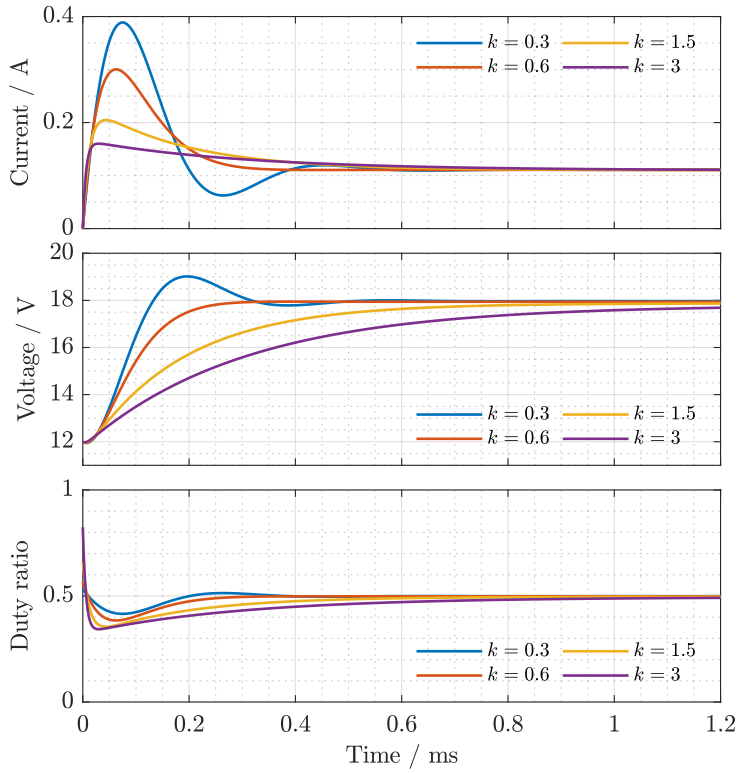


Figure 2.7: Waveforms of passivity-based control for buck converter with specific feedback gain settings.

### 2.5.3 Buck-boost converter

PBC for the buck-boost converter also follows the same derivation process. The buck-boost converter shown in Fig. 2.3(c) is modeled as

$$\begin{bmatrix} L & 0 \\ 0 & C \end{bmatrix} \begin{bmatrix} \dot{i} \\ \dot{v} \end{bmatrix} = \begin{bmatrix} 0 & -(1-\mu) \\ (1-\mu) & -1/R \end{bmatrix} \begin{bmatrix} i \\ v \end{bmatrix} + \begin{bmatrix} \mu \\ 0 \end{bmatrix} E. \tag{2.29}$$

The steady-state equations for the buck-boost converter are obtained as

$$\begin{cases} \mu = \dfrac{v}{v+E}, \\ i = \dfrac{v(v+E)}{RE}, \end{cases} \tag{2.30}$$

by setting the left hand side of (2.29) to zero. The condition for the asymptotic stability is

$$\begin{aligned} \tilde{\boldsymbol{x}}^{\mathrm{T}} \tilde{\boldsymbol{g}}(\mu) \tilde{\boldsymbol{u}} &= \begin{bmatrix} i - i_{\mathrm{d}} \\ v - v_{\mathrm{d}} \end{bmatrix}^{\mathrm{T}} \begin{bmatrix} 0 & -(1-\mu) & \mu \\ (1-\mu) & -1/R & 0 \end{bmatrix} \begin{bmatrix} i_{\mathrm{d}} \\ v_{\mathrm{d}} \\ E \end{bmatrix} \\ &= (\mu - \mu_{\mathrm{d}})\{i(v_{\mathrm{d}} + E) - i_{\mathrm{d}}(v + E)\} < 0, \ \tilde{\boldsymbol{x}} \neq 0. \end{aligned} \tag{2.31}$$

This condition is satisfied by

$$\mu = \mu_{\mathrm{d}} - k\{i(v_{\mathrm{d}} + E) - i_{\mathrm{d}}(v + E)\}, \ k > 0. \tag{2.32}$$

Thus, (2.32) is the PBC for the buck-boost converter.

The transient characteristics of the PBC law for buck converter are shown in Fig. 2.8. The parameters are set as $L = 470\,\mu\mathrm{H}$, $C = 10\,\mu\mathrm{F}$, $E = 18\,\mathrm{V}$, $R = 36\,\Omega$, $v_{\mathrm{d}} = 18\,\mathrm{V}$, $i_{\mathrm{d}} = 1\,\mathrm{A}$. Similarly to the boost converter's case, it is possible to reduce both overshoot and settling time by increasing the feedback gain. Fig. 2.9 shows the actual waveforms obtained for specific feedback gain settings. It is confirmed that increasing the feedback gain improves the transient characteristics. However, the duty ratio must be ensured that it does not saturate due to large feedback gain.

## 2.6 Adaptive passivity-based control

In this section, APBC is explained for buck and boost converters. APBC is a control method that enables asymptotic stabilization without the knowledge of the output load.

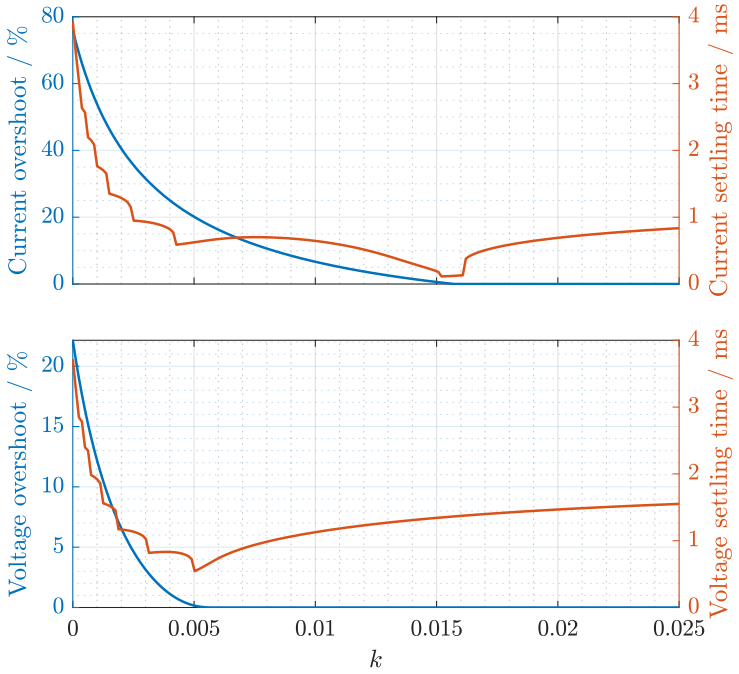


Figure 2.8: Transient characteristics of passivity-based control for buck-boost converter.

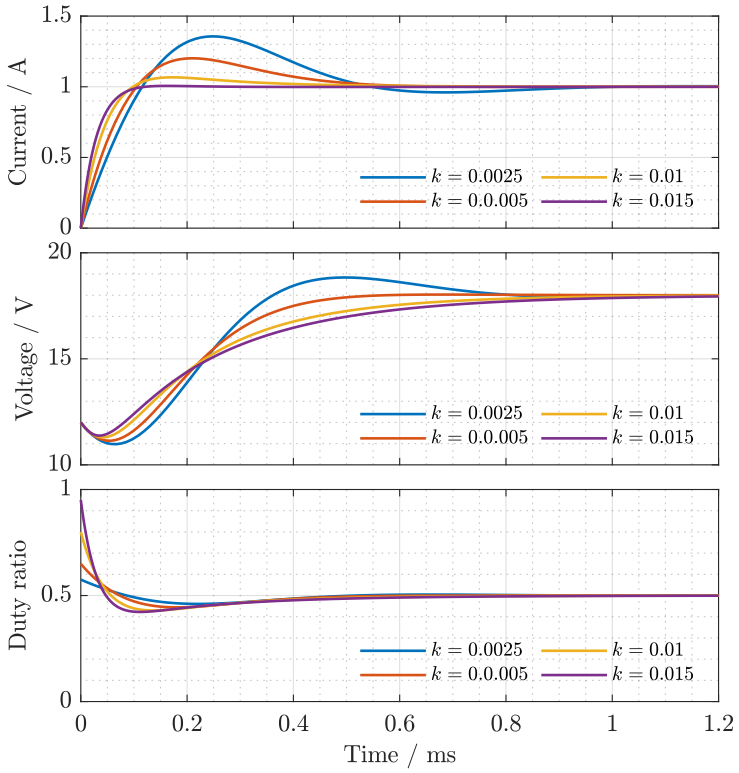


Figure 2.9: Waveforms of passivity-based control for buck-boost converter with specific feedback gain settings.

This feature is obtained by introducing an adaptive variable with dynamics that does not violate the passivity of the system. The advantage of APBC is that it can automatically maintain the output voltage among the series-paralleled converters [77, 78]. Previous research on APBC of power converters can be found in [79–81]. The detail of the control method is explained below.

### 2.6.1 Buck converter

According to the second equation of (2.26), the desired current and voltage for the PBC of buck converters must satisfy

$$i_{\mathrm{d}} = \frac{v_{\mathrm{d}}}{R}. \tag{2.33}$$

This equation implies the balance between the current and the voltage at the steady-state. Hence, the PBC for a buck converter (2.28) assumes the knowledge of the output load $R$.

Suppose that we have the desired output voltage $v_{\mathrm{d}}$ for the buck converter. Also, suppose that we have no knowledge of the output load $R$ and cannot determine the desired current $i_{\mathrm{d}}$ from the steady-state equation (2.26). Here, we can introduce an adaptive desired current $\widehat{i_{\mathrm{d}}}$ to replace the actual desired current $i_{\mathrm{d}}$ in the control law of (2.28). Thus, we have

$$\mu = \frac{v_{\mathrm{d}}}{E} - k(i - \widehat{i_{\mathrm{d}}}),\ k > 0, \tag{2.34}$$

as the APBC for the buck converter. The dynamics of the adaptive variable $\widehat{i_{\mathrm{d}}}$ are defined as

$$L_{\mathrm{a}}\dot{\widehat{i_{\mathrm{d}}}} = kE(i - \widehat{i_{\mathrm{d}}}),\ L_{\mathrm{a}} > 0, \tag{2.35}$$

where $L_{\mathrm{a}}$ is an additional control parameter. Note that (2.34) and (2.35) do not require any knowledge of output load $R$ or desired current $i_{\mathrm{d}}$ for control.

Substituting (2.34) and (2.35) to the buck converter model (2.25) yields the extended system of

$$\begin{cases} L\dot{i} = -v + v_{\mathrm{d}} - kE(i - \widehat{i_{\mathrm{d}}}), \\ C\dot{v} = i - \dfrac{v}{R}, \\ L_{\mathrm{a}}\dot{\widehat{i_{\mathrm{d}}}} = kE(i - \widehat{i_{\mathrm{d}}}). \end{cases} \tag{2.36}$$

Equation (2.36) represents the buck converter regulated by APBC. The storage function of (2.36) is

$$\mathcal{H} = \frac{1}{2}L(i - i_{\mathrm{d}})^2 + \frac{1}{2}C(v - v_{\mathrm{d}})^2 + \frac{1}{2}L_{\mathrm{a}}(\widehat{i_{\mathrm{d}}} - i_{\mathrm{d}})^2. \tag{2.37}$$

The time derivative of the storage function along the trajectory of (2.36) is obtained as

$$\begin{aligned}\dot{\mathcal{H}} &= L\dot{i}(i - i_{\mathrm{d}}) + C\dot{v}(v - v_{\mathrm{d}}) + L_{\mathrm{c}}\dot{\widehat{i_{\mathrm{d}}}}(\widehat{i_{\mathrm{d}}} - i_{\mathrm{d}}) \\ &= -\frac{(v - v_{\mathrm{d}})^2}{R} - kE(i - \widehat{i_{\mathrm{d}}})^2 \leq 0,\end{aligned} \tag{2.38}$$

which indicates the asymptotic stability of (2.36) in the sense of Lyapunov. The APBC given in (2.34) and (2.35) is shown to asymptotically stabilize the buck converter at the output voltage of $v = v_{\mathrm{d}}$ without the knowledge of the load $R$. It implies the robustness of APBC against load fluctuations and uncertainties.

APBC has two control parameters $k$ and $L_{\mathrm{a}}$ as seen from (2.34) and (2.35). Figs. 2.10(a) and (b) show the transient properties of buck converter regulated by APBC depending on the control parameters. Here, the circuit parameters are chosen based on the components of the fabricated converter introduced in Section 5.3 listed in Table 5.1. The transient characteristics are analyzed from the step response of (2.36) with the initial state at the origin. The desired output voltage and the output load is chosen as $v_{\mathrm{d}} = 24\,\mathrm{V}$ and $R = 9.6\,\Omega$. The control parameters are limited in the region where the duty ratio $\mu$ satisfies $0 \leq \mu \leq 1$ throughout the transient. The numerical simulation was executed by MATLAB/Simulink 2020b.

The dependence of current overshoot on the control parameters is shown in Fig. 2.10(a). It indicates that setting a larger value for both control parameters decreases the current overshoot. However, if either one of the parameter is set insufficiently small, then it will drastically reduce the effectiveness of the control. According to Fig. 2.10(a), the control parameters should be set $k \geq 0.19, L_{\mathrm{a}} \geq 0.8 \times 10^{-3}$ in order to have zero current overshoot in the transient.

The dependence of settling time on the control parameters is shown in Fig. 2.10(b). Here, the settling time is defined as the time it takes for the buck converter current to remain within 0.5% error from the steady-state current. Fig. 2.10(b) shows a waved surface due to the damped oscillations in the current waveform. The surface has a region around $k = 0.2, L_{\mathrm{a}} = 0.92 \times 10^{-3}$, where the settling time becomes relatively smaller than the other regions inside the figure.

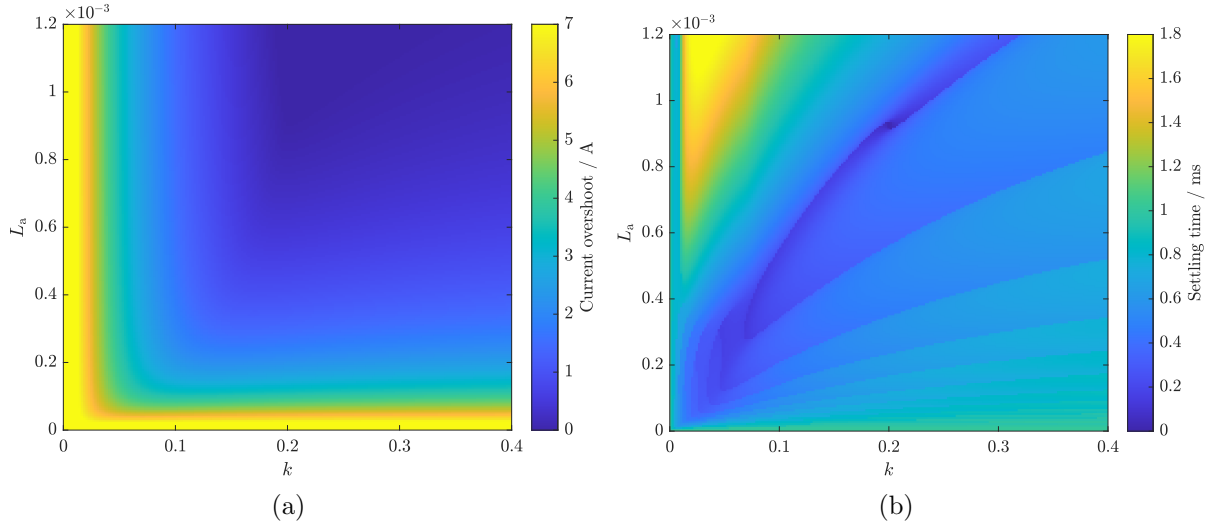


Figure 2.10: Transient properties of buck converter regulated by APBC depending on the control parameters. (a) Current overshoot. (b) Settling time.

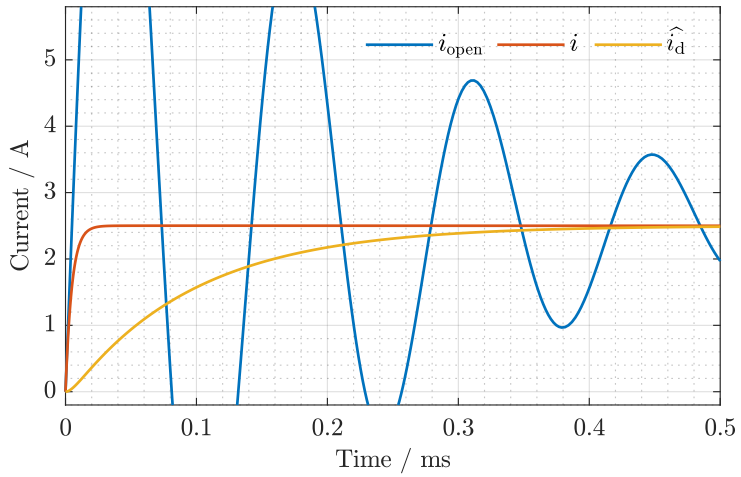


Figure 2.11: Waveform of buck converter current at $k = 0.2$ and $L_{\text{a}} = 0.92 \times 10^{-3}$ compared with open loop system.

Figure. 2.11 is the simulated current waveform of the buck converter with APBC at $k = 0.2, L_{\text{a}} = 0.92 \times 10^{-3}$. Here, $i_{\text{open}}$ is the current waveform of the open loop system, where the buck converter is operating without control. The controlled buck converter current shows significantly better transient in terms of overshoot and settling time. The dynamics of the adaptive variable $\widehat{i}_{\text{d}}$ can also be observed. Note that the feedback control is purely based on the error between $i$ and $\widehat{i}_{\text{d}}$, and no information of the load $R$ or the desired current $i_{\text{d}}$ is necessary.

### 2.6.2 Boost converter

The APBC for the boost converter is given by

$$\mu = 1 - \frac{E}{v_{\rm d}} - k(iv_{\rm d} - \widehat{i_{\rm d}}v),\ k > 0, \tag{2.39}$$

where dynamics of the adaptive variable $\widehat{i_{\rm d}}$ is defined as

$$L_{\rm a}\dot{\widehat{i_{\rm d}}} = kv(iv_{\rm d} - \widehat{i_{\rm d}}v),\ L_{\rm a} > 0. \tag{2.40}$$

This control law is able to be derived in the same way as the buck converter.

Substituting (2.39) and (2.40) to the boost converter model (2.20) yields the extended system of

$$\begin{cases} L\dot{i} = -\dfrac{E}{v_{\rm d}}v - kv_{\rm d}iv - kv^2\widehat{i_{\rm d}} + E, \\ C\dot{v} = \dfrac{E}{v_{\rm d}}i + kv_{\rm d}i^2 - kiv\widehat{i_{\rm d}} - \dfrac{v}{R}, \\ L_{\rm a}\dot{\widehat{i_{\rm d}}} = kv(iv_{\rm d} - \widehat{i_{\rm d}}v). \end{cases} \tag{2.41}$$

Equation (2.41) represents the boost converter with APBC. The storage function of (2.41) is

$$\mathcal{H} = \frac{1}{2}L(i - i_{\rm d})^2 + \frac{1}{2}C(v - v_{\rm d})^2 + \frac{1}{2}L_{\rm a}(\widehat{i_{\rm d}} - i_{\rm d})^2. \tag{2.42}$$

The time derivative of the storage function along the trajectory of (2.41) is obtained as

$$\begin{aligned} \dot{\mathcal{H}} &= L\dot{i}(i - i_{\rm d}) + C\dot{v}(v - v_{\rm d}) + L_{\rm c}\dot{\widehat{i_{\rm d}}}(\widehat{i_{\rm d}} - i_{\rm d}) \\ &= -\frac{(v - v_{\rm d})^2}{R} - k(iv_{\rm d} - \widehat{i_{\rm d}}v)^2 \le 0, \end{aligned} \tag{2.43}$$

which indicates the asymptotic stability of (2.41) in the sense of Lyapunov. Similarly to the buck converter, the APBC given in (2.39) and (2.40) is shown to asymptotically stabilize the boost converter at the output voltage of $v = v_{\rm d}$ without the knowledge of the load $R$.

The dependence of the current overshoot on the control parameters for the APBC of the boost converter is shown in Fig. 2.12(a). Similarly to the buck converter's case, setting a larger value for both control parameters decreases the current overshoot. Also, if either one of the parameters is set insufficiently small, it drastically reduces the effectiveness

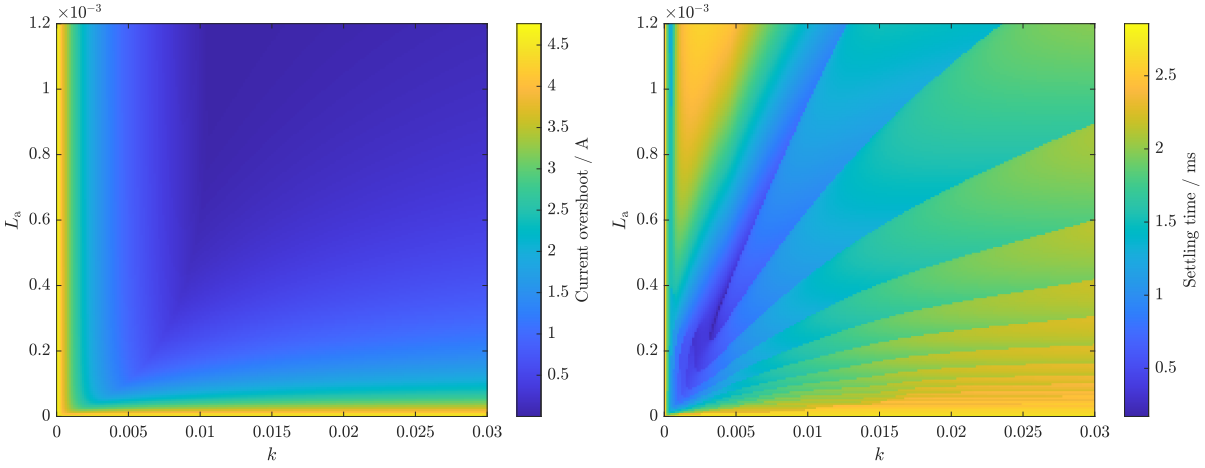


(a) (b)

Figure 2.12: Transient properties of boost converter regulated by APBC depending on the control parameters. (a) Current overshoot. (b) Settling time.

of the control. According to Fig. 2.12(a), the control parameters should be set $k \geq 0.01$, $L_{\mathrm{a}} \geq 0.7 \times 10^{-3}$ in order to have zero current overshoot in the transient.

The dependence of settling time on the control parameters is shown in Fig. 2.12(b). It should be noted that he surface has a thin region around $k = 0.0035$, $L_{\mathrm{a}} = 0.23 \times 10^{-3}$, where the settling time becomes relatively smaller than the other regions. The feedback parameters then should be set in this region with higher values in order to optimize the transient performance.

To summarize this section, we explained the APBC of the boost and buck converters and examined its transient performance numerically. The results in this section are based on the fabricated dc-dc converter introduced in Section 5.3. The optimal control parameter settings obtained in this section will be utilized in the power management of series-paralleled converters, examined in Chapter 5. The application of APBC to the series-paralleled converters is verified in [77, 78]. Note that the transient performance depend on the circuit parameters, and therefore the optimal control parameters may vary between the converter designs.

## 2.7 Decoupled passivity-based control

This section is devoted to the explanation of DPBC for a boost converter. DPBC is a control method that decouples the input current characteristics from the output

voltage fluctuations. This feature is obtained by the modification of feedback gain by state feedback. The detail is explained below.

Applying the PBC law (2.24) to the boost converter model (2.20) gives

$$\begin{cases} L\dot{i} = -\left\{\dfrac{E}{v_\mathrm{d}} + k(v_\mathrm{d} i - v i_\mathrm{d})\right\} v + E, \\ C\dot{v} = \left\{\dfrac{E}{v_\mathrm{d}} + k(v_\mathrm{d} i - v i_\mathrm{d})\right\} i - \dfrac{v}{R}. \end{cases} \tag{2.44}$$

By expanding the equations, we have

$$\begin{cases} \dfrac{L i_\mathrm{d}}{E i_\mathrm{d}}\dot{i} = 1 - \dfrac{v}{v_\mathrm{d}} - k\dfrac{{v_\mathrm{d}}^2 i_\mathrm{d}}{E}\left(\dfrac{iv}{i_\mathrm{d} v_\mathrm{d}} - \dfrac{v^2}{{v_\mathrm{d}}^2}\right), \\ \dfrac{CR}{v_\mathrm{d}}\dot{v} = \dfrac{i}{i_\mathrm{d}} - \dfrac{v}{v_\mathrm{d}} - k\dfrac{{v_\mathrm{d}}^2 i_\mathrm{d}}{E}\left(\dfrac{iv}{i_\mathrm{d} v_\mathrm{d}} - \dfrac{i^2}{{i_\mathrm{d}}^2}\right). \end{cases} \tag{2.45}$$

Here, if we give $k$ as

$$k = \frac{E}{v i_\mathrm{d} v_\mathrm{d}}, \tag{2.46}$$

we obtain

$$\begin{cases} \dfrac{L i_\mathrm{d}}{E i_\mathrm{d}}\dot{i} = 1 - \dfrac{i}{i_\mathrm{d}}, \\ \dfrac{CR}{v_\mathrm{d}}\dot{v} = -\dfrac{v}{v_\mathrm{d}} + \dfrac{i^2}{{i_\mathrm{d}}^2}\dfrac{v_\mathrm{d}}{v}, \end{cases} \tag{2.47}$$

We can clearly see that the first equation of (2.47) becomes independent of the output voltage $v$, which implies that the dynamics of the input current $i$ has been decoupled from the output voltage $v$. By substituting (2.46) to (2.24), we obtain the actual DPBC law for the boost converter as

$$\mu = 1 - \frac{Ei}{i_\mathrm{d} v}. \tag{2.48}$$

DPBC law for the boost converter (2.48) allows keeping the dynamics of the input current independent while ensuring the stability in the sense of Lyapunov.

Figure 2.13 shows the transient waveform of boost converter regulated by DPBC. An initial error from the desired state is given to the output voltage. Here, the current of the boost converter stays constant at the desired state with no fluctuations with DPBC, compared to PBC with constant feedback gains. Therefore, the decoupled feature of the control method is confirmed numerically. This feature is confirmed to be applicable to series-parallel connection of the converters in [78].

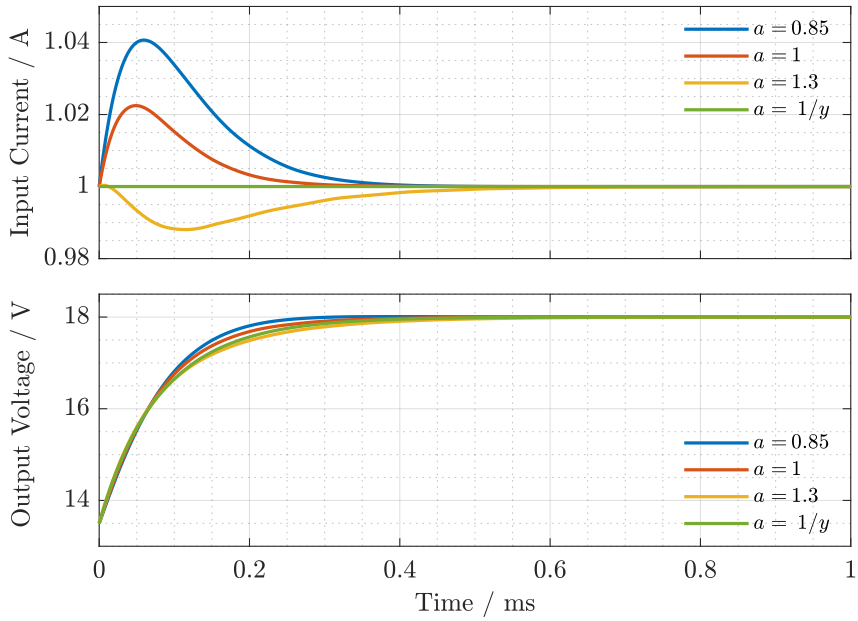


Figure 2.13: Waveform of boost converter regulated by DPBC.

## 2.8 Summary

In this chapter, the basic concepts of this study were introduced in detail. Passivity, Lyapunov stability, and PCHS were first explained. Then, averaged models of boost, buck, and buck-boost converters were described as PCHS. APBC and DPBC were also introduced for advanced transient features. The characteristics and performance of the control methods were numerically analyzed to determine the feedback gain settings. The contents of this chapter provide theoretical support for the numerical and experimental results in the subsequent chapters.

# Chapter 3

# Output series-parallel connection of dc-dc converters regulated by passivity-based control

In this chapter, the asymptotic stability of the output series-paralleled dc-dc converters regulated by PBC is theoretically discussed. The asymptotic stability of the system is rigorously shown in terms of stored energy and Lyapunov stability theory. First, the dc-dc converter model is introduced with an additional external variable representing the mutual interaction between the converters. Then, circuit restrictions are given to the variables for the model to describe a series or parallel connection. Through the process, the output series-paralleled converters are shown to be reclassified into the PCHS of (2.13). Thus, the asymptotic stability of the series-paralleled converters is able to be discussed in the same manner as a single dc-dc converter. It follows that the application of PBC to each converter asymptotically stabilizes the series-paralleled converters. The results of the numerical simulations are shown to confirm the theoretical discussions. Here, several scenarios for external disturbance will be considered to verify the stability and robustness of the output series-paralleled converters regulated by PBC.

## 3.1 DC-DC converter model with output interaction

The dc-dc converter with output interaction is modeled as

$$\mathcal{A}\dot{\tilde{\boldsymbol{x}}} = \{\mathcal{J}(\boldsymbol{s}) - \mathcal{R}\}\tilde{\boldsymbol{x}} + \tilde{\boldsymbol{g}}(\boldsymbol{s})\tilde{\boldsymbol{u}} + \boldsymbol{b}, \tag{3.1}$$

where $\boldsymbol{b} \in \mathbb{R}^n$ implies the interaction at the output. This dc-dc converter model is shown diagrammatically in Fig. 3.1. As shown in the figure, the interaction $\boldsymbol{b}$ is treated as an

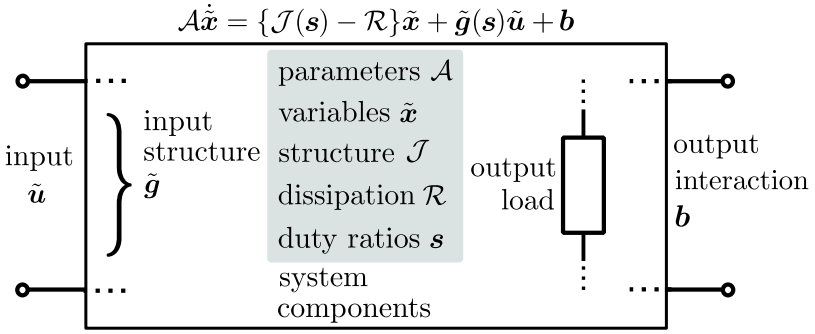


Figure 3.1: DC-DC converter model with interaction at output. © 2021 IEEE

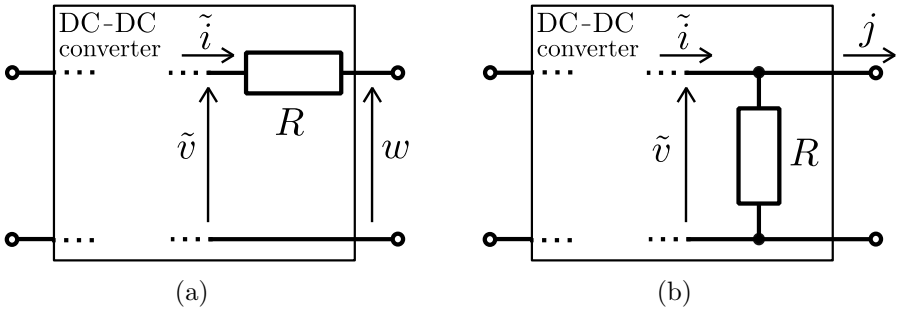


Figure 3.2: Possible circuit structures for series or parallel output interaction. (a) Series interaction. (b) Parallel interaction. © 2021 IEEE

external variable. The storage function of (3.1) is kept as

$$\mathcal{H} = \frac{1}{2}\tilde{\boldsymbol{x}}^{\mathrm{T}}\mathcal{A}\tilde{\boldsymbol{x}}. \tag{3.2}$$

However, its time derivative is altered to be

$$\begin{aligned}\dot{\mathcal{H}} &= \tilde{\boldsymbol{x}}^{\mathrm{T}}\mathcal{A}\dot{\tilde{\boldsymbol{x}}} \\ &= -\tilde{\boldsymbol{x}}^{\mathrm{T}}\mathcal{R}\tilde{\boldsymbol{x}} + \tilde{\boldsymbol{x}}^{\mathrm{T}}\tilde{\boldsymbol{g}}(\boldsymbol{s})\tilde{\boldsymbol{u}} + \tilde{\boldsymbol{x}}^{\mathrm{T}}\boldsymbol{b},\end{aligned} \tag{3.3}$$

where the term $\tilde{\boldsymbol{x}}^{\mathrm{T}}\boldsymbol{b}$ implies the power supplied from the output interaction.

Two possible circuit structures are assumed for the output interaction; series or parallel connection as shown in Figs. 3.2(a) and (b), respectively. The variables $\tilde{v}$ and $\tilde{i}$ represent the output voltage and the output current of the converter. In Fig. 3.2(a), the interaction appears as the voltage $w$ in series to the load. From the assumption that the only dissipative element of the converter is the output load $R$, we have

$$-\tilde{\boldsymbol{x}}^{\mathrm{T}}\mathcal{R}\tilde{\boldsymbol{x}} = -\frac{\tilde{v}^2}{R},\ \tilde{\boldsymbol{x}}^{\mathrm{T}}\boldsymbol{b} = \frac{\tilde{v}w}{R}, \tag{3.4}$$

for the series interaction. Clearly, adding the two equations in (3.4) gives the power consumption at the load. Here, we can see that the output interaction affects the dissipation of the model. Similarly, we have

$$-\tilde{\boldsymbol{x}}^{\mathrm{T}}\mathcal{R}\tilde{\boldsymbol{x}} = -R\tilde{i}^2,\ \tilde{\boldsymbol{x}}^{\mathrm{T}}\boldsymbol{b} = R\tilde{i}j, \tag{3.5}$$

for the parallel case shown in Fig. 3.2(b).

## 3.2 Output series or parallel connection of two dc-dc converters

Fig. 3.3(a) shows a pair of dc-dc converters with output interaction. Each converter has output load $R$, output voltage $\tilde{v}$, output current $\tilde{i}$, and output interaction $\boldsymbol{b}$. The subscripts '1' and '2' correspond to converters #1 and #2, respectively.

### 3.2.1 Model and energy property

The pair of dc-dc converters shown in Fig. 3.3(a) are modeled as

$$\begin{cases} \mathcal{A}_1\dot{\tilde{\boldsymbol{x}}}_1 = \{\mathcal{J}_1(\boldsymbol{s}_1) - \mathcal{R}_1\}\tilde{\boldsymbol{x}}_1 + \tilde{\boldsymbol{g}}_1(\boldsymbol{s}_1)\tilde{\boldsymbol{u}}_1 + \boldsymbol{b}_1, \\ \mathcal{A}_2\dot{\tilde{\boldsymbol{x}}}_2 = \{\mathcal{J}_2(\boldsymbol{s}_2) - \mathcal{R}_2\}\tilde{\boldsymbol{x}}_2 + \tilde{\boldsymbol{g}}_2(\boldsymbol{s}_2)\tilde{\boldsymbol{u}}_2 + \boldsymbol{b}_2. \end{cases} \tag{3.6}$$

Note that these equations are independent due to the fact that no conditions are fixed to the variables yet. Equation (3.6) is rewritten as

$$\mathcal{A}_{12}\dot{\tilde{\boldsymbol{x}}}_{12} = \{\mathcal{J}_{12}(\boldsymbol{s}_{12}) - \mathcal{R}'_{12}\}\tilde{\boldsymbol{x}}_{12} + \tilde{\boldsymbol{g}}_{12}(\boldsymbol{s}_{12})\tilde{\boldsymbol{u}}_{12} + \boldsymbol{b}_{12}, \tag{3.7}$$

by using

$$\begin{cases} \tilde{\boldsymbol{x}}_{12} = \begin{bmatrix} \tilde{\boldsymbol{x}}_1 \\ \tilde{\boldsymbol{x}}_2 \end{bmatrix},\ \tilde{\boldsymbol{u}}_{12} = \begin{bmatrix} \tilde{\boldsymbol{u}}_1 \\ \tilde{\boldsymbol{u}}_2 \end{bmatrix},\ \mathcal{A}_{12} = \begin{bmatrix} \mathcal{A}_1 & 0 \\ 0 & \mathcal{A}_2 \end{bmatrix}, \\ \mathcal{J}_{12} = \begin{bmatrix} \mathcal{J}_1 & 0 \\ 0 & \mathcal{J}_2 \end{bmatrix},\ \mathcal{R}'_{12} = \begin{bmatrix} \mathcal{R}_1 & 0 \\ 0 & \mathcal{R}_2 \end{bmatrix}, \\ \tilde{\boldsymbol{g}}_{12} = \begin{bmatrix} \tilde{\boldsymbol{g}}_1 & 0 \\ 0 & \tilde{\boldsymbol{g}}_2 \end{bmatrix},\ \boldsymbol{b}_{12} = \begin{bmatrix} \boldsymbol{b}_1 \\ \boldsymbol{b}_2 \end{bmatrix},\ \boldsymbol{s}_{12} = \begin{bmatrix} \boldsymbol{s}_1 \\ \boldsymbol{s}_2 \end{bmatrix}. \end{cases} \tag{3.8}$$

Then, the storage function of (3.7) is

$$\mathcal{H}_{12} = \frac{1}{2}\tilde{\boldsymbol{x}}_{12}^{\mathrm{T}}\mathcal{A}_{12}\tilde{\boldsymbol{x}}_{12}. \tag{3.9}$$

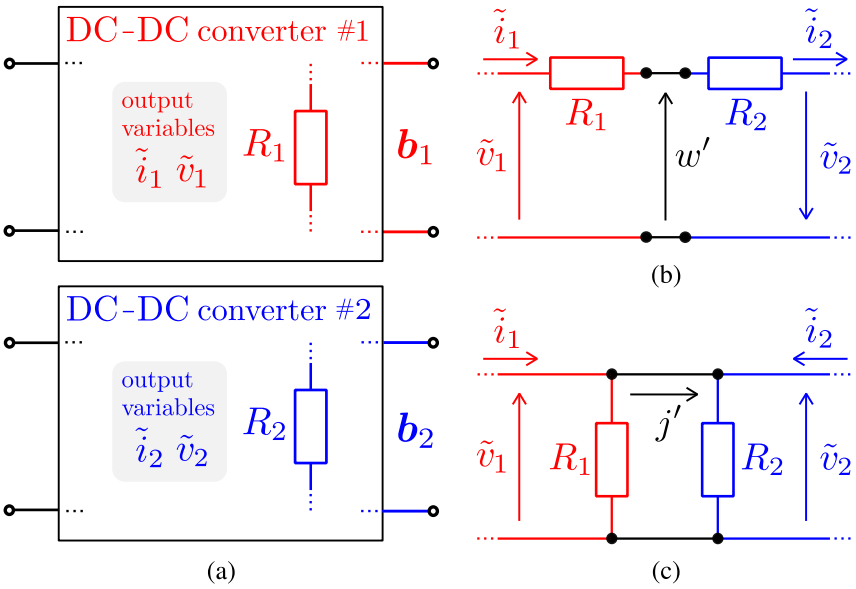


Figure 3.3: Pair of dc-dc converters with output interaction. (a) Drawn individually. (b) Series connection at output. (c) Parallel connection at output. © 2021 IEEE

The time derivative of the storage function is obtained as

$$\begin{aligned}\dot{\mathcal{H}}_{12} &= \tilde{\boldsymbol{x}}_{12}^{\mathrm{T}}\mathcal{A}_{12}\dot{\tilde{\boldsymbol{x}}}_{12} \\ &= -\tilde{\boldsymbol{x}}_{12}^{\mathrm{T}}\mathcal{R}'_{12}\tilde{\boldsymbol{x}}_{12} + \tilde{\boldsymbol{x}}_{12}^{\mathrm{T}}\tilde{\boldsymbol{g}}_{12}(\boldsymbol{s}_{12})\tilde{\boldsymbol{u}}_{12} + \tilde{\boldsymbol{x}}_{12}^{\mathrm{T}}\boldsymbol{b}_{12},\end{aligned} \tag{3.10}$$

where

$$\begin{cases}\tilde{\boldsymbol{x}}_{12}^{\mathrm{T}}\mathcal{R}'_{12}\tilde{\boldsymbol{x}}_{12} = \tilde{\boldsymbol{x}}_1^{\mathrm{T}}\mathcal{R}_1\tilde{\boldsymbol{x}}_1 + \tilde{\boldsymbol{x}}_2^{\mathrm{T}}\mathcal{R}_2\tilde{\boldsymbol{x}}_2, \\ \tilde{\boldsymbol{x}}_{12}^{\mathrm{T}}\boldsymbol{b}_{12} = \tilde{\boldsymbol{x}}_1^{\mathrm{T}}\boldsymbol{b}_1 + \tilde{\boldsymbol{x}}_2^{\mathrm{T}}\boldsymbol{b}_2,\end{cases} \tag{3.11}$$

from (3.8).

### 3.2.2 Series connection

Fig. 3.3(b) is the schematic of the outputs connected in series. In this configuration, both loads have the identical current flow. The converters interact through the voltage $w'$, which represents the voltage imbalance among the outputs. Therefore, we have

$$\tilde{i}_1 = \tilde{i}_2,\ w_1 = -w_2, \tag{3.12}$$

where $w_1$ and $w_2$ indicates the voltage interaction for converters #1 and #2, respectively. Also from the voltage law,

$$w_1 = \tilde{v}_1 - R_1\tilde{i}_1,\ w_2 = \tilde{v}_2 - R_2\tilde{i}_2, \tag{3.13}$$

is obtained. Then, the load current is

$$\tilde{i}_1 = \tilde{i}_2 = \frac{\tilde{v}_1 + \tilde{v}_2}{R_1 + R_2}, \tag{3.14}$$

from (3.12) and (3.13).

Since Fig. 3.3(b) corresponds to the series interaction shown in Fig. 3.2(a), we have

$$\begin{cases} \tilde{\boldsymbol{x}}_1^{\mathrm{T}} \mathcal{R}_1 \tilde{\boldsymbol{x}}_1 = \dfrac{\tilde{v}_1{}^2}{R_1}, \ \tilde{\boldsymbol{x}}_2^{\mathrm{T}} \mathcal{R}_2 \tilde{\boldsymbol{x}}_2 = \dfrac{\tilde{v}_2{}^2}{R_2}, \\ \tilde{\boldsymbol{x}}_1^{\mathrm{T}} \boldsymbol{b}_1 = \dfrac{\tilde{v}_1 w_1}{R_1}, \ \tilde{\boldsymbol{x}}_2^{\mathrm{T}} \boldsymbol{b}_2 = \dfrac{\tilde{v}_2 w_2}{R_2}, \end{cases} \tag{3.15}$$

from (3.4). Moreover, from (3.13) and (3.14), we have

$$\begin{cases} \tilde{\boldsymbol{x}}_1^{\mathrm{T}} \boldsymbol{b}_1 = \dfrac{\tilde{v}_1{}^2}{R_1} - \dfrac{\tilde{v}_1(\tilde{v}_1 + \tilde{v}_2)}{R_1 + R_2}, \\ \tilde{\boldsymbol{x}}_2^{\mathrm{T}} \boldsymbol{b}_2 = \dfrac{\tilde{v}_2{}^2}{R_2} - \dfrac{\tilde{v}_2(\tilde{v}_1 + \tilde{v}_2)}{R_1 + R_2}. \end{cases} \tag{3.16}$$

Substituting (3.16) to (3.11) results in

$$\begin{aligned} \tilde{\boldsymbol{x}}_{12}^{\mathrm{T}} \boldsymbol{b}_{12} &= \frac{\tilde{v}_1{}^2}{R_1} + \frac{\tilde{v}_2{}^2}{R_2} - \frac{(\tilde{v}_1 + \tilde{v}_2)^2}{R_1 + R_2} \\ &= \tilde{\boldsymbol{x}}_{12}^{\mathrm{T}} \mathcal{R}'_{12} \tilde{\boldsymbol{x}}_{12} - \tilde{\boldsymbol{x}}_{12}^{\mathrm{T}} \mathcal{R}_{\mathrm{s}} \tilde{\boldsymbol{x}}_{12}, \end{aligned} \tag{3.17}$$

by introducing a positive semi-definite matrix $\mathcal{R}_{\mathrm{s}}$ that satisfies

$$\tilde{\boldsymbol{x}}_{12}^{\mathrm{T}} \mathcal{R}_{\mathrm{s}} \tilde{\boldsymbol{x}}_{12} = \frac{(\tilde{v}_1 + \tilde{v}_2)^2}{R_1 + R_2}. \tag{3.18}$$

Hence, we obtain

$$\boldsymbol{b}_{12} = \mathcal{R}'_{12} \tilde{\boldsymbol{x}}_{12} - \mathcal{R}_{\mathrm{s}} \tilde{\boldsymbol{x}}_{12} \tag{3.19}$$

for the series connection in Fig. 3.3(b). From above discussions, we can confirm that the connection at the output replaces the dissipation of the model. Moreover, the introduced dissipation matrix $\mathcal{R}_{\mathrm{s}}$ represents the series connection of the loads.

### 3.2.3 Parallel connection

Similar discussions can be made for the parallel connection. Fig. 3.3(c) is the schematic of the outputs connected in parallel. In this configuration, both loads have identical load

voltage. The current $j'$ implies the interaction between the converters. Therefore, we have

$$\tilde{v}_1 = \tilde{v}_2,\ j_1 = -j_2, \tag{3.20}$$

where $j_1$ and $j_2$ indicates the current interaction for converters #1 and #2, respectively. Also from the current law,

$$j_1 = \tilde{i}_1 - \frac{\tilde{v}_1}{R_1},\ j_2 = \tilde{i}_2 - \frac{\tilde{v}_2}{R_2}, \tag{3.21}$$

is obtained. Then, the load voltage is

$$\tilde{v}_1 = \tilde{v}_2 = \frac{R_1 R_2}{R_1 + R_2}(\tilde{i}_1 + \tilde{i}_2), \tag{3.22}$$

from (3.20) and (3.21).

Since Fig. 3.3(c) corresponds to the series interaction shown in Fig. 3.2(b), we have

$$\begin{cases} \tilde{\boldsymbol{x}}_1^{\mathrm{T}} \mathcal{R}_1 \tilde{\boldsymbol{x}}_1 = R_1 \tilde{i}_1{}^2,\ \tilde{\boldsymbol{x}}_2^{\mathrm{T}} \mathcal{R}_2 \tilde{\boldsymbol{x}}_2 = R_2 \tilde{i}_2{}^2, \\ \tilde{\boldsymbol{x}}_1^{\mathrm{T}} \boldsymbol{b}_1 = R_1 \tilde{i}_1 j_1,\ \tilde{\boldsymbol{x}}_2^{\mathrm{T}} \boldsymbol{b}_2 = R_2 \tilde{i}_2 j_2, \end{cases} \tag{3.23}$$

from (3.5). Moreover, from (3.21) and (3.22), we have

$$\begin{cases} \tilde{\boldsymbol{x}}_1^{\mathrm{T}} \boldsymbol{b}_1 = R_1 \tilde{i}_1{}^2 - \dfrac{R_1 R_2}{R_1 + R_2} \tilde{i}_1 (\tilde{i}_1 + \tilde{i}_2), \\ \tilde{\boldsymbol{x}}_2^{\mathrm{T}} \boldsymbol{b}_2 = R_2 \tilde{i}_2{}^2 - \dfrac{R_1 R_2}{R_1 + R_2} \tilde{i}_2 (\tilde{i}_1 + \tilde{i}_2). \end{cases} \tag{3.24}$$

Substituting (3.24) to (3.11) results in

$$\begin{aligned} \tilde{\boldsymbol{x}}_{12}^{\mathrm{T}} \boldsymbol{b}_{12} &= R_1 \tilde{i}_1{}^2 + R_2 \tilde{i}_2{}^2 - \frac{R_1 R_2}{R_1 + R_2} (\tilde{i}_1 + \tilde{i}_2)^2 \\ &= \tilde{\boldsymbol{x}}_{12}^{\mathrm{T}} \mathcal{R}'_{12} \tilde{\boldsymbol{x}}_{12} - \tilde{\boldsymbol{x}}_{12}^{\mathrm{T}} \mathcal{R}_{\mathrm{p}} \tilde{\boldsymbol{x}}_{12}, \end{aligned} \tag{3.25}$$

by introducing a positive semi-definite matrix $\mathcal{R}_{\mathrm{p}}$ that satisfies

$$\tilde{\boldsymbol{x}}_{12}^{\mathrm{T}} \mathcal{R}_{\mathrm{p}} \tilde{\boldsymbol{x}}_{12} = \frac{R_1 R_2}{R_1 + R_2} (\tilde{i}_1 + \tilde{i}_2)^2. \tag{3.26}$$

Hence, we obtain

$$\boldsymbol{b}_{12} = \mathcal{R}'_{12} \tilde{\boldsymbol{x}}_{12} - \mathcal{R}_{\mathrm{p}} \tilde{\boldsymbol{x}}_{12}, \tag{3.27}$$

for the parallel connection in Fig. 3.3(c).

### 3.2.4 Replacement of dissipation

From (3.19) and (3.27), the external input $\boldsymbol{b}_{12}$ replaces the original dissipation matrix. Thus, it is possible to rewrite the model of (3.7) as

$$\mathcal{A}_{12}\dot{\tilde{\boldsymbol{x}}}_{12} = \{\mathcal{J}_{12}(\boldsymbol{s}_{12}) - \mathcal{R}_{12}\}\tilde{\boldsymbol{x}}_{12} + \tilde{\boldsymbol{g}}_{12}(\boldsymbol{s}_{12})\tilde{\boldsymbol{u}}_{12},\ \mathcal{R}_{12} = \begin{cases} \mathcal{R}_{\rm s} & \text{(series)}, \\ \mathcal{R}_{\rm p} & \text{(parallel)}, \end{cases} \tag{3.28}$$

by substituting (3.19) or (3.27) to (3.7). Here, $\mathcal{R}_{12}$ is equal to $\mathcal{R}_{\rm s}$ or $\mathcal{R}_{\rm p}$ depending on the series or parallel connection at the output. The model (3.28) has the same structure as (2.13), which is the general PCHS of the dc-dc converter. Therefore, we have shown that a pair of dc-dc converters connected in either series or parallel at the output is described in the general form of PCHS.

## 3.3 Output series-parallel connection of $n$ numbers of dc-dc converters

Let us first clarify that the system consisting of $n \in \mathbb{N}$ numbers of converters connected repeatedly in either series or parallel at their outputs to share a single load is defined as output series-paralleled $n$ converters. Fig. 3.4 shows the diagram of the output series-paralleled $n$ converters. The output interaction for this system is also given in series or parallel to the output load, similarly to Fig. 3.2. The single dc-dc converter is included in the definition for the case of $n = 1$.

Suppose, for all $m \in \mathbb{N}$ s.t. $m \leq n$, any output series-paralleled $m$ converters are described by PCHS in (2.13). Consider the natural numbers $\alpha$, $\beta \in \mathbb{N}$ s.t. $\alpha + \beta = n + 1$. Then, a specific output series-paralleled $n + 1$ converters can be described by the model

$$\begin{cases} \mathcal{A}_\alpha\dot{\tilde{\boldsymbol{x}}}_\alpha = \{\mathcal{J}_\alpha(\boldsymbol{s}_\alpha) - \mathcal{R}_\alpha\}\tilde{\boldsymbol{x}}_\alpha + \tilde{\boldsymbol{g}}_\alpha(\boldsymbol{s}_\alpha)\tilde{\boldsymbol{u}}_\alpha + \boldsymbol{b}_\alpha, \\ \mathcal{A}_\beta\dot{\tilde{\boldsymbol{x}}}_\beta = \{\mathcal{J}_\beta(\boldsymbol{s}_\beta) - \mathcal{R}_\beta\}\tilde{\boldsymbol{x}}_\beta + \tilde{\boldsymbol{g}}_\beta(\boldsymbol{s}_\beta)\tilde{\boldsymbol{u}}_\beta + \boldsymbol{b}_\beta. \end{cases} \tag{3.29}$$

The first and the second equations in (3.29) describe the output series-paralleled converters with interactions consisting of $\alpha$ and $\beta$ numbers of converters, respectively. The equations are PCHS and the matrices and variables have the same properties as listed in Table 2.1. Note that (3.29) corresponds to (3.6). In both of these models, the circuit restrictions shown in Fig. 3.3 have to be applied so that the models describe series or parallel connections. Thus, the same discussions as Section 3.2 can be made. Since the

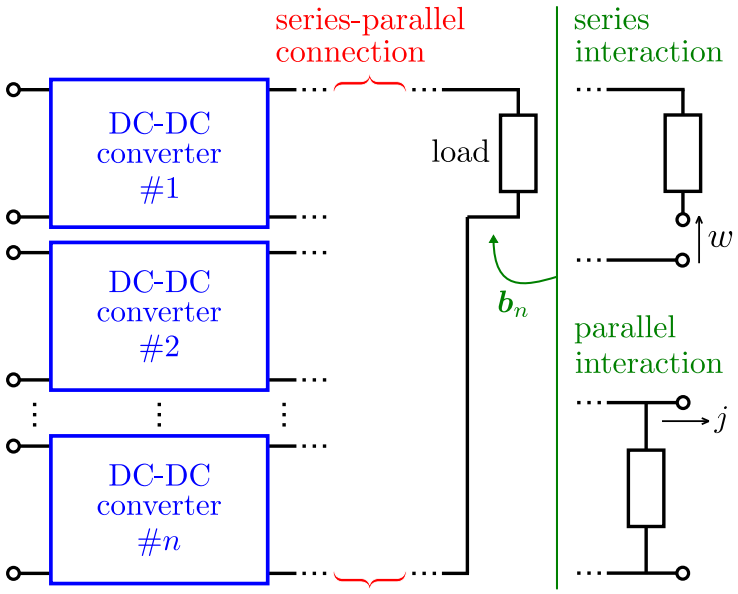


Figure 3.4: Output series-paralleled $n$ converters. © 2021 IEEE

natural numbers $\alpha$ and $\beta$ can be chosen arbitrarily, it concludes that any structure of output series-paralleled $n+1$ converters is described by the general PCHS in (2.13).

In the previous sections, we have already shown for $n = 1, 2$ that the output series-paralleled $n$ converters are described by PCHS in (2.13). This statement can be proved for all $n$ by the mathematical induction based on the above discussions for (3.29). Therefore, we have proved that the output series-paralleled $n$ converters are described by PCHS in (2.13), for $n \in \mathbb{N}$.

## 3.4 Passivity-based control and asymptotic stability

Suppose that the whole output series-paralleled $n$ converters are modeled in PCHS as

$$\mathcal{A}_n \dot{\tilde{\boldsymbol{x}}}_n = \{\mathcal{J}_n(\boldsymbol{s}_n) - \mathcal{R}_n\}\tilde{\boldsymbol{x}}_n + \tilde{\boldsymbol{g}}_n(\boldsymbol{s}_n)\tilde{\boldsymbol{u}}_n. \tag{3.30}$$

Also suppose that they consist of $n$ numbers of single dc-dc converters. Each of these converters can be modeled as PCHS

$$\mathcal{A}_{1.m} \dot{\tilde{\boldsymbol{x}}}_{1.m} = \{\mathcal{J}_{1.m}(\boldsymbol{s}_{1.m}) - \mathcal{R}_{1.m}\}\tilde{\boldsymbol{x}}_{1.m} + \tilde{\boldsymbol{g}}_{1.m}(\boldsymbol{s}_{1.m})\tilde{\boldsymbol{u}}_{1.m}, \tag{3.31}$$

where $m \in \mathbb{N}$ s.t. $m \leq n$. The symbols used in (3.30) and (3.31) follow the definitions for PCHS listed in Table 2.1. The subscript '$1.m$' indicates each single converter consisting the output series-paralleled $n$ converters.

Since (3.30) is written in the general PCHS of (2.13), the condition for the asymptotic stability is given from (2.17) as

$$\tilde{\boldsymbol{x}}_n^{\mathrm{T}} \tilde{\boldsymbol{g}}_n(\boldsymbol{s}_n) \tilde{\boldsymbol{u}}_n < 0, \ \tilde{\boldsymbol{x}}_n \neq 0. \tag{3.32}$$

Note from the previous discussions that the series-parallel connection only alters the dissipative properties of the model. According to (3.8), $\tilde{\boldsymbol{x}}_{1.m}$ and $\tilde{\boldsymbol{u}}_{1.m}$ are combined vertically throughout the series-parallel connection. On the other hand, $\tilde{\boldsymbol{g}}_{1.m}$ is combined diagonally. Thus, we have

$$\begin{cases} \tilde{\boldsymbol{x}}_n = \begin{bmatrix} \tilde{\boldsymbol{x}}_{1.1} \\ \tilde{\boldsymbol{x}}_{1.2} \\ \vdots \\ \tilde{\boldsymbol{x}}_{1.n} \end{bmatrix}, \ \tilde{\boldsymbol{u}}_n = \begin{bmatrix} \tilde{\boldsymbol{u}}_{1.1} \\ \tilde{\boldsymbol{u}}_{1.2} \\ \vdots \\ \tilde{\boldsymbol{u}}_{1.n} \end{bmatrix}, \\ \tilde{\boldsymbol{g}}_n = \begin{bmatrix} \tilde{\boldsymbol{g}}_{1.1} & 0 & \cdots & 0 \\ 0 & \tilde{\boldsymbol{g}}_{1.2} & & \vdots \\ \vdots & & \ddots & 0 \\ 0 & \cdots & 0 & \tilde{\boldsymbol{g}}_{1.n} \end{bmatrix}, \end{cases} \tag{3.33}$$

and accordingly,

$$\tilde{\boldsymbol{x}}_n^{\mathrm{T}} \tilde{\boldsymbol{g}}_n(\boldsymbol{s}_n) \tilde{\boldsymbol{u}}_n = \sum_{m=1}^{n} \tilde{\boldsymbol{x}}_{1.m}^{\mathrm{T}} \tilde{\boldsymbol{g}}_{1.m}(\boldsymbol{s}_{1.m}) \tilde{\boldsymbol{u}}_{1.m}. \tag{3.34}$$

Controlling each converter by PBC gives

$$\tilde{\boldsymbol{x}}_{1.m}^{\mathrm{T}} \tilde{\boldsymbol{g}}_{1.m}(\boldsymbol{s}_{1.m}) \tilde{\boldsymbol{u}}_{1.m} < 0, \ \tilde{\boldsymbol{x}}_{1.m} \neq 0, \tag{3.35}$$

for all $m \leq n$. The condition (3.32) is satisfied by (3.34) and (3.35). Therefore, it is proved that the output series-paralleled $n$ converters are asymptotically stable by the PBC of each converter.

In conclusion of this section, we have proved that output series-paralleled dc-dc converters regulated by PBC maintain their asymptotic stability. Also, throughout the section, we have shown that any structure of output series-paralleled converters is described by PCHS in (2.13). The diversity and scalability of the structure lies in the generality of the discussion. Note that the restrictions made in the discussion were only for the circuit constraints due to the output connection. It implies the robust, diverse, and scalable feature of PBC that the asymptotic stability is not restricted by the circuit topologies, parameters, and steady-states of the series-paralleled converters. The theoretical results are confirmed in the next section by numerical simulation.

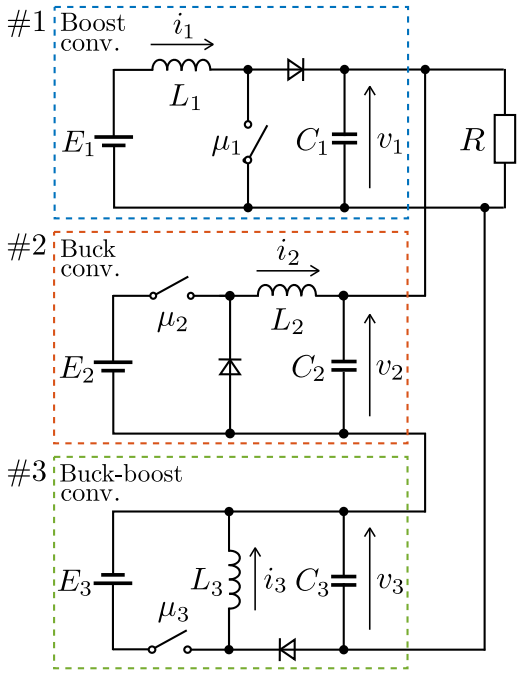


Figure 3.5: Boost, buck, and buck-boost converters connected in series-parallel at the output. © 2021 IEEE

## 3.5 Numerical simulation

In this section, the PBC of the output series-paralleled converters is examined based on numerical simulation using MATLAB/Simulink 2020b.

### 3.5.1 Setups for simulation

The simulated circuit is shown in Fig. 3.5. It is composed of boost, buck, and buck-boost converters. The subscripts '1', '2', and '3', correspond to the boost, buck, and buck-boost converter, respectively. This circuit configuration was chosen to demonstrate the minimum series-parallel connection of various converters. The circuit parameters for the simulated circuit are shown in Table 3.1. Here, the parameters are chosen to be diverse. The parameter $k$ is the feedback control gain set for the PBC of each converter. The load resistance is $R = 12\,\Omega$. The switches and the diodes are considered ideal.

As for control, the PBC explained in Section 2.4 are applied to each converter. The duty ratios for the switches of boost, buck, and buck-boost converters are governed by (2.24), (2.28), and (2.32), respectively. The calculated duty ratios are converted to the switching signal by PWM at 1 MHz. The sampling frequency of the state variables is also

Table 3.1: Parameters of dc-dc converters. © 2021 IEEE

| #1 Boost | | #2 Buck | | #3 Buck-boost | |
|---|---|---|---|---|---|
| Parameter | Values | Parameter | Values | Parameter | Values |
| $L_1$ | $470\,\mu$H | $L_2$ | $500\,\mu$H | $L_3$ | $330\,\mu$H |
| $C_1$ | $10\,\mu$F | $C_2$ | $33\,\mu$F | $C_3$ | $20\,\mu$F |
| $E_1$ | 18 V | $E_2$ | 40 V | $E_3$ | 24 V |
| $k_1$ | 0.02 | $k_2$ | 0.3 | $k_3$ | 0.02 |

Table 3.2: Initial state of dc-dc converters. © 2021 IEEE

| #1 Boost | | #2 Buck | | #3 Buck-boost | |
|---|---|---|---|---|---|
| Variable | State | Variable | State | Variable | State |
| $i_1$ | 1.4 A | $i_2$ | 1.3 A | $i_3$ | 2.8 A |
| $v_1$ | 10 V | $v_2$ | 16 V | $v_3$ | 12 V |

Table 3.3: Desired state of dc-dc converters. © 2021 IEEE

| #1 Boost | | #2 Buck | | #3 Buck-boost | |
|---|---|---|---|---|---|
| Variable | State | Variable | State | Variable | State |
| $i_{1\mathrm{d}}$ | 1.950 A | $i_{2\mathrm{d}}$ | 2.025 A | $i_{3\mathrm{d}}$ | 3.375 A |
| $v_{1\mathrm{d}}$ | 36 V | $v_{2\mathrm{d}}$ | 20 V | $v_{3\mathrm{d}}$ | 16 V |
| $\mu_{1\mathrm{d}}$ | 0.5 | $\mu_{2\mathrm{d}}$ | 0.5 | $\mu_{3\mathrm{d}}$ | 0.4 |

set at 1 MHz, and the calculation of the duty ratios is executed instantly. The feedback control scheme follows the schematic diagram shown in Fig. 2.2.

The initial state and the desired state of the simulated circuit are given in Table 3.2 and Table 3.3, respectively. The desired state is determined for the converters to have various voltage, current, and power levels at the steady-state. In the simulation, we first consider the case that there is no disturbance in the system, to confirm the asymptotic stability numerically. Then, we also consider the cases that there are perturbations or fluctuations at the input voltage source or the output load, in order to examine the robustness of the proposed control method. These simulation scenarios are based on the previous works in [43, 44].

### 3.5.2 Simulation without disturbance

The simulated waveforms of the output series-paralleled converters in the ideal case are shown in Fig. 3.6. It can be seen from Fig. 3.6 that the waveforms converge to the

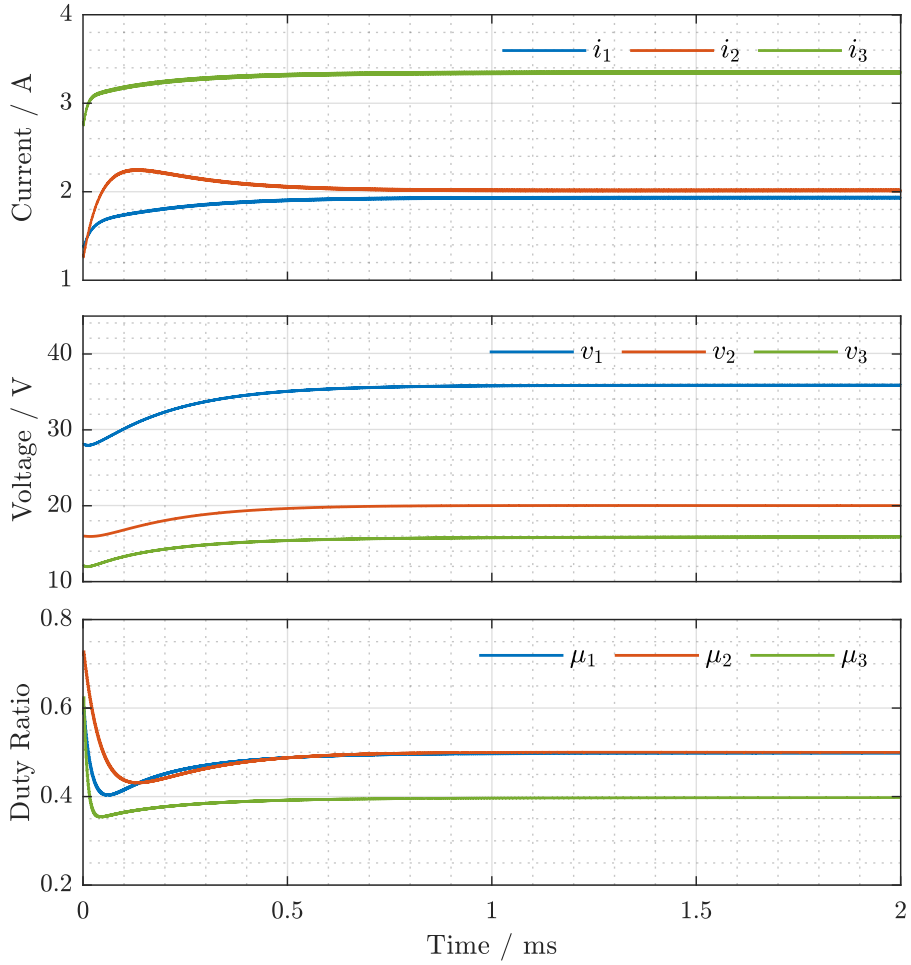


Figure 3.6: Numerical waveforms of output series-paralleled converters for the ideal case with no disturbances. © 2021 IEEE

desired state shown in Table 3.3. Therefore, PBC was numerically confirmed to achieve the asymptotic stability of the series-paralleled boost, buck, and buck-boost converters. It was also confirmed that the diversity in each converter did not violate the asymptotic stability. This implies the feature of PBC that it allows the diverse voltage, current, and power levels among various circuit parameters in the series-parallel connection.

### 3.5.3 Perturbation at input voltage source

For this simulation, a stochastic perturbation that follows a normal distribution was added to the input voltage sources $E_1$, $E_2$, and $E_3$. The maximum peak-to-peak magnitude of the perturbation was chosen to be approximately 10 V. This is 55.6 %, 41.7 %,

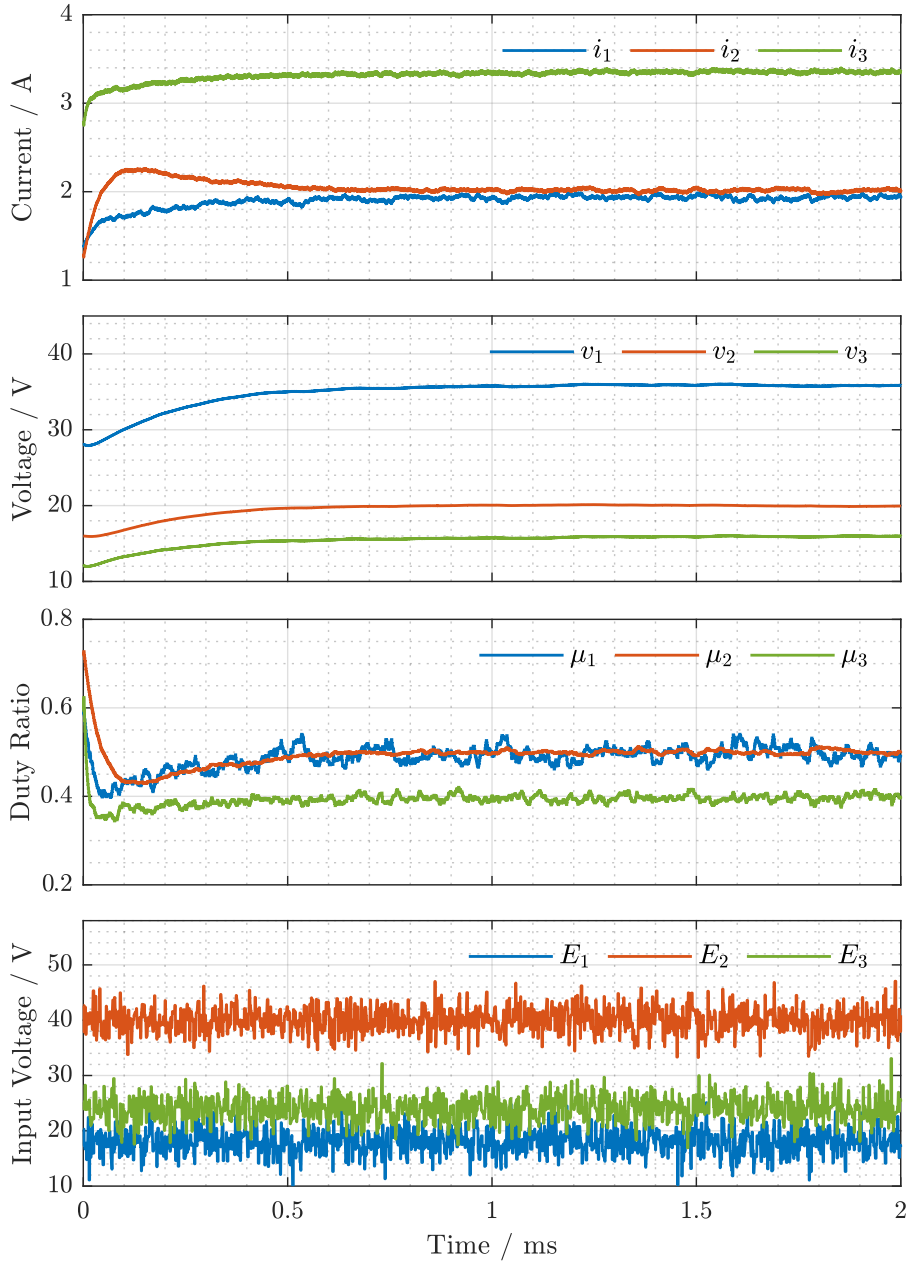


Figure 3.7: Numerical waveforms of output series-paralleled converters with random perturbation input. © 2021 IEEE

and 25.0 % of the values of $E_1$, $E_2$, and $E_3$, respectively.

Fig. 3.7 shows the simulated waveforms of the output series-paralleled converters with the perturbation inputs. The bottom graph shows the perturbed input voltage. As can be seen, the proposed PBC achieves the stability of the system around the desired state of Table 3.3. The instantaneous errors of the input currents and the output voltages from

their desired states are less than 4.1 % and 1.9 %, respectively. The variations of computed duty ratios are within 5.0 % of the total range of the closed interval [0,1]. Hence, the error in the system is found to be significantly reduced compared to the input perturbation. PBC exhibited high robustness with regard to the perturbed inputs. It is worth noting that the low-pass nature of the converter itself also contributes to the reduction of the error as well as the control.

### 3.5.4 Temporary fluctuation of output load

Unknown load resistance variations generally affect the behavior of the closed-loop performance of the controlled converter [44]. In this simulation, temporary fluctuation of the output load resistance $R$ was given. The obtained waveforms are shown in Fig. 3.8. As seen in the bottom graph, the output load resistance temporarily decreases to 70 % of its nominal value. It is confirmed that the PBC restores its asymptotic stability after the change, converging towards the desired state of Table 3.3. The temporary change of the load did not violate the stability nor the proper steady-state operation of the output series-paralleled converters regulated by PBC.

In this section, we numerically confirmed the stability and the robustness of the output series-paralleled converters regulated by PBC. The simulated results showed correspondence to the theoretical discussions in that PBC achieved the stabilization of output series-paralleled converters with various circuit topologies, parameters, and steady-states. The robustness of the proposed control was also examined through the perturbations. Although the obtained waveforms highly depend on the settings of the circuit parameters, desired states, and disturbances, the overall features of stability and robustness are likely to remain widely, since our consideration does not require any specific settings of the system. These features correspond to the experimental result in [82], where PBC was shown to asymptotically stabilize the paralleled boost and buck converters with various parameters and steady-states.

## 3.6 Summary

In this chapter, we examined the asymptotic stability of the output series-paralleled dc-dc converters regulated by PBC. We introduced the dc-dc converter model with the additional variable representing the output interaction to describe the series-parallel con-

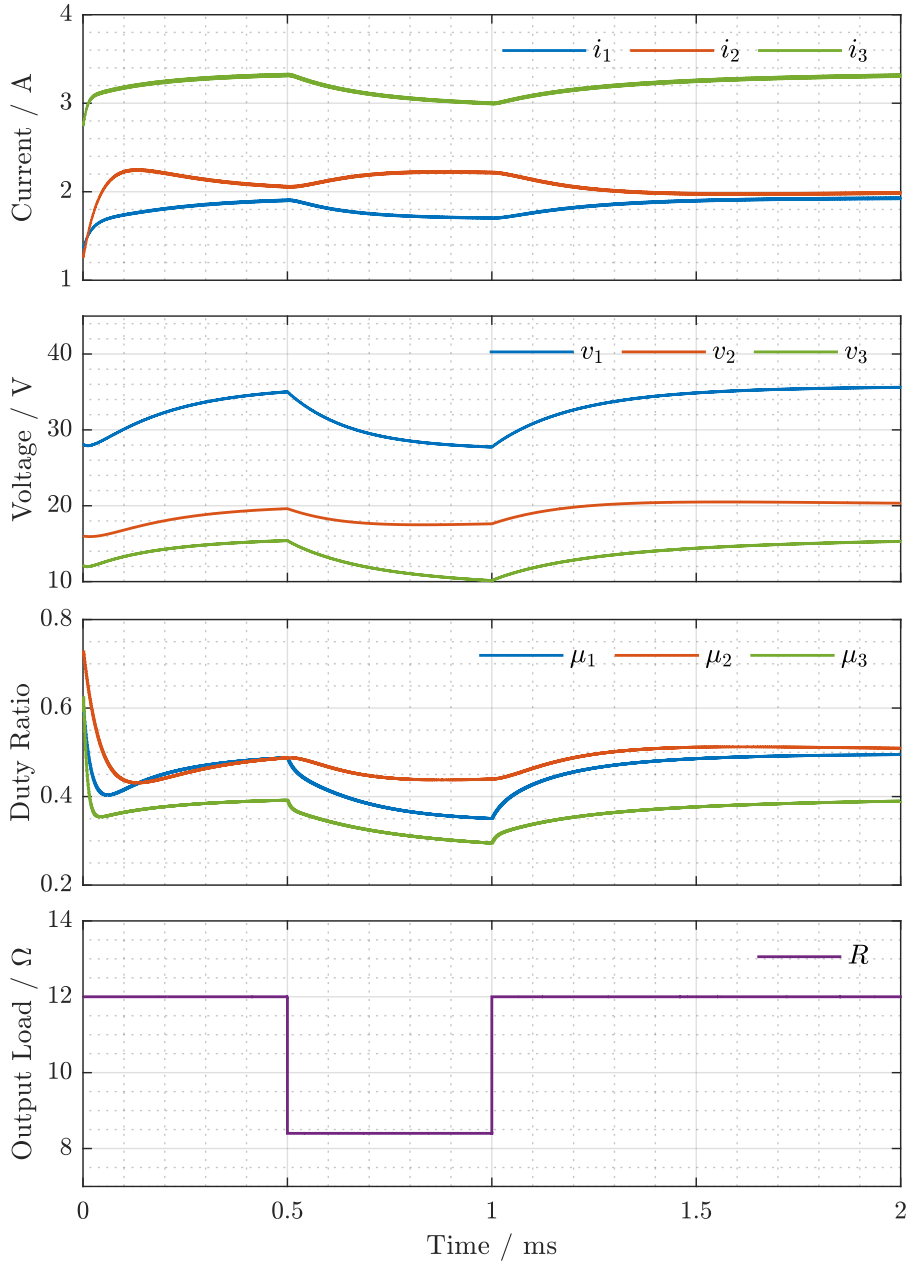


Figure 3.8: Numerical waveforms of output series-paralleled converters with temporary load fluctuation. © 2021 IEEE

nection of the converters. Then, the output series-paralleled converters were shown to be reclassified into the general dc-dc converter model. This feature enabled us to discuss the asymptotic stability of the series-paralleled converters based on the condition obtained from the general converter model. Consequently, the converters regulated by PBC were proven to maintain their stability at the output series-parallel connection. The theoretical

result was verified in the numerical simulation of series-paralleled boost, buck, and buck-boost converters. The stable and robust features of the proposed control were confirmed in the simulation. PBC allowed diverse circuit topologies, parameters, and steady-states of the output series-paralleled dc-dc converters. This contribution is able to theoretically support the previous numerical and experimental studies [63, 82] for the series-paralleled converters regulated by PBC, justifying the further extension of the system.

# Chapter 4

# Passivity-based control of parallel connected boost and buck converters

This chapter discusses the parallelization of boost and buck converters regulated by PBC. The PBC law derived in Section 2.4 is applied to each converter individually to achieve the asymptotic stability of the system. The steady-state ripple and error characteristics as well as time constants of the paralleled converters are discussed considering their dependency on the feedback gains. The feedback gain settings in the experiment are determined based on these numerical results. Moreover, the numerical results are confirmed to coincide with the results of the experiment.

The chapter is organized as follows. We will first analytically show that the individual PBC assures the whole parallel connected system to be asymptotically stable. Then, numerical simulation is provided to analyze the dependence of circuit characteristics on the feedback gain settings of PBC. Lastly, we have experimental confirmation.

## 4.1 Parallel connected boost and buck converters

Figure 4.1 is a schematic circuit of parallel connected boost and buck converters. The converters are sharing a load at the output. Each converter consists of voltage source $E$, inductance $L$, capacitance $C$, switch $u$, and diode $D$. Here, $i$ denotes the inductor current and $v$ the capacitor voltage. The subscripts '1' and '2' correspond to converter #1 (boost converter) and converter #2 (buck converter), respectively. Note that all circuit elements mentioned in this section are ideal.

The Kirchhoff's laws give the differential equations of the parallelized circuit shown

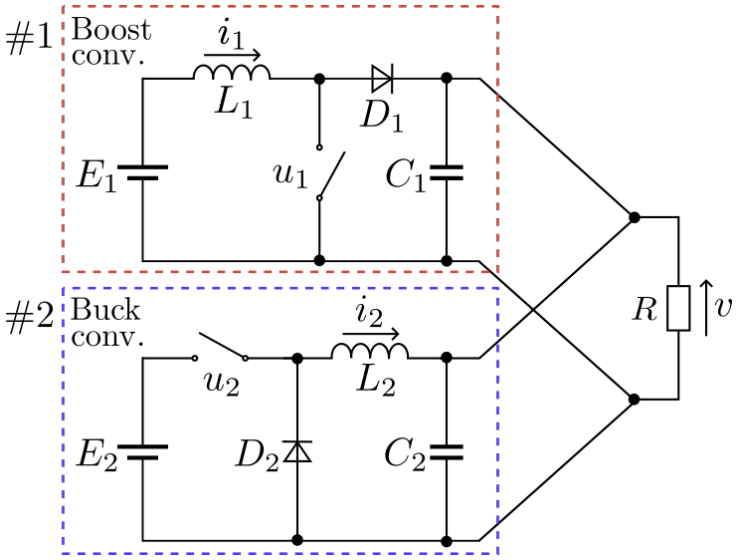


Figure 4.1: Schematic circuit of parallel connected boost and buck converters. © 2020 IEICE

in Fig. 4.1 as

$$\begin{cases} L_1\dot{i}_1 = -(1-u_1)v + E_1, \\ L_2\dot{i}_2 = -v + u_2E_2, \\ C_{12}\dot{v} = (1-u_1)i_1 + i_2 - \dfrac{v}{R}, \end{cases} \tag{4.1}$$

where $C_{12} = C_1 + C_2$. The dot $(\dot{})$ on the variable is a notation for time differentiation. The system is discontinuous with the switching variables $u_1, u_2 \in \{0, 1\}$, switching the system structure. Regulation of power converters implies switching operation, which corresponds to the switching variables $u_1$ and $u_2$.

Assuming a sufficiently high-frequency switching operation, the state-averaging model of DC-DC converters is obtained [43, 45]. By averaging (4.1), we obtain

$$\begin{cases} L_1\dot{i}_1 = -(1-\mu_1)v + E_1, \\ L_2\dot{i}_2 = -v + \mu_2E_2, \\ C_{12}\dot{v} = (1-\mu_1)i_1 + i_2 - \dfrac{v}{R}. \end{cases} \tag{4.2}$$

The switching variables $u_1, u_2$ are replaced with duty ratios $\mu_1, \mu_2 \in [0, 1]$. Here, we are able to see that (4.2) has the form of PCHS in (2.4).

The control objective would be to obtain the asymptotical stability at the desired state $[i_1,\, i_2,\, v] = [i_{1\mathrm{d}},\, i_{2\mathrm{d}},\, v_{\mathrm{d}}]$ by modifying the duty ratios $\mu_1$ and $\mu_2$. Null curve of (4.2)

is obtained as

$$\begin{cases} \mu_1 = 1 - \dfrac{E_1}{v}, \\ \mu_2 = \dfrac{v}{E_2}, \\ E_1 i_1 + \mu_2 E_2 i_2 = \dfrac{v^2}{R}. \end{cases} \tag{4.3}$$

The desired state $[i_1\, i_2\, v] = [i_{1\mathrm{d}}\, i_{2\mathrm{d}}\, v_\mathrm{d}]$ must be chosen to satisfy (4.3). The steady-state implies that all input energy is consumed at the load, and a specific duty ratio will be chosen for a specific output voltage. Thus the desired duty ratios become

$$\begin{cases} \mu_{1\mathrm{d}} = 1 - \dfrac{E_1}{v_\mathrm{d}}, \\ \mu_{2\mathrm{d}} = \dfrac{v_\mathrm{d}}{E_2}, \end{cases} \tag{4.4}$$

which correspond to the desired output voltage $v_\mathrm{d}$.

According to Section 4.2, PBC law for each individual converter is given by

$$\begin{cases} \mu_1 = \mu_{1\mathrm{d}} - k_1(v_\mathrm{d} i_1 - v i_{1\mathrm{d}}) & (k_1 > 0), \\ \mu_2 = \mu_{2\mathrm{d}} - k_2(i_2 - i_{2\mathrm{d}}) & (k_2 > 0). \end{cases} \tag{4.5}$$

The storage functions for each converter are

$$\begin{cases} \mathcal{H}_1(i_1,\, v) = \dfrac{1}{2} L_1 (i_1 - i_{1\mathrm{d}})^2 + \dfrac{1}{2} C_1 (v - v_\mathrm{d})^2, \\ \mathcal{H}_2(i_2,\, v) = \dfrac{1}{2} L_2 (i_2 - i_{2\mathrm{d}})^2 + \dfrac{1}{2} C_2 (v - v_\mathrm{d})^2. \end{cases} \tag{4.6}$$

Then, the storage function $\mathcal{H}_{12}$ for the whole system is their summation

$$\begin{aligned} &\mathcal{H}_{12}(i_1,\, i_2,\, v) = \mathcal{H}_1(i_1,\, v) + \mathcal{H}_2(i_2,\, v) \\ &= \frac{1}{2} L_1 (i_1 - i_{1\mathrm{d}})^2 + \frac{1}{2} L_2 (i_2 - i_{2\mathrm{d}})^2 + \frac{1}{2} C_{12} (v - v_\mathrm{d})^2. \end{aligned} \tag{4.7}$$

Differentiating the storage function gives

$$\begin{aligned} \frac{\mathrm{d}\mathcal{H}_{12}}{\mathrm{d}t} =& \frac{\partial \mathcal{H}_{12}}{\partial i_1} \frac{\mathrm{d}i_1}{\mathrm{d}t} + \frac{\partial \mathcal{H}_{12}}{\partial i_2} \frac{\mathrm{d}i_2}{\mathrm{d}t} + \frac{\partial \mathcal{H}_{12}}{\partial v} \frac{\mathrm{d}v}{\mathrm{d}t} \\ =& (\mu_1 - \mu_{1\mathrm{d}})\,(v_\mathrm{d} i_1 - v i_{1\mathrm{d}}) + (\mu_2 - \mu_{2\mathrm{d}})\, E (i_2 - i_{2\mathrm{d}}) - \frac{(v - v_\mathrm{d})^2}{R}. \end{aligned} \tag{4.8}$$

By applying the control law (4.5), we obtain

$$\frac{\mathrm{d}\mathcal{H}_{12}}{\mathrm{d}t} = -k_1(v_\mathrm{d} i_1 - v i_{1\mathrm{d}})^2 - k_2 E(i_2 - i_{2\mathrm{d}})^2 - \frac{(v - v_\mathrm{d})^2}{R}, \tag{4.9}$$

which implies that $\mathcal{H}_{12}$ decreases monotonically. Therefore, the storage function $\mathcal{H}_{12}$ is a candidate for the Lyapunov function of the paralleled system. It ensures the asymptotic stability around $[i_1\, i_2\, v] = [i_{1\mathrm{d}}\, i_{2\mathrm{d}}\, v_\mathrm{d}]$.

The above discussion has analytically shown that individual application of PBC to each converter stabilizes the paralleled system. This is due to the fact that passivity is kept throughout the parallel connection. Also, this result clearly coincides with the theoretical result in Chapter 3. Note that the discussions made in this section are based on ideal circuit elements. Hence, we must take the nonideality into account when we apply these control laws to the practical converters.

## 4.2 Numerical simulation

In this section, we will numerically examine the characteristics of the paralleled converters regulated PBC. The result focuses on the dependence of the circuit characteristics on control gains $k_1$ and $k_2$, which govern both the steady-state and the transient of the system.

### 4.2.1 Setups of simulation

In the simulation, the circuit is modeled using MATLAB/SIMULINK 2020b. Here, we introduce the parameters of circuit elements listed in Table 4.1. Those resistances are all parasitic resistances except for the load $R$ and are considered to be connected in series to each element. They correspond to the products used in the experimental circuit.

The duty ratios $\mu_1$ and $\mu_2$ for each converter are estimated by (4.5) as continuous variables. The switches, however, have discrete on and off states. Therefore we must have an A/D conversion method maintaining the calculated on and off ratio. PWM is widely used due to its simplicity and easy implementation. However, according to the increase in switching frequency, it must require a significantly fast clock speed of the controller to maintain its resolution of the pulse width. Therefore, we adopt a pulse density modulation, from the expectation of increased switching speed. One of the modulations is $\Delta\Sigma$ modulation [83, 84]. Substituting $\Delta\Sigma$ modulation, the averaged characteristics

Table 4.1: Circuit elements and parameters. © 2020 IEICE

| Element | Product | Values |
|---|---|---|
| Inductance $L_1$ | Murata 1447440C | 470 $\mu$H, 125 m$\Omega$ |
| Inductance $L_2$ | Wurth Elektronik 744137 | 630 $\mu$H, 175 m$\Omega$ |
| Capacitance $C_1$ | CL21-DC250V106 | 10 $\mu$F |
| Capacitance $C_2$ | Panasonic ECQE2475KF | 4.7 $\mu$F |
| Voltage source $E_1$ | Matsusada P4K18-2 | 9 V |
| Voltage source $E_2$ | Matsusada P4K36-1 | 36 V |
| Load $R$ | 0-1614782-1 100RK $\times$ 2 | 50 $\Omega$ |
| Switches | ROHM SCT2450KE | 450 m$\Omega$ |
| Diodes | ROHM SCS206AMC | 100 m$\Omega$ |

Table 4.2: Initial desired state. © 2020 IEICE

| $v_{\mathrm{d}}$ | $i_{1\mathrm{d}}$ | $i_{2\mathrm{d}}$ | $\mu_{1\mathrm{d}}$ | $\mu_{2\mathrm{d}}$ |
|---|---|---|---|---|
| 18 V | 0.235 A | 0.252 A | 0.535 | 0.518 |

Table 4.3: Modified desired state. © 2020 IEICE

| $v_{\mathrm{d}}$ | $i_{1\mathrm{d}}$ | $i_{2\mathrm{d}}$ | $\mu_{1\mathrm{d}}$ | $\mu_{2\mathrm{d}}$ |
|---|---|---|---|---|
| 18 V | 0.548 A | 0.108 A | 0.535 | 0.518 |

of dc-dc converters are kept at sufficiently large frequency [76, 85, 86]. In the following simulation, the pulse width is fixed at 1 $\mu$s for both converters.

With the aforementioned circuit and controller settings, we consider the supplied power adjustment. While the desired output voltage stays unchanged, the desired input current of each converter is modified. The target is set initially as shown in Table 4.2. At the instance $t = 0$, we will give a step-like change to the target to be shown in Table 4.3, which is chosen not to alter the power consumption of the whole system.

The elements we have used in the simulation are nonideal, which makes it difficult for us to obtain the exact values of the steady-state. Here, we have considered exclusively the diode's voltage drop $v_{\mathrm{on}}\,(= 1.35\,\mathrm{V})$ and its power consumption. Hence, the target

depends on the relationship

$$\begin{cases} \mu_{1\mathrm{d}} = 1 - \dfrac{E_1}{v_\mathrm{d} + v_\mathrm{on}}, \\ \mu_{2\mathrm{d}} = \dfrac{v_\mathrm{d} + v_\mathrm{on}}{E_2 + v_\mathrm{on}}, \\ E_1 i_{1\mathrm{d}} + \mu_{2\mathrm{d}} E_2 i_{2\mathrm{d}} = \dfrac{{v_\mathrm{d}}^2}{R} + (1 - \mu_{1\mathrm{d}}) v_\mathrm{on} i_{1\mathrm{d}} + (1 - \mu_{2\mathrm{d}}) v_\mathrm{on} i_{2\mathrm{d}}. \end{cases} \tag{4.10}$$

However, they do not exactly describe the steady-state, since the inner resistances are out of consideration. Therefore, the steady-state errors remain. In particular, the desired state with an extremely high boost ratio leads to significant errors due to the inner resistances with large power consumption. In this case, the error cannot be compensated by the feedback control. The decision of the desired state is restricted to have sufficiently low inner power consumption.

### 4.2.2 Simulation results

The steady-state characteristics are shown in Figs. 4.3 and 4.4. Here, the steady-state ripple and the errors of input currents and output voltage are evaluated. Subscripts 'r' and 'e' stand for ripple and steady-state error, respectively. The ripple is the amplitude of fluctuating ac component in the rectified dc output. The steady-state error is the difference between the desired value and the actual value of a system when the response has reached the steady-state.

In Figs. 4.2(a) and (b), there appear large ripples when feedback gains are set higher than a certain threshold. It is caused by high gain settings which makes the ripple be fed unnecessarily to the feedback controller. Also, in Fig. 4.2(a), the contours are almost parallel to $k_2$ axis. It means that the ripple of $i_1$ is independent of $k_2$. A similar feature can be seen in Fig. 4.2(b). The ripple of $i_2$ is independent of $k_1$. Each gain setting should be set less than its threshold in order to avoid large ripples. The thresholds can be obtained individually because the ripple characteristics were independent.

Figures 4.2(c) and (d) show the steady-state error depending on the feedback gains. It is shown that the errors become significantly large at a small gain region in which the effect of feedback control is exceedingly reduced. If one of the feedback gains is set sufficiently high, then both steady-state errors can be restricted significantly. This is due to the load-sharing between the converters. The gains, set larger than the thresholds, cannot keep the error lower due to the saturation of duty ratios and large ripples. The

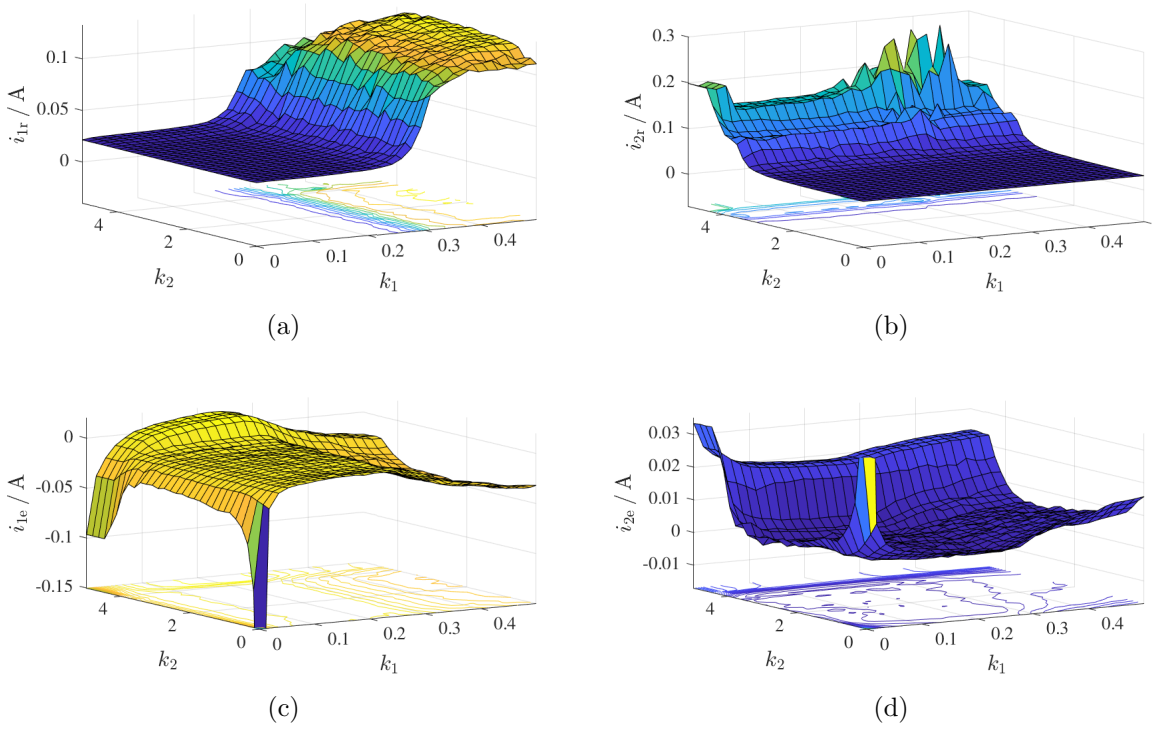


Figure 4.2: steady-state current characteristics with regards to $k_1$ and $k_2$. (a) Ripple characteristics of boost converter input current $i_1$. (b) Ripple characteristics of buck converter input current $i_2$. (c) Steady-state error of input current boost converter $i_1$. (d) Steady-state error of buck converter input current $i_2$. 

above discussions insist that the gains are limited in a range for appropriate steady-state operation.

In Fig. 4.3, steady-state characteristics of the output voltage are shown. Fig. 4.3(a) is similar to Fig. 4.2(a). The threshold seen in both figures has almost no difference. It is because the boost converter is more sensitive to output noise than the buck converter. Fig. 4.3(b) shows a flat surface in the center. This portion corresponds to the appropriate gain settings seen in Fig. 4.2. It is confirmed that the ripple and error characteristics of output voltage and input currents are related.

Figure 4.4 shows the time constant $\tau$ of the system. Here, $\tau$ is defined as the estimated duration of $\mathcal{H}_{12}$ to be 1/e of the initial value. The constant e is the Napier's constant. In the figure, the larger gains are set, the smaller $\tau$ appears. However, it saturates due to the limit of duty ratio from 0 to 1. In addition, the contours are almost parallel to one of the axes. It implies that the time constant of converters is independent of each

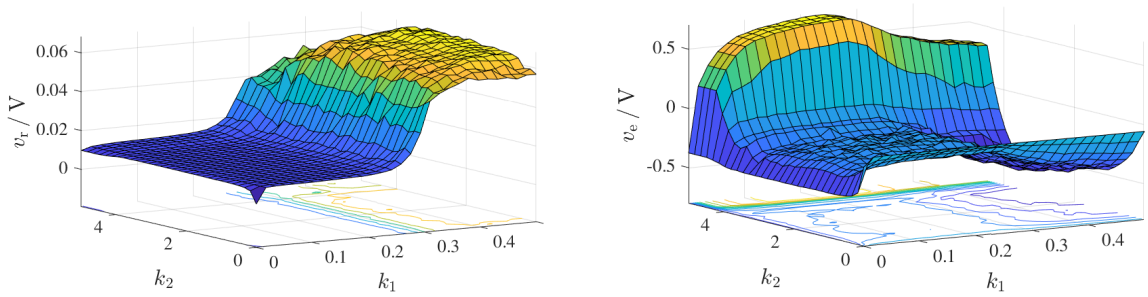


(a) (b)

Figure 4.3: Steady-state voltage characteristics with regards to $k_1$ and $k_2$. (a) Ripple characteristics of output voltage $v$. (b) Steady-state error of output voltage $v$. © 2020 IEICE

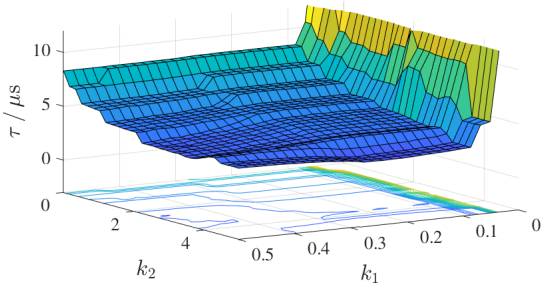


Figure 4.4: Surface of time constant $\tau$ with regards to $k_1$ and $k_2$. © 2020 IEICE

other. The time constant of the whole system is governed by the slower of the two. These characteristics assure the extension of parallelization into multiple converters.

Figure 4.5 shows the transient waveforms of $i_1$ and $i_2$ for some couples of $k_1$ and $k_2$. In Fig. 4.5(a), it is shown that the time for the convergence of $i_1$ is almost independent of $k_2$. It corresponds to the results in Fig. 4.2. The same feature can be seen in Fig. 4.5(b). In addition, it is confirmed that large gain settings lead to significantly large ripples.

In summary, we have discussed the characteristics of the parallelized system governed by the gains $k_1$ and $k_2$. The simulation concludes that both the steady-state and transient characteristics of paralleled converters keep independent. The feedback gains of each converter is able to be determined independently by setting it at the highest possible value that is less than the ripple threshold. This knowledge is applied to the design of paralleled converter systems. In the next section, the parameter in the region will be examined in experiments.

Note that these results are obtained for a fixed circuit parameter and the desired

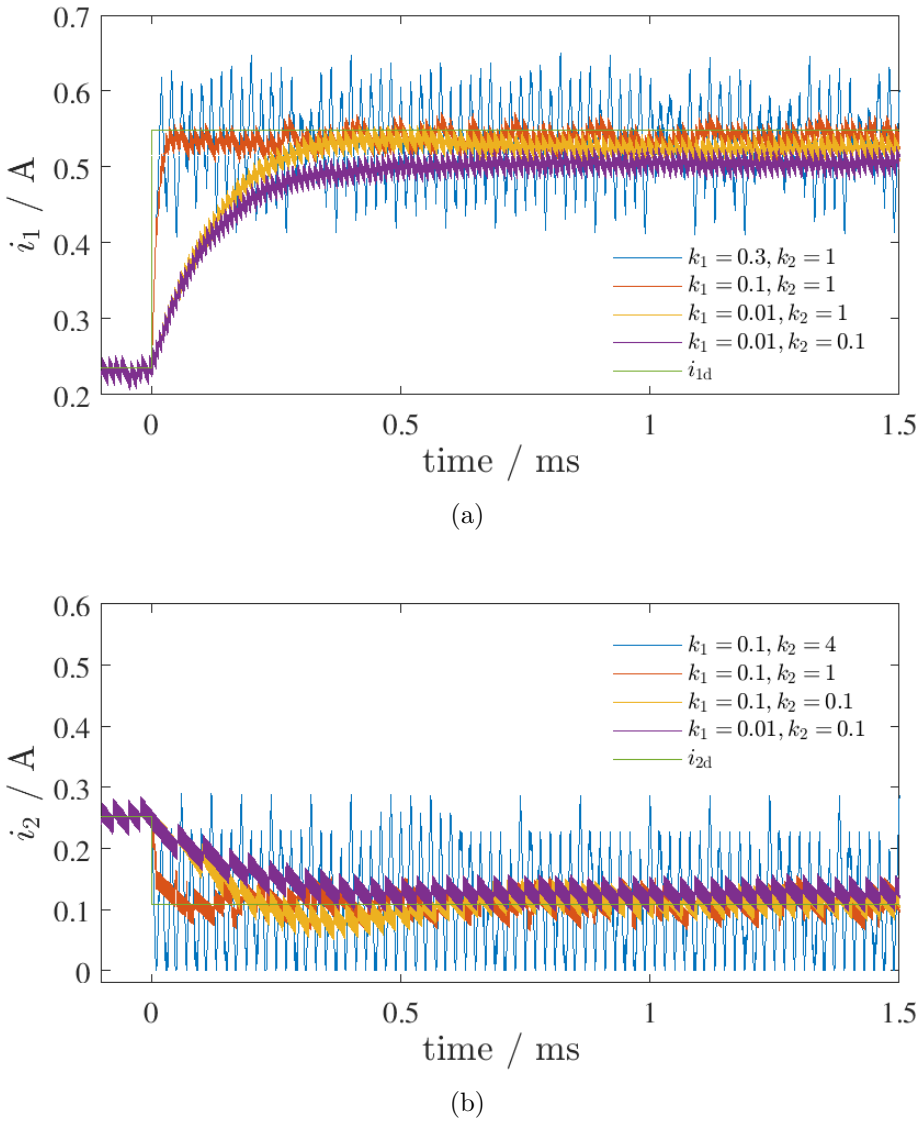


Figure 4.5: Transient waveform of input currents. (a) Boost converter. (b) Buck converter.


state. The region of the feedback gains for a valid converter operation definitely depends on the circuit parameters and the desired states. Though they are not examined here, it is expected that they have a region for achieving similar results. From the numerical results and discussions in this section, it is anticipated that the region of the circuit parameters and the desired states have a relationship, particularly to internal power consumption and output capacitance.

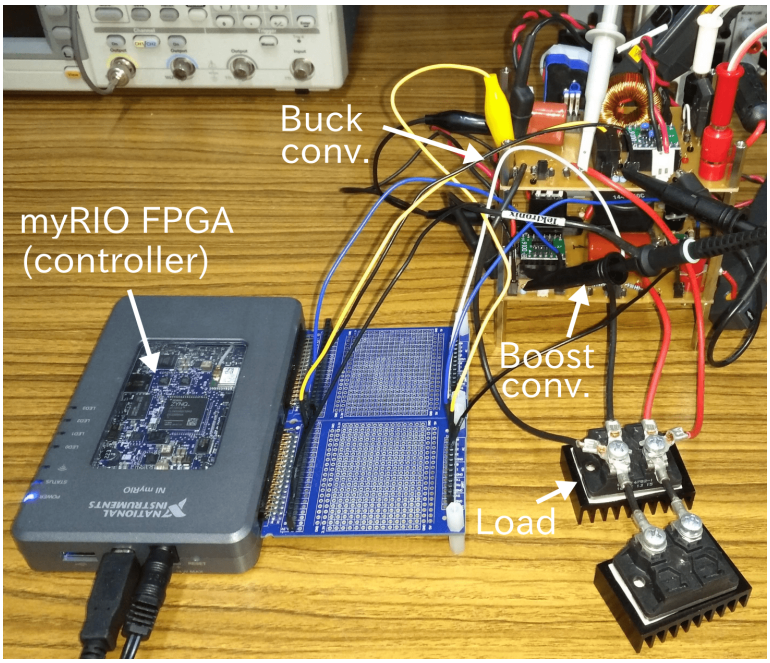


Figure 4.6: Photo of the experimental system. © 2020 IEICE

## 4.3 Experimental verification

In this section, the experimental results of the parallel connected system are shown. Supplied power is adjusted corresponding to the simulation. The target states are adopted as shown in Tables 4.2 and 4.3.

### 4.3.1 Settings of experiment

Figure 4.7 shows the photo of the experimental system. The parallel connected boost and buck converters are implemented with elements shown in Table 4.1. Here, current sensors are adopted to measure the inductor currents of converters. They are Analog Devices LTC6102 for the boost converter and LEM LTS6-NP for the buck converter. The measured currents are applied for feedback control. Furthermore, the main switches of the converters are driven by the gate driver Silicon Labs SI823BB.

In the experiment, myRIO FPGA is used as the controller to calculate the duty ratio and generate the switching signal. The duty ratio is calculated according to (4.5). The feedback gains are set at $k_1 = 0.03$ and $k_2 = 1$ based on the results in Section 4.2. The switching signal is generated based on the duty ratio by $\Delta\Sigma$ modulation, which is applied to the gate driver.

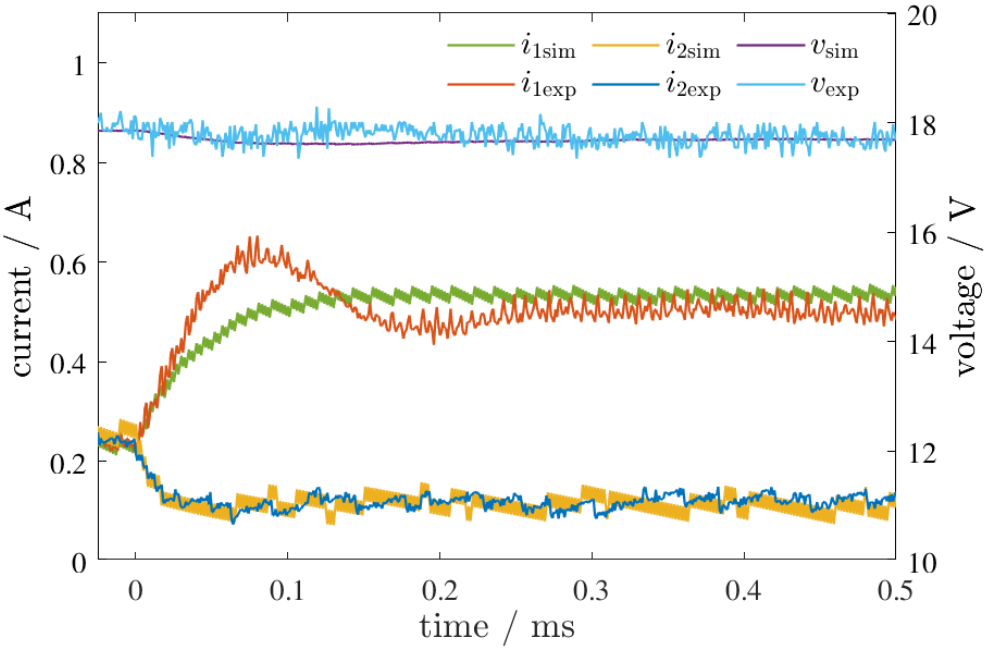


Figure 4.7: Experimental and numerical result of parallel connected converters. © 2020 IEICE

### 4.3.2 Experimental results

Both the experimental and numerical results are shown in Fig. 4.7 for comparison. The waveforms of $i_1$, $i_2$, and $v$ are obtained both experimentally and numerically for the setting explained above. The subscription 'sim' and 'exp' stand for simulation and experiment, respectively.

First of all, it is confirmed that the experimental system becomes asymptotically stable at the steady-state. The steady-state well coincides with the simulation after the adjustment of input power. Current $i_1$ shows a larger error at steady-state. It is found to be caused by parasitic resistances and low gain settings.

At the transient, the experimentally obtained $i_1$ shows overshoots in waveforms, which are not observed in the corresponding simulation. This is likely to be due to the sensor characteristics. The quick response time or the low-pass characteristics of the sensor may possibly cause overshoots or even instability with large gain settings. The low gain setting was appropriate. In order to avoid this conflict, a sufficiently quick response is requested for the sensors.

On the other hand, buck converter current $i_2$ showed a good coincidence of simulation

and experimental results. This clearly shows the independent characteristics, in that the overshoot of $i_1$ did not affect the transient of $i_2$. The experimental result also showed that their transient waveforms are governed by their individual time constant.

The simulation and experimental results of output voltage $v$ also well coincide. During the transient, $v$ almost shows no fluctuation from the steady-state, due to sufficient output capacitance. Therefore, the interaction among the converters is reduced since the interconnection between the converters is limited. The independency of the converters are achieved from the circuit parameters as well as the control technique.

## 4.4 Summary

The parallel connection of boost and buck converters and their PBC were examined numerically and experimentally. Individual application of PBC to the boost and buck converters achieved asymptotic stabilization of the paralleled system. Through numerical simulation, the dependence on the feedback gains was investigated in terms of ripple characteristics, error characteristics, and time constant. It was concluded that the gain settings were found for steady-state operation. It was also confirmed that each converter had independent characteristics. Therefore, the feedback gain settings were able to be determined individually. Stability and independent characteristics were also confirmed through the experiment. These results enable the design for more diverse parallelization of converters by PBC.

# Chapter 5

# Power management of series-parallel connected dc-dc converter system by passivity-based control

In this chapter, a power management method of series-parallel connected converters using PBC is examined. Power management refers to the regulation of power supply ratio among series-paralleled converters in response to changes in load and target conditions. PBC, APBC, and DPBC introduced in Chapter 2 are applied to the converters in order for them to respond autonomously to the fluctuations.

The fabricated dc-dc converter for series-parallel connection is first introduced. Then, the series-paralleled converter circuit considered in this chapter is presented. The numerical results are provided to confirm the asymptotic stability, transient feature, and power management of the converters. Lastly, the construction of the experimental setup is also explained.

## 5.1 Fabricated nonisolated dc-dc converter for series-parallel connection

Fig. 5.1 shows the photography of the fabricated dc-dc converter for the experiment of series-parallel connection. It is a nonisolated and bidirectional synchronous dc-dc converter as shown in the circuit schematic of Fig. 5.2. The power stage has high and low voltage sides that can be used as either the input or the output. Thus, the converter can be used as either buck or boost converter depending on the situation. Also, the fabricated converter is designed for easy series or parallel connection at the input/output. As

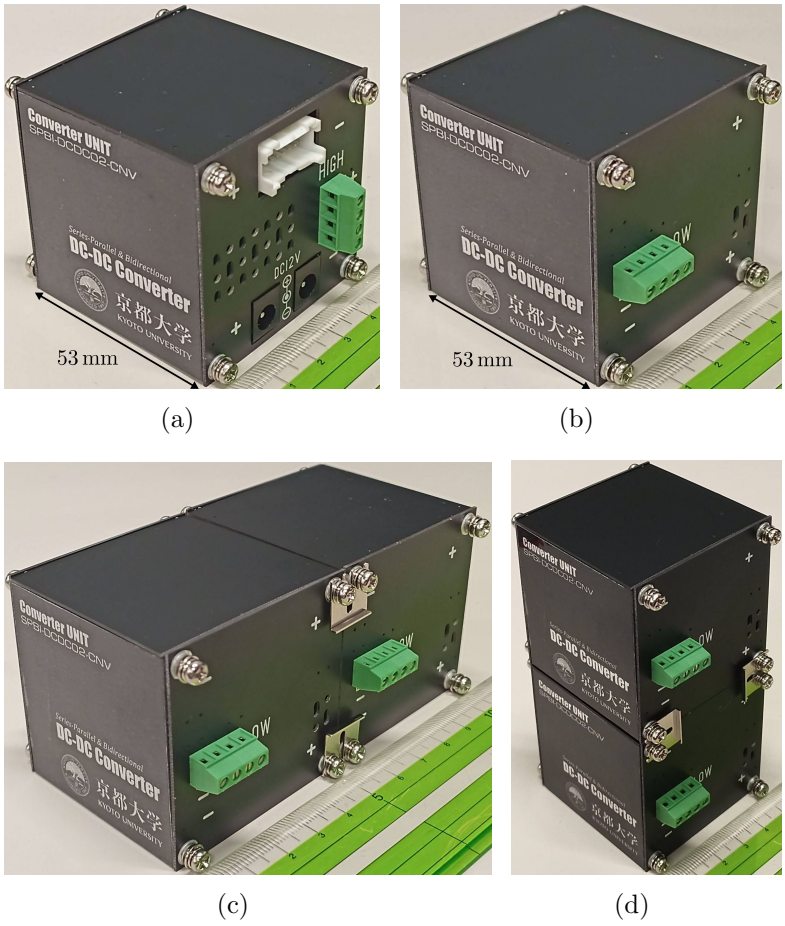


Figure 5.1: Fabricated nonisolated bidirectional synchronous rectification dc-dc converter for series-parallel connection (SPBI-DCDC02-CNV). (a) High voltage input/output. (b) Low voltage input/output. (c) Series connection. (d) Parallel connection.

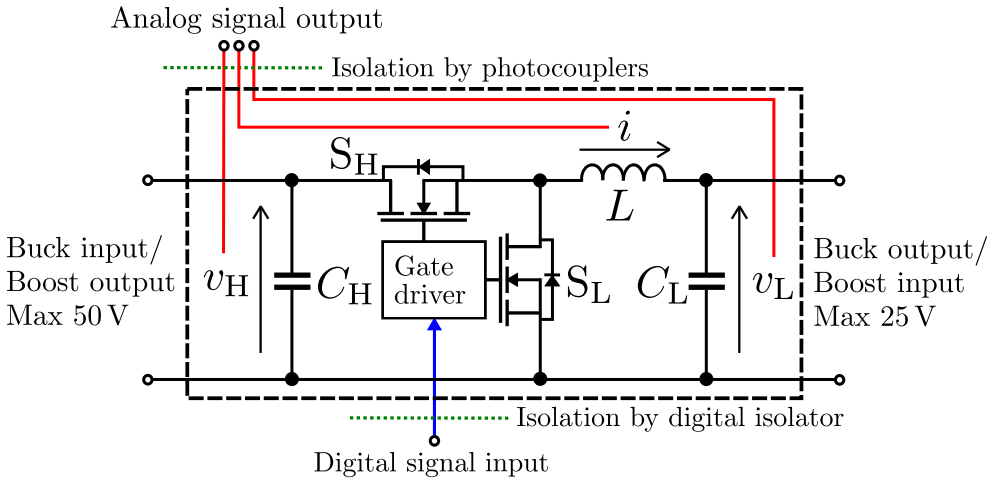


Figure 5.2: Simplified circuit schematic of fabricated dc-dc converter.


Figure 5.3: MyRIO FPGA controller.

shown in Fig. 5.1(c) and (d), the converters can easily be connected in series-parallel by stacking or lining them up. The considerations provided in this chapter are based on this fabricated dc-dc converter.

The fabricated converter has an isolated communication terminal as seen in Fig. 5.2. The actual communication terminal of the circuit is shown in the photograph of Fig. 5.1(a). The terminal has analog signal outputs for the voltage and the current feedback. The digital inputs for the switching signals are also provided. Hence, the voltage and current feedback control of the converter is able to be implemented by an external controller. The programmable myRIO FPGA by National Instruments shown in Fig. 5.3 is adopted for the external controller in our experimental setup. MyRIO FPGA is capable of 20 ns minimum pulse width digital output with a 500 kHz aggregated sample rate of analog signals. Therefore, it is able to reliably provide up to 2MHz switching signal by $\Delta\Sigma$ modulation with feedback control.

The detailed list of the circuit components is shown in Table 5.1. The parameters of the inductor and capacitor are chosen for the 2 MHz switching operation with no significant steady-state ripples in the current and voltage waveforms. They are also chosen to reliably endure 3 A and 50 V, respectively. A photocoupler and digital isolator are provided for the isolation of the analog and digital signals, respectively. In addition, the signals are transformed into differential signals during transfer between the controller and the converter for noise reduction. The gate of the switches is driven by the MOSFET US6M1 manufactured by ROHM. From the above components, the specifications of the

Table 5.1: Component Listing

| Device | Model | Manufacturer | Symbol | Value |
|---|---|---|---|---|
| Inductor | 74435574700 | Wurth | $L$ | $47\,\mu$H |
| Capacitor | PCV2A100MCL1 | nichicon | $C_{\mathrm{H}}$, $C_{\mathrm{L}}$ | $10\,\mu$F |
| Switch | IRL540NPBF | Infineon | $S_{\mathrm{H}}$, $S_{\mathrm{L}}$ | |
| Photocoupler | ACPL-C87A | Broadcom | | |
| Digital isolator | SI8610BC-B-IS | Skyworks | | |
| Gate driver | US6M1 | ROHM | | |
| Current sensor | AD8210 | Analog Devices | | |

Table 5.2: Converter Specifications

| | |
|---|---|
| High voltage input/output | 10-50 V |
| Low voltage input/output | 5-25 V |
| Maximum inductance current | 3 A |
| Maximum switching frequency | 2 MHz |

fabricated dc-dc converters are given in Table 5.2.

The switch adopted in the fabricated converter is a Si device IRL540NPBF by Infineon. The test operation of a single fabricated converter used as a buck converter is shown in Fig. 5.4. The converter successfully steps down the voltage input of 50 V and 100 W down to 25 V. Here, the efficiency of the device was more than 90%. The substrate temperature during the steady-state operation was 82.3°C as shown in Fig. 5.5. This is sufficiently lower than the maximum operating temperature of the device which is 175°C. Thus, we have confirmed the successful operation of the fabricated converter.

## 5.2 Series-paralleled boost and buck converters

The series-parallel connection of buck and boost converters shown in Fig. 5.6 is considered in this chapter. The circuit parameters of each converter are based on the fabricated dc-dc converter explained in the previous section. This circuit configuration imitates HPS and cascaded PV systems considered in the previous studies. HPS is often modeled as power sources, including PV panels, and converters connected in parallel at the load [17–30]. On the other hand, cascaded PV systems consider the dc-dc converters connected in series at the output [10–16]. Therefore, in order to precisely describe an

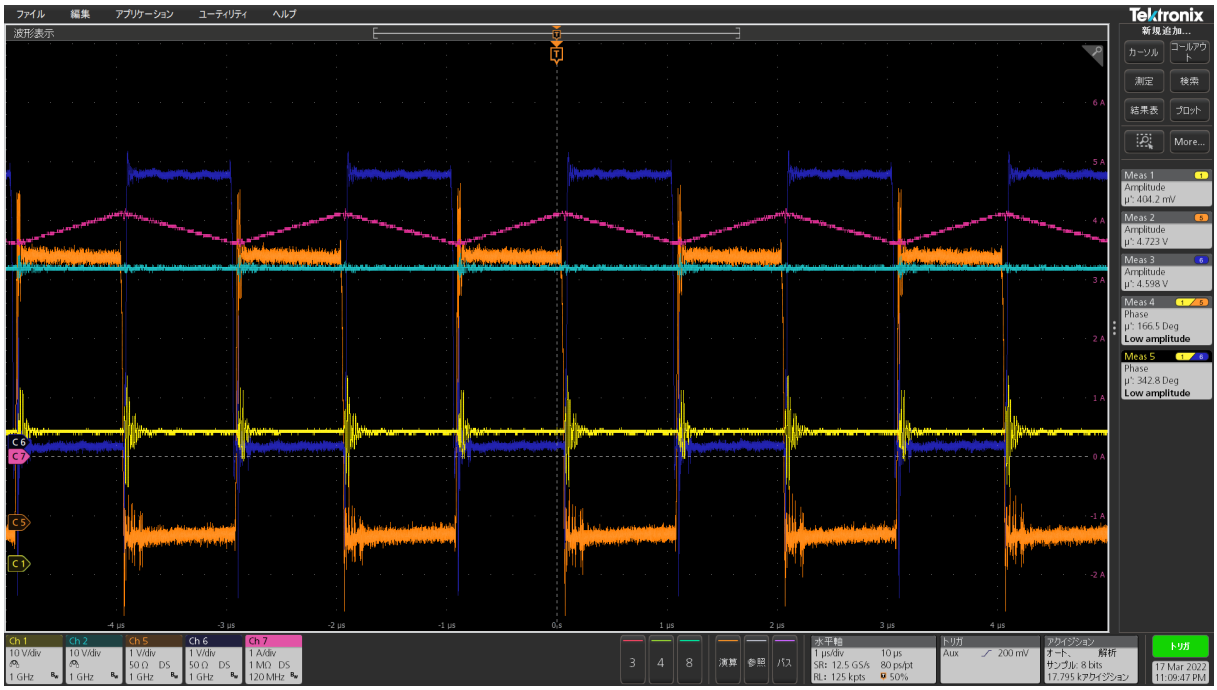


Figure 5.4: Waveform of fabricated converter operating as buck converter at 50V 100W input. Light blue indicates high-voltage side, yellow indicates low-voltage side, pink indicates inductor current, orange indicates high-side gate voltage, and blue indicates low-side gate voltage.

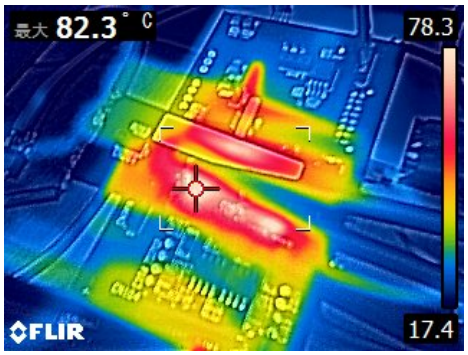


Figure 5.5: The substrate temperature at 100 W opereation of fabricated converter.

HPS with cascaded PV panels, we have combined the series and parallel connection at the output of the dc-dc converters.

APBC explained in Section 2.6 is applied to buck converter # 1 for adaptively maintaining the constant voltage output of the series-paralleled converters. The control parameters are set as $k_1 = 0.1, L_{1a} = 0.2 \times 10^{-7}$. DPBC derived in Section 2.7 is applied

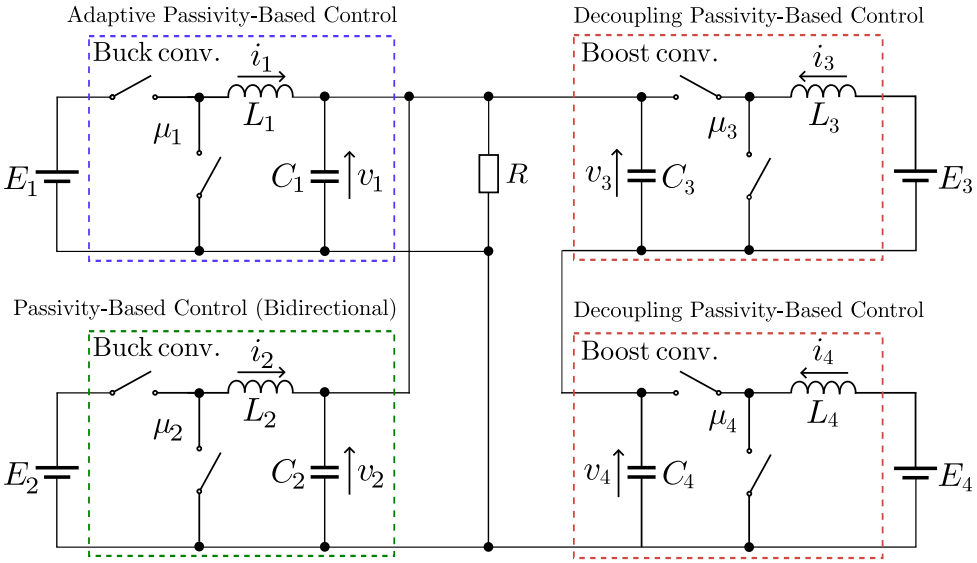


Figure 5.6: Series-paralleled boost and buck converters.

Table 5.3: Initial state of dc-dc converters

| #1 Buck | | #2 Buck | | #3 Boost | | #4 Boost | |
|---|---|---|---|---|---|---|---|
| Variable | State | Variable | State | Variable | State | Variable | State |
| $i_1$ | 0.8 A | $i_2$ | 0.5 A | $i_3$ | 2.0 A | $i_4$ | 2.0 A |
| $v_1$ | 24 V | $v_2$ | 24 V | $v_3$ | 12 V | $v_4$ | 12 V |
| $E_1$ | 48 V | $E_2$ | 36 V | $E_3$ | 6 V | $E_4$ | 6 V |

to the series connected boost converters # 3 and # 4 for the decoupled operation of the power sources. PBC with constant desired state explained in Section 2.5 is applied to the buck converter #2. Here, the negative desired state is tested for bidirectional current flow. The feedback gain for the PBC of buck converter #2 is set as $k_2 = 0.1$. These control rules are obtained in the form of duty ratios, thus we adopt the $\Delta\Sigma$ modulation in order to transform these continuous variables into the switching signals, similarly to Chapter 4. The switching frequency will be set at 2 MHz, which is the maximum switching frequency of the fabricated converter. The output load is 8 Ω without any fluctuations.

## 5.3 Numerical simulation

The series-paralleled buck and boost converters shown in Fig. 5.6 are numerically simulated by MATLAB/Simulink 2020b. In the simulation, the converters are initially operating at steady-state shown in Table 5.3. The simulation is focused on the transient

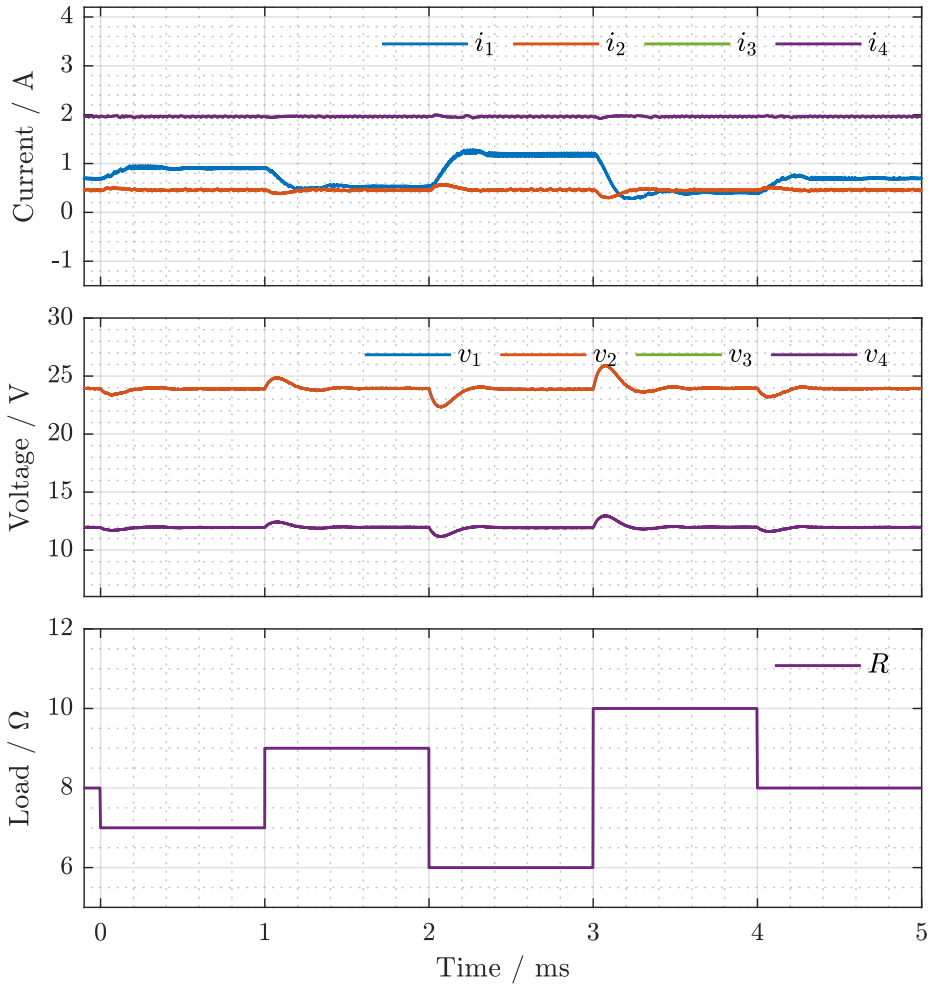


Figure 5.7: Simulated waveform for ouput load fluctuation.

response of the system against load fluctuations and modification of the desired state. These disturbances will be shown with the simulated waveforms. We also focus on whether the transient performance is kept throughout the series-parallel connection. The feedback of the variables is assumed to have no time delay during the simulation.

The simulated waveforms for the load fluctuation are shown in Fig. 5.7. It is confirmed that the buck converter current $i_1$ adaptively changes its steady-state to maintain the output voltage at 24 V. Therefore, the asymptotic stability of the system remained in the load fluctuation. On the other hand, the boost converter voltage and current remained constant at their initial state values by DPBC. Thus, we have numerically confirmed that APBC and DPBC are able to be applied to the series-paralleled converters combined with PBC. In addition, APBC and DPBC maintain their transient features during the

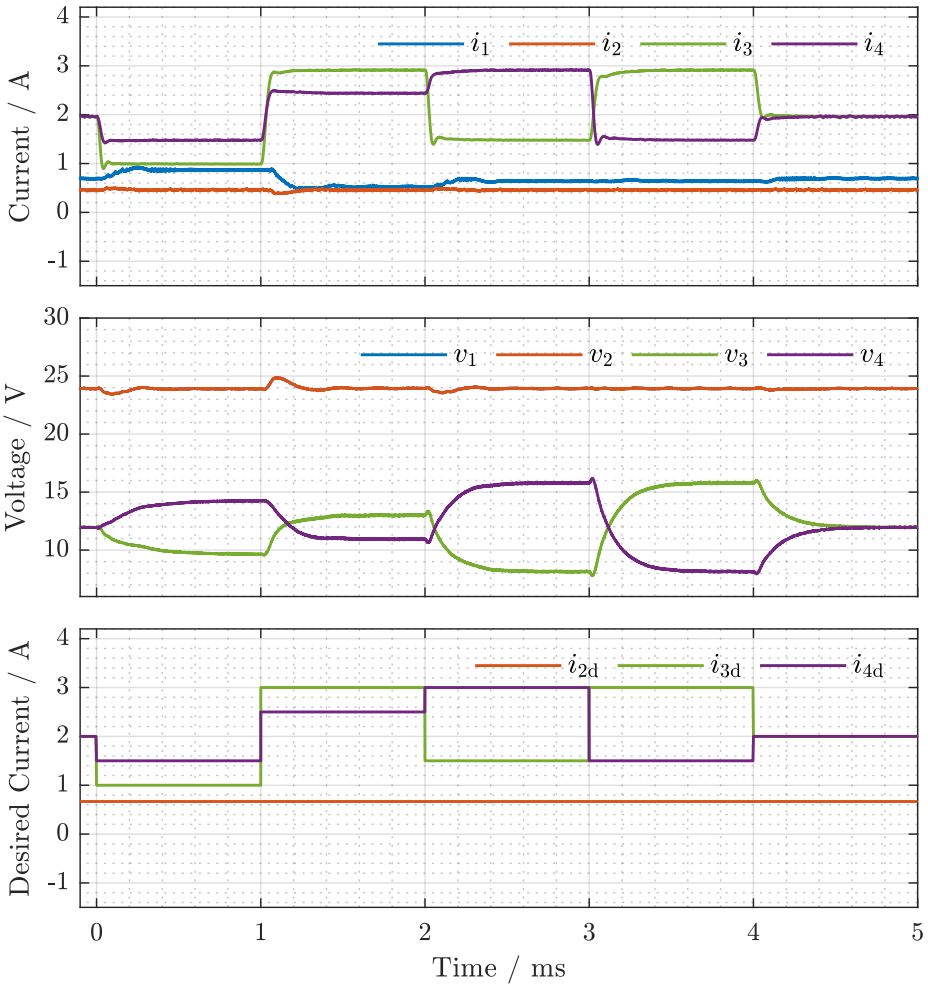


Figure 5.8: Simulated waveform for modification of desired state for boost converters.

connection. These features can contribute to cooperative power management between the power sources.

The transient response to the modification of desired states for boost converters #3 and #4 are shown in Fig. 5.8. In this case, the desired currents for the boost converters are modified during the simulation. The current waveforms of boost converters #3 and #4 are clearly decoupled from the output voltage, operating at their own time constant. Meanwhile, the buck converter current #1 adapts its steady-state to assure the asymptotic stability and the output voltage of 24 V. It is confirmed that DPBC allowed the inputs of the boost converters to operate independently of the disturbances. This feature enables efficient and protective use of power sources.

Lastly, the transient response to the modification of desired state for the buck converter

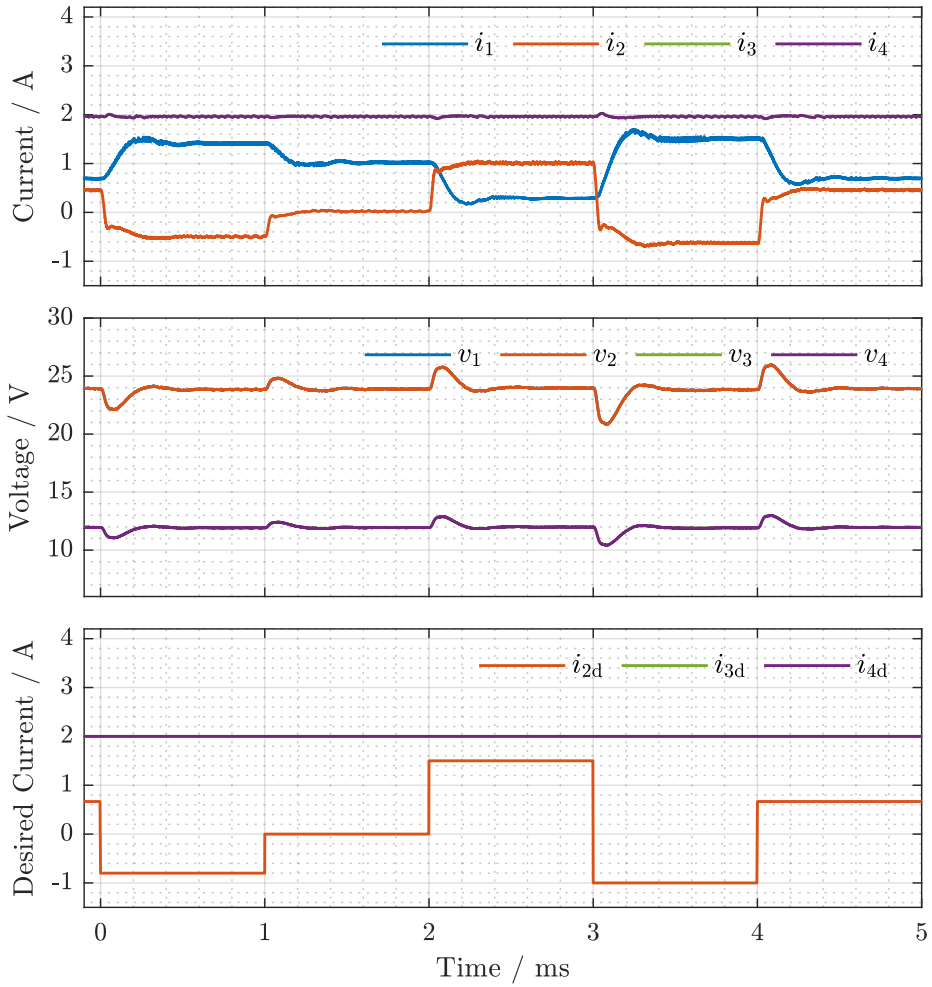


Figure 5.9: Simulated waveform for modification of desired state for buck converter.

#2 is shown in Fig. 5.9. Here, the desired current of the buck converter is allowed to be set as either a positive or negative value, in order to realize bidirectional current flow. Note that the current waveform of the buck converter #2 smoothly changes its direction depending on the desired value. It was made clear that PBC allows the negative current at the steady-state by setting a negative desired state. This feature enables the charging and discharging of the power source. It was shown that the PBC allows bidirectional current flow without any mode changes. APBC and DPBC are also confirmed to maintain their transient performances.

In summary of this section, we numerically considered the power management of series-paralleled dc-dc converters shown in Fig. 5.6 by PBC. APBC and DPBC were adopted for advanced transient features. It was shown in the simulation that APBC and DPBC are

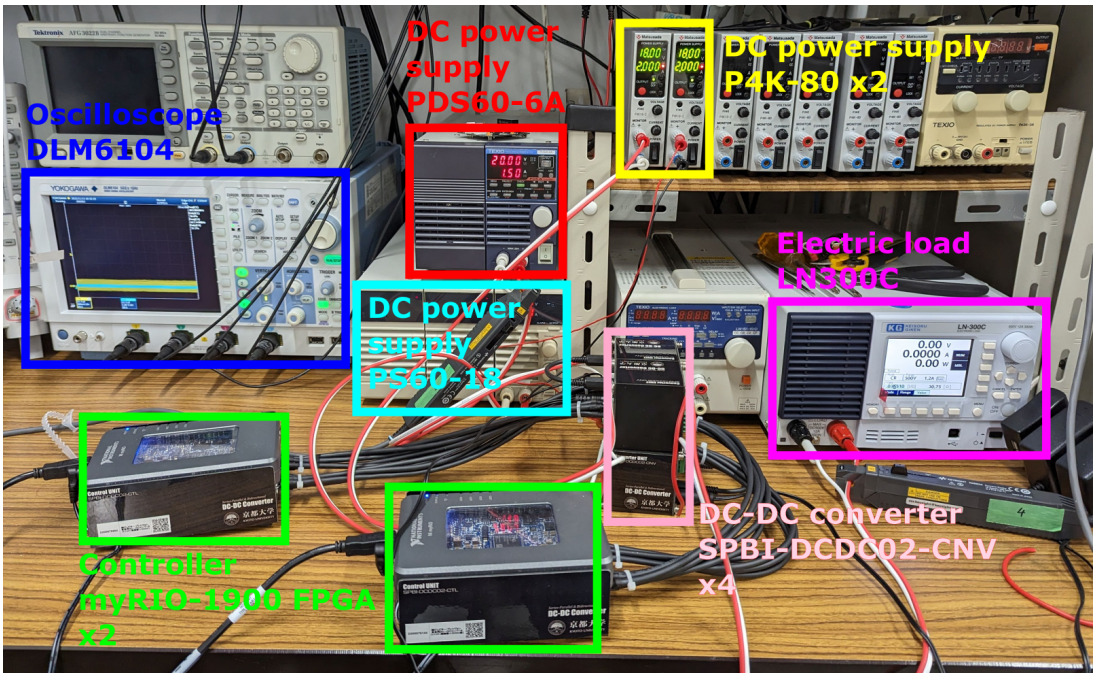


Figure 5.10: Photo of experimental setup.

Table 5.4: Experimental Equipment Listing

| Equipment | Product | Manufacturer | Symbol |
|---|---|---|---|
| DC power supply | PDS60-6A | TEXIO | $E_1$ |
| DC power supply | PS60-18 | TEXIO | $E_2$ |
| DC power supply | P4K-80 | Matsusada | $E_3, E_4$ |
| Electronic load | LN300C | Keisoku Giken | $R$ |
| Controller | myRIO-1900 FPGA | National Instruments | |
| DC-DC converter | SPBI-DCDC02-CNV | Jupiter Precision | |

capable of maitaining the output voltage and decoupling the power sources, respectively. Though several types of disturbances were added to the system, the asymptotic stability and the transient characteristics were kept. The power management by PBC was shown to be feasible for the series-paralleled converters.

## 5.4 Experimental setup

This section is devoted to the explanation of the experimental setup. The experiment aims to implement the simulation results achieved in Section 5.3. The photo of the


Figure 5.11: Output connection structure of fabricated dc-dc converters. Input side has no connection due to separate voltage sources.

experimental setup is shown in Fig. 5.10. Here, the equipment listed in Table 5.4 are assembled to compose the simulated circuit shown in Fig. 5.6.

The dc power supplies listed in Table 5.4 are adopted based on their output voltage and power. They are able to reliably supply the voltage and power used in the simulation. They also have isolation in the power stage which allows series connection. For the bidirectional operation of buck converter #2, a constant load must be connected parallel to the output of the power supply PS60-18 to allow negative current flow. LN300C is a programmable electric load manufactured by Keisoku Giken. It is able to reproduce the simulated load fluctuations. The change of desired states is given by myRIO FPGA controller. The details of the dc-dc converter and controller are explained previously in Section 5.1.

In Fig. 5.11, the connection structure of the converters is shown in a photograph. Here, the series-parallel connection of dc-dc converters shown in Fig. 5.6 is achieved. The terminals of the dc-dc converter are connected by metallic plates, except for the nonadjacent terminal which is using a red cable for connection. The converters shown in Fig. 5.10 are connected as shown in Fig. 5.11. The input side has no connection since the converters have individual power sources.

To summarize, we have shown that the experimental system for the circuit configuration in Fig. 5.6 is able to be constructed. The fabricated dc-dc converter and controller explained and tested in Section 5.1 were adopted. Equipment capable of reproducing the

external inputs and fluctuations was selected and assembled for the experimental setup.

The experiments for this chapter showed saturation in the input current sensing feedback signal for the fabricated converter as seen in Fig. 5.12. Here, the fabricated converter is operating as a buck converter with alternate output resistances. In Fig. 5.12, the output signal of the current sensor is saturated and distorted regardless of the input current value. This leads to measurement errors in the feedback control. On the other hand, the correspondence between the input current value and the feedback signal is confirmed when there is no switching operation as shown in Fig. 5.13. Here, the current sensor output signal corresponds to the input current values. Therefore, the saturation of this signal is expected to be caused by the high-frequency switching noise in the current waveform. To avoid the saturation of the signal, appropriate noise filtering is necessary at the input of the current sensor. By the reduction of the high-frequency switching noise, it is possible to obtain an accurate feedback signal and implement PBC. In conclusion of this section, we explained the setups, equipment, and requirements for the experimental verification.

## 5.5 Summary

In this chapter, we discussed the power management methods of series-parallel connected dc-dc converters by PBC. APBC and DPBC were adopted for the advanced transient features of the converters. They were shown to be applicable for the series-paralleled converters, maintaining the asymptotical stability, the output voltage, and the decoupled characteristics of the system. These features can contribute to the stable and cooperative use of converters and power sources.

The considerations in this dissertation were based on the fabricated dc-dc converter for series-parallel connection shown in Fig. 5.1. Therefore, the numerical results should provide information and insights for the experiment of the series-paralleled converters. Then, the setups for the experiment were shown. The individual equipment has been verified. Their combined use must be prioritized for future work.


(a)


(b)

Figure 5.12: Waveforms of fabricated nonisolated bidirectional synchronous rectification dc-dc converter (SPBI-DCDC02-CNV) with switching operation. (a) 12 Ω output resistance. (b) 25 Ω output resistance. Yellow, green, blue, and pink waveforms imply converter input voltage, current sensing IC output signal, converter input current, and photocoupler input signal, respectively. Current sensing is not obtained due to saturation and distortion of the signals regardless of different input current values.

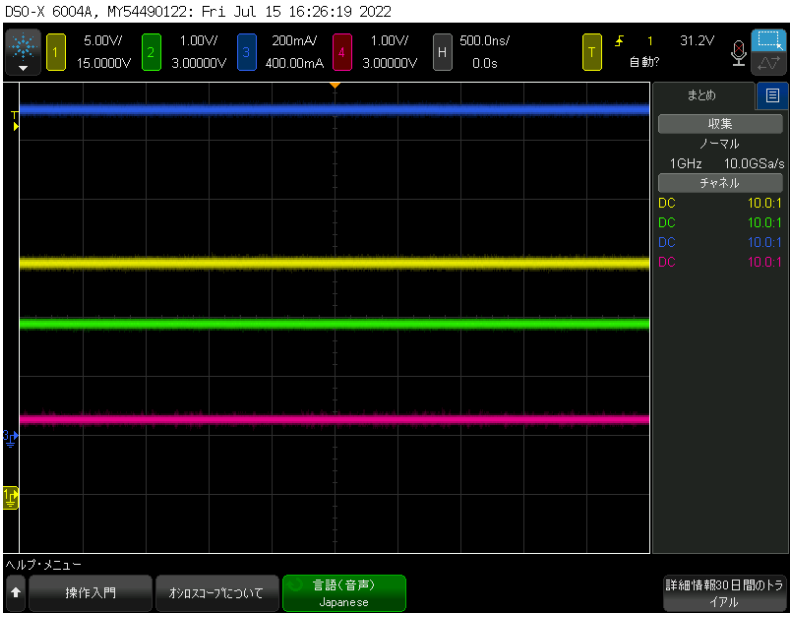


(a)


(b)

Figure 5.13: Waveforms of fabricated nonisolated bidirectional synchronous rectification dc-dc converter (SPBI-DCDC02-CNV) with no switching operation. (a) 18 Ω output resistance. (b) 27 Ω output resistance. Yellow, green, blue, and pink waveforms imply converter input voltage, current sensing IC output signal, converter input current, and photocoupler input signal, respectively. Current sensing is confirmed to be available due to the signals corresponing to different input current values.

# Chapter 6

# Conclusion and future directions

In this dissertation, we considered the PBC of series-parallel connected dc-dc converters from the viewpoints of asymptotic stability and control performance. It was theoretically shown that series-parallel connected dc-dc converters regulated by PBC are asymptotically stable. Then, this result was confirmed numerically and experimentally. In addition, APBC and DPBC were introduced for the power management of series-paralleled converters. The transient characteristics of these control methods were analyzed numerically. It was also confirmed that the transient performance of these control methods remains throughout the series-parallel connection. The results of this dissertation contribute to providing more diversity and scalability in the series-parallel connection of power converters. A summary for the contributions of each chapter is provided in the following section. Then, the future directions of this research are discussed.

## 6.1 Summary of contribution

In Chapter 2, the basic concepts of this research were explained. Passivity, Lyapunov stability theory, and PCHS were first introduced from past references. Then, based on these concepts, PBC was described in a general manner. The derivation process of PBC laws for boost, buck, and buck-boost converters was shown. APBC and DPBC were also introduced for advanced control performance. Their transient characteristics were analyzed numerically. The numerical results gave insights into determining the control parameters for optimal transient performance. The control parameters adopted in the series-parallel connection were based on the results in this chapter.

In Chapter 3, we theoretically investigated the output series-paralleled dc-dc con-

verters regulated by PBC. An additional variable was introduced to the dc-dc converter model to represent the output interaction which describes the series-parallel connection. It was demonstrated that the output series-paralleled converters are reclassified into the general dc-dc converter model, represented in PCHS. It enabled us to discuss the asymptotic stability of the series-paralleled converters based on PCHS, similar to a single dc-dc converter. As a result, the converters regulated by PBC were proven to maintain their stability at the output series-parallel connection. Theoretical results were validated by the numerical simulation of series-paralleled boost, buck, and buck-boost converters. The simulation verified the stable and robust features of PBC. PBC enabled a wide range of circuit topologies, parameters, and steady-states of the output series-paralleled dc-dc converters. This contribution can theoretically complement the previous numerical and experimental research for the series-paralleled converters regulated by PBC, allowing the further extension of the system.

In Chapter 4, the parallel connection of boost and buck converters regulated by PBC was examined numerically and experimentally. The individual application of PBC to each converter led to asymptotic stabilization of the paralleled system. This result corresponds to the results in Chapter 3. The dependence of ripple characteristics, error characteristics, and time constant on the feedback gains was investigated numerically. Here, the feedback gain settings for the experiment were identified. It was also confirmed in the simulation that the characteristics of each converter were independent. Therefore, the feedback gain settings were shown to be modified individually. The experiment also demonstrated asymptotic stability and independent properties of the converters. The results in this chapter have shown the capability of PBC for designing a more diverse parallelization of converters.

In Chapter 5, we addressed the power management methods of series-parallel connected dc-dc converters using PBC. APBC and DPBC were adopted for the advanced transient features of the converters. They were numerically demonstrated to be applicable for the series-paralleled converters while preserving asymptotical stability, output voltage, and decoupled properties of the system. These features can contribute to the stable and cooperative operation of the power converters and power sources. The numerical results should provide insights into the experiment of the series-paralleled converters. The non-isolated bidirectional synchronous rectification dc-dc converter for series-parallel connection was fabricated for the experiment. The setups for the experiment were also

shown. The test operation of the fabricated converter was demonstrated, and the individual equipment for the experiment was verified.

In conclusion, this dissertation developed a general discussion on the series-parallel connection of dc-dc converters regulated by PBC. Then, it was confirmed through numerical simulation and experiments. The generality and scalability of the results of this dissertation will greatly contribute to the development of the research field for the series-parallel connection of power converters. The restrictions given in the considerations were extremely few, compared to previous research. Hence, the results provided in this dissertation should be applicable to various domains of electrical engineering.

## 6.2 Future directions

As for future directions, the following three viewpoints should be addressed. The first viewpoint is the experimental considerations for the power management of series-paralleled dc-dc converters using PBC. The second viewpoint is the expansion of this research. The third viewpoint is the series-parallel integration of power converters. A detailed explanation of each viewpoint is given below.

Firstly, the most important and immediate issue is to obtain experimental data from the setups introduced in Chapter 5. Although the operation of individual experimental equipment has been verified, the operation of the equipment used in combination has not been confirmed. Unexpected interactions between the equipment may lead to the discrepancy with the simulation or even instability. In this case, a specific startup method or device synchronization is necessary. In addition, parasitic elements and feedback delays may be required to be included in the simulation to reproduce experimental results. The identification of these nonideal factors is also vital as well as the confirmation of asymptotic stability and transient features. It is critical to obtain the experimental data to validate the power management method of series-paralleled converters using PBC.

Secondly, the results provided in this dissertation should be expanded toward multiple fields of study. For instance, dc-ac, ac-dc, and ac-ac converters could be included in the series-parallel connection. This issue may be solved theoretically by obtaining the PCHS of these power converters, and deriving the PBC law. However, it is ideal for the experimental consideration to be provided as well. The isolated power converters should also be included. Series-parallel connection at the input side should be prioritized to be

examined theoretically, numerically, and experimentally. The considerations in regard to the output series-parallel connection of the converters cannot be directly applied to the connection at the input side. Above mentioned expansions of this research would lead to more diverse series-parallel connections and cooperative use of power converters and energy sources.

Finally, we address the series-parallel integration of power converters. In this dissertation, Si devices were adopted for the fabrication of experimental dc-dc converters. This is due to Si devices being the most widely used switching devices. This research has focused on achieving the series-parallel connection of the converters, rather than the improvement of a signle converter. However, with the recent trend toward adopting next-generation power devices such as SiC and GaN, series-paralleled power converters should also incorporate them to achieve even higher performance in the future. It is necessary not only to integrate each converter by using these devices but also to establish a method to integrate multiple converters in series-parallel. A completely new method of designing a power converter can be developed, in which the number of power converters and their connection structures are examined, rather than the selection of switching devices and passive elements. It will bring us a new paradigm in this research field as a more straightforward and simple power converter design method.

# Bibliography

[1] S. Luo, Z. Ye, R. L. Lin, and F. C. Lee, "A classification and evaluation of paralleling methods for power supply modules," in *30th Annual IEEE Power Electronics Specialists Conference Record*, vol. 2, 1999, pp. 901–908.

[2] Y. Huang and C. K. Tse, "Circuit theoretic classification of parallel connected dc-dc converters," *IEEE Transactions on Circuits and Systems I: Regular Papers*, vol. 54, no. 5, pp. 1099–1108, 2007.

[3] R. Ayyanar, R. Giri, and N. Mohan, "Active input-voltage and load-current sharing in input-series and output-parallel connected modular dc-dc converters using dynamic input-voltage reference scheme," *IEEE Transactions on Power Electronics*, vol. 19, no. 6, pp. 1462–1473, 2004.

[4] R. Giri, V. Choudhary, R. Ayyanar, and N. Mohan, "Common-duty-ratio control of input-series connected modular dc-dc converters with active input voltage and load-current sharing," *IEEE Transactions on Industry Applications*, vol. 42, no. 4, pp. 1101–1111, 2006.

[5] X. Ruan, W. Chen, L. Cheng, C. K. Tse, H. Yan, and T. Zhang, "Control strategy for input-series output-parallel converters," *IEEE Transactions on Industrial Electronics*, vol. 56, no. 4, pp. 1174–1185, 2009.

[6] W. Chen, X. Ruan, H. Yan, and C. K. Tse, "Dc/dc conversion systems consisting of multiple converter modules: Stability, control, and experimental verifications," *IEEE Transactions on Power Electronics*, vol. 24, no. 6, pp. 1463–1474, 2009.

[7] D. Sha, Z. Guo, T. Luo, and X. Liao, "A general control strategy for input-series output-series modular dc–dc converters," *IEEE Transactions on Power Electronics*, vol. 29, no. 7, pp. 3766–3775, 2014.

[8] D. Ma, W. Chen, and X. Ruan, "A review of voltage/current sharing techniques for series–parallel-connected modular power conversion systems," *IEEE Transactions on Power Electronics*, vol. 35, no. 11, pp. 12383–12400, 2020.

[9] A. J. B. Bottion and I. Barbi, "Input-series and output-series connected modular output capacitor full-bridge pwm dc–dc converter," *IEEE Transactions on Industrial Electronics*, vol. 62, no. 10, pp. 6213–6221, 2015.

[10] G. R. Walker and P. C. Sernia, "Cascaded dc-dc converter connection of photovoltaic modules," *IEEE Transactions on Power Electronics*, vol. 19, no. 4, pp. 1130–1139, 2004.

[11] N. Femia, G. Lisi, G. Petrone, G. Spagnuolo, and M. Vitelli, "Distributed maximum power point tracking of photovoltaic arrays: novel approach and system analysis," *IEEE Transactions on Industrial Electronics*, vol. 55, no. 7, pp. 2610–2621, 2008.

[12] M. S. Zaman, S. Poshtkouhi, V. Palaniappan, K. W. Li, H. J. Bergveld, S. Myskorg, and O. Trescases, "Distributed power-management architecture for a low-profile concentrating-pv system," in *2012 15th International Power Electronics and Motion Control Conference*, 2012, pp. LS2d.4–1–LS2d.4–8.

[13] S. Poshtkouhi, V. Palaniappan, M. Fard, and O. Trescases, "A general approach for quantifying the benefit of distributed power electronics for fine grained mppt in photovoltaic applications using 3-d modeling," *IEEE Transactions on Power Electronics*, vol. 27, no. 11, pp. 4656–4666, 2012.

[14] R. C. N. Pilawa-Podgurski and D. J. Perreault, "Submodule integrated distributed maximum power point tracking for solar photovoltaic applications," *IEEE Transactions on Power Electronics*, vol. 28, no. 6, pp. 2957–2967, 2013.

[15] M. H. Taghvaee, M. A. M. Radzi, S. M. Moosavain, H. Hizam, and M. Hamiruce Marhaban, "A current and future study on non-isolated dc–dc converters for photovoltaic applications," *Renewable and Sustainable Energy Reviews*, vol. 17, pp. 216–227, 2013.

[16] G. C. Konstantopoulos and A. T. Alexandridis, "Non-linear voltage regulator design for dc/dc boost converters used in photovoltaic applications: analysis and experimental results," *IET Renewable Power Generation*, vol. 7, no. 3, pp. 296–308, 2013.

[17] M. Uzunoglu, O. Onar, and M. Alam, "Modeling, control and simulation of a pv/fc/uc based hybrid power generation system for stand-alone applications," *Renewable Energy*, vol. 34, no. 3, pp. 509–520, 2009.

[18] H. Zhou, T. Bhattacharya, D. Tran, T. S. T. Siew, and A. M. Khambadkone, "Composite energy storage system involving battery and ultracapacitor with dynamic energy management in microgrid applications," *IEEE Transactions on Power Electronics*, vol. 26, no. 3, pp. 923–930, 2011.

[19] X. Xiong, C. K. Tse, and X. Ruan, "Bifurcation analysis of standalone photovoltaic-battery hybrid power system," *IEEE Transactions on Circuits and Systems I: Regular Papers*, vol. 60, no. 5, pp. 1354–1365, 2013.

[20] X. Zhang, X. Ruan, and C. K. Tse, "Impedance-based local stability criterion for dc distributed power systems," *IEEE Transactions on Circuits and Systems I: Regular Papers*, vol. 62, no. 3, pp. 916–925, 2015.

[21] K. F. Krommydas and A. T. Alexandridis, "Modular control design and stability analysis of isolated pv-source/battery-storage distributed generation systems," *IEEE Journal on Emerging and Selected Topics in Circuits and Systems*, vol. 5, no. 3, pp. 372–382, 2015.

[22] N. Mukherjee and D. Strickland, "Control of Cascaded dc–dc converter-based hybrid battery energy storage systems—part i: stability issue," *IEEE Transactions on Industrial Electronics*, vol. 63, no. 4, pp. 2340–2349, 2016.

[23] N. Mukherjee and D. Strickland, 'Control of Cascaded dc–dc converter-based hybrid battery energy storage systems—part ii: lyapunov approach," *IEEE Transactions on Industrial Electronics*, vol. 63, no. 5, pp. 3050–3059, 2016.

[24] A. Mirzaei, M. Forooghi, A. A. Ghadimi, A. H. Abolmasoumi, and M. R. Riahi, "Design and construction of a charge controller for stand-alone pv/battery hybrid system by using a new control strategy and power management," *Solar Energy*, vol. 149, pp. 132–144, 2017.

[25] D. Peng, M. Huang, J. Li, J. Sun, X. Zha, and C. Wang, "Large-signal stability criterion for parallel-connected dc–dc converters with current source equivalence,"

*IEEE Transactions on Circuits and Systems II: Express Briefs*, vol. 66, no. 12, pp. 2037–2041, 2019.

[26] M. Ayad, M. Becherif, A. Henni, A. Aboubou, M. Wack, and S. Laghrouche, "Passivity-based control applied to dc hybrid power source using fuel cell and supercapacitors," *Energy Conversion and Management*, vol. 51, no. 7, pp. 1468–1475, 2010.

[27] A. Tofighi and M. Kalantar, "Power management of pv/battery hybrid power source via passivity-based control," *Renewable Energy*, vol. 36, no. 9, pp. 2440–2450, 2011.

[28] M. Ahmed, A. Elhassane, and A. Mohamed, "Modelling and passivity-based control of a non-isolated dc-dc converter in a fuel cell system," *International Journal of Electrical and Computer Engineering*, vol. 8, no. 5, pp. 3436–3443, 2018.

[29] M. A. Hassan, E. Li, X. Li, T. Li, C. Duan, and S. Chi, "Adaptive passivity-based control of dc–dc buck power converter with constant power load in dc microgrid systems," *IEEE Journal of Emerging and Selected Topics in Power Electronics*, vol. 7, no. 3, pp. 2029–2040, 2019.

[30] M. Patrone and D. Feroldi, "Passivity-based control design for a grid-connected hybrid generation system integrated with the energy management strategy," *Journal of Process Control*, vol. 74, pp. 99–109, 2019.

[31] F. Blaabjerg, Zhe Chen, and S. B. Kjaer, "Power electronics as efficient interface in dispersed power generation systems," *IEEE Transactions on Power Electronics*, vol. 19, no. 5, pp. 1184–1194, 2004.

[32] J. M. Guerrero, F. Blaabjerg, T. Zhelev, K. Hemmes, E. Monmasson, S. Jemei, M. P. Comech, R. Granadino, and J. I. Frau, "Distributed generation: toward a new energy paradigm," *IEEE Industrial Electronics Magazine*, vol. 4, no. 1, pp. 52–64, 2010.

[33] F. Blaabjerg, R. Teodorescu, M. Liserre, and A. Timbus, "Overview of control and grid synchronization for distributed power generation Systems," *IEEE Transactions on Industrial Electronics*, vol. 53, no. 5, pp. 1398–1409, 2006.

[34] J. M. Carrasco, L. G. Franquelo, J. T. Bialasiewicz, E. Galvan, R. C. Portillo-Guisado, M. A. M. Prats, J. I. Leon, and N. Moreno-Alfonso, "Power-electronic

systems for the grid integration of renewable energy sources: a survey," *IEEE Transactions on Industrial Electronics*, vol. 53, no. 4, pp. 1002–1016, 2006.

[35] B. Kroposki, C. Pink, R. DeBlasio, H. Thomas, M. Simoes, and P. K. Sen, "Benefits of power electronic interfaces for distributed energy systems," in *2006 IEEE Power Engineering Society General Meeting*, 2006.

[36] S. Chakraborty, B. Kramer, and B. Kroposki, "A review of power electronics interfaces for distributed energy systems towards achieving low-cost modular design," *Renewable and Sustainable Energy Reviews*, vol. 13, no. 9, pp. 2323–2335, 2009.

[37] C. K. Tse, "Flip bifurcation and chaos in three-state boost switching regulators," *IEEE Transactions on Circuits and Systems I: Fundamental Theory and Applications*, vol. 41, no. 1, pp. 16–23, 1994.

[38] E. Fossas and G. Olivar, "Study of chaos in the buck converter," *IEEE Transactions on Circuits and Systems I: Fundamental Theory and Applications*, vol. 43, no. 1, pp. 13–25, 1996.

[39] C. K. Tse and M. D. Bernardo, "Complex behavior in switching power converters," *Proceedings of the IEEE*, vol. 90, no. 5, pp. 768–781, 2002.

[40] H. H. C. Iu and C. K. Tse, "Bifurcation behavior in parallel-connected buck converters," *IEEE Transactions on Circuits and Systems I: Fundamental Theory and Applications*, vol. 48, no. 2, pp. 233–240, 2001.

[41] S. K. Mazumder, A. H. Nayfeh, and A. Borojevic, "Robust control of parallel dc-dc buck converters by combining integral-variable-structure and multiple-sliding-surface control schemes," *IEEE Transactions on Power Electronics*, vol. 17, no. 3, pp. 428–437, 2002.

[42] H. R. Baghaee, M. Mirsalim, G. B. Gharehpetian, and H. A. Talebi, "A generalized descriptor-system robust $H_\infty$ control of autonomous microgrids to improve small and large signal stability considering communication delays and load nonlinearities," *International Journal of Electrical Power & Energy Systems*, vol. 92, pp. 63–82, 2017.

[43] H. Sira-Ramirez, R. Perez-Moreno, R. Ortega, and M. Garcia-Esteban, "Passivity-based controllers for the stabilization of dc-to-dc power converters," *Automatica*, vol. 33, no. 4, pp. 499–513, 1997.

[44] R. Ortega, J. Perez, P. Nicklasson, and H. Sira-Ramirez, *Passivity-based Control of Euler-Lagrange Systems: Mechanical, Electrical and Electromechanical Applications*, ser. Communications and Control Engineering, Springer-Verlag, 1998.

[45] G. Escobar, A. J. Van der Schaft, and R. Ortega, "Hamiltonian viewpoint in the modeling of switching power converters," *Automatica*, vol. 35, no. 3, pp. 445–452, 1999.

[46] R. Ortega, A. J. Van Der Schaft, I. Mareels, and B. Maschke, "Putting energy back in control," *IEEE Control Systems Magazine*, vol. 21, no. 2, pp. 18–33, 2001.

[47] R. Ortega, A. van der Schaft, B. Maschke, and G. Escobar, "Interconnection and damping assignment passivity-based control of port-controlled hamiltonian systems," *Automatica*, vol. 38, no. 4, pp. 585–596, 2002.

[48] H. Sira-Ramirez and R. Silva-Ortigoza, *Control Design Techniques in Power Electronics Devices*, 2006th ed., Springer-Verlag, 2006.

[49] M. Takegaki and S. Arimoto, "A new feedback method for dynamic control of manipulators," *Journal of Dynamic Systems Measurement and Control*, vol. 102, no. 3 pp. 119–125, 1981.

[50] J. Slotine and W. Li, "On the adaptive control of robot manipulators," *International Journal of Robotics Research*, vol. 6, no. 3, pp. 49–59, 1987.

[51] R. Ortega and M. W. Spong, "Adaptive motion control of rigid robots: A tutorial," *Automatica*, vol. 25, no. 6, pp. 877–888, 1989.

[52] G. Escobar, R. Ortega, H. Sira-Ramirez, J.-P. Vilain, and I. Zein, "An experimental comparison of several nonlinear controllers for power converters," *IEEE Control Systems Magazine*, vol. 19, no. 1, pp. 66–82, 1999.

[53] M. Perez, R. Ortega, and J. R. Espinoza, "Passivity-based PI control of switched power converters," *IEEE Transactions on Control Systems Technology*, vol. 12, no. 6, pp. 881–890, 2004.

[54] R. Leyva, A. Cid-Pastor, C. Alonso, I. Queinnec, S. Tarbouriech, and L. Martinez-Salamero, "Passivity-based integral control of a boost converter for large-signal stability," *IEE Proceedings Control Theory and Applications*, vol. 153, no. 2, pp. 139–146, 2006.

[55] H. Komurcugil, "Steady-state analysis and passivity-based control of single-phase pwm current-source inverters," *IEEE Transactions on Industrial Electronics*, vol. 57, no. 3, pp. 1026–1030, 2010.

[56] R. Leyva, C. Olalla, I. Queinnec, S. Tarbouriech, C. Alonso, and L. Martinez-Salamero, "Passivity-based control for large-signal stability of high-order switching converters," *Asian Journal of Control*, vol. 14, no. 2, pp. 335–347, 2012.

[57] J. Zeng, Z. Zhang, and W. Qiao, "An interconnection and damping assignment passivity-based controller for a dc-dc boost converter with a constant power load," *IEEE Transactions on Industry Applications*, vol. 50, no. 4, pp. 2314–2322, 2014.

[58] H. Komurcugil, "Improved passivity-based control method and its robustness analysis for single-phase uninterruptible power supply inverters," *IET Power Electronics*, vol. 8, no. 8, pp. 1558–1570, 2015.

[59] S. Pang, B. Nahid-Mobarakeh, S. Pierfederici, M. Phattanasak, Y. Huangfu, G. Luo, and F. Gao, "Interconnection and damping assignment passivity-based control applied to on-board dc-dc power converter system supplying constant power load," *IEEE Transactions on Industry Applications*, vol. 55, no. 6, pp. 6476–6485, 2019.

[60] C. Desoer and E. Kuh, *Basic Circuit Theory*, ser. McGraw Hill international editions: Electrical and electronic engineering series. McGraw-Hill, 1969.

[61] J. Kassakian, M. Schlecht, and G. Verghese, *Principles of Power Electronics*, ser. Addison-Wesley series in electrical engineering. Addison-Wesley, 1991.

[62] R. W. Erickson and D. Maksimović, *Fundamentals of Power Electronics*. Boston, MA: Springer US, 2001, vol. 53, no. 9.

[63] T. Hikihara and Y. Murakami, "Regulation of parallel converters with respect to stored energy and passivity characteristics," *IEICE Transactions on Fundamentals*

*of Electronics, Communications and Computer Sciences*, vol. E94-A, no. 3, pp. 1010–1014, 2011.

[64] R. Manohar and T. Hikihara, "Phase synchronization of autonomous AC grid system with passivity-based control," *International Journal of Circuit Theory and Applications*, vol. 48, no. 6, pp. 906–918, 2020.

[65] R. Manohar and T. Hikihara, "Dynamic behaviour of a ring coupled boost converter system with passivity-based control," *Nonlinear Theory and Its Applications, IEICE*, vol. 11, no. 1, pp. 109–122, 2020.

[66] V. M. Popov and R. Georgescu, *Hyperstability of Control Systems*, Springer-Verlag, 1973.

[67] J. C. Willems, "Dissipative dynamical systems part i: General theory," *Archive for rational mechanics and analysis*, vol. 45, no. 5, pp. 321–351, 1972.

[68] B. M. Maschke and A. J. van der Schaft, "Port-controlled hamiltonian systems: modelling origins and systemtheoretic properties," in *Nonlinear Control Systems Design 1992*. Elsevier, 1993, pp. 359–365.

[69] A. J. van der Schaft, "Port-controlled hamiltonian systems: Towards a theory for control and design of nonlinear physical systems," *Journal of the Society of Instrument and Control Engineers*, vol. 39, no. 2, pp. 91–98, 2000.

[70] P. T. Krein, J. Bentsman, R. M. Bass, and B. L. Lesieutre, "On the use of averaging for the analysis of power electronic systems," *IEEE Transactions on Power Electronics*, vol. 5, no. 2, pp. 182–190, 1990.

[71] S. Sanders, J. Noworolski, X. Liu, and G. Verghese, "Generalized averaging method for power conversion circuits," *IEEE Transactions on Power Electronics*, vol. 6, no. 2, pp. 251–259, 1991.

[72] J. Sun, D. Mitchell, M. Greuel, P. Krein, and R. Bass, "Averaged modeling of pwm converters operating in discontinuous conduction mode," *IEEE Transactions on Power Electronics*, vol. 16, no. 4, pp. 482–492, 2001.

[73] A. M. Lyapunov, "The general problem of the stability of motion," *International journal of control*, vol. 55, no. 3, pp. 531–534, 1992.

[74] H. K. Khalil, *Nonlinear systems; 3rd ed.*, Upper Saddle River, Prentice-Hall, 2002.

[75] H. Rodriguez, R. Ortega, and G. Escobar, "A robustly stable output feedback saturated controller for the boost dc-to-dc converter," in *Proceedings of the 38th IEEE Conference on Decision and Control*, vol. 3, 1999, pp. 2100–2105 vol.3.

[76] R. Silva-Ortigoza, F. Carrizosa-Corral, J. Gálvez-Gamboa, M. Marcelino-Aranda, D. Muñoz Carrillo, and H. Taud, "Assessment of an average controller for a dc/dc converter via either a pwm or a sigma-delta-modulator," *Abstract and Applied Analysis*, 2014.

[77] Y. Murakawa and T. Hikihara, "Adaptive passivity-based control for constant voltage output of series-paralleled dc-dc converters," in *2021 IEEE 30th International Symposium on Industrial Electronics (ISIE)*, 2021, pp. 1–5.

[78] Y. Murakawa and T. Hikihara, "Passivity-based adaptive control and decoupling control for series-parallel connection of dc-dc converters," in *International Symposium on Nonlinear Theory and its Applications (NOLTA 2020)*, 2021, pp. 44–47.

[79] G. Escobar, D. Chevreau, R. Ortega, and E. Mendes, "An adaptive passivity-based controller for a unity power factor rectifier," *IEEE Transactions on Control Systems Technology*, vol. 9, no. 4, pp. 637–644, 2001.

[80] S. I. Seleme, A. H. R. Rosa, L. M. F. Morais, P. F. Donoso-Garcia, and P. C. Cortizo, "Evaluation of adaptive passivity-based controller for power factor correction using a boost converter," *IET Control Theory & Applications*, vol. 6, no. 14, pp. 2168–2178, 2012.

[81] D. M. Sánchez-Javier, J. A. Hernández-Reyes, J. L. Palomeque-Loyo, D. Langarica-Cordoba, P. R. Martinez-Rodriguez, and L. H. Diaz-Saldierna, "Adaptive passivity-based control for a fuel cell-quadratic boost converter system," in *2021 IEEE International Autumn Meeting on Power, Electronics and Computing (ROPEC)*, vol. 5, 2021, pp. 1–6.

[82] Y. Murakawa, Y. Sadanda, and T. Hikihara, "Parallelization of boost and buck type dc-dc converters by individual passivity-based control," *IEICE Transactions on Fundamentals of Electronics, Communications and Computer Sciences*, vol. E103.A, no. 3, pp. 589–595, 2020.

[83] R. Steele, *Delta Modulation Systems*. Pentech Press, 1975.

[84] S. Norsworthy, R. Schreier, and G. Temes, *Delta Sigma Data Converters: Theory, Design, and Simulation*. IEEE Press-Wiley, 1997.

[85] S. K. Dunlap and T. S. Fiez, "A noise-shaped switching power supply using a delta-sigma modulator," *IEEE Transactions on Circuits and Systems I: Regular Papers*, vol. 51, no. 6, pp. 1051–1061, 2004.

[86] H. Sira-Ramírez and R. Silva-Ortigoza, "Sliding mode $\Sigma$-$\Delta$ modulation control of the boost converter," *Asian Journal of Control*, vol. 7, no. 4, pp. 349–355, 2005.

# List of publications

## Journal articles

[1] Y. Murakawa and T. Hikihara, "Output series-parallel connection of passivity-based controlled dc-dc converters: generalization of asymptotic stability," *IEEE Transactions on Circuits and Systems I: Regular Papers*, vol. 68, no. 4, pp. 1750–1759, 2021.

[2] Y. Murakawa, Y. Sadanda, and T. Hikihara, "Parallelization of boost and buck type dc-dc converters by individual passivity-based control," *IEICE Transactions on Fundamentals of Electronics, Communications and Computer Sciences*, vol. E103.A, no. 3, pp. 589–595, 2020.

## Peer-reviewed international conference proceedings

[3] Y. Murakawa and T. Hikihara, "Adaptive Passivity-Based Control for Constant Voltage Output of Series-Paralleled DC-DC Converters," *2021 IEEE 30th International Symposium on Industrial Electronics (ISIE 2021)*, Kyoto, Japan, virtual conference, June 2021.

[4] Y. Murakawa and T. Hikihara, "Passivity-Based Adaptive Control and Decoupling Control for Series-Parallel Connection of DC-DC Converters," *2020 International Symposium on Nonlinear Theory and its Applications (NOLTA 2020)*, Okinawa, Japan, virtual conference, Nov. 2020.

[5] Y. Murakawa and T. Hikihara, "Regulation of Parallel Connected Boost and Buck Converters by Passivity-Based Control," *2020 IEEE Workshop on Wide Bandgap Power Devices and Applications in Asia (WiPDA Asia 2020)*, Suita, Japan, virtual conference, Sept. 2020.

# Other conference proceedings and presentations

[6] Y. Murakawa and T. Hikihara, "Numerical Study on Control Parameter Settings of Passivity-Based Adaptive Control for DC-DC Converters," *2021 IEICE NOLTA Society Conference*, PM-2-2, virtual conference, June 2021 (in Japanese).

[7] Y. Murakawa and T. Hikihara, "Theoretical Study on Asymptotic Stability of Passivity-Based Controlled DC-DC Converters Connected in Series-Parallel," *65th Annual Conference of the Institute of Systems, Control and Information Engineers (SCI'21)*, Gsb-07-5, virtual conference, May 2021 (in Japanese).

[8] Y. Murakawa and T. Hikihara, "Theoretical Study of Output Series-Paralleled DC-DC Converters Regulated by Passivity-Based Control," *2021 IEICE General Conference*, A-1-14, virtual conference, Mar. 2021 (in Japanese).

[9] Y. Murakawa and T. Hikihara, "Generalization for Asymptotic Stability of Series-Parallel Connected DC-DC Converters Regulated by Passivity-Based Control," *IEEJ Technical Meeting on Electronic Circuits*, ECT-021-008, virtual conference, Jan. 2021 (in Japanese).

[10] Y. Murakawa and T. Hikihara, "Theoretical Study of Output Series-Paralleled DC-DC Converters Regulated by Passivity-Based Control," *2020 Taiwan and Japan Conference on Circuits and Systems (TJCAS 2020)*, virtual conference, Nov. 2020.

[11] Y. Murakawa and T. Hikihara, "Numerical Study on Applying Passivity-Based Control to Series-Parallel Connected DC-DC Converters," *IEEJ Technical Meeting on Electronic Circuits*, ECT-018-046, Kyoto, Japan, June 2018 (in Japanese).

[12] Y. Murakawa and T. Hikihara, "A Study on Passivity-Based Control of Boost Converters Connected in Series-Parallel," *62th Annual Conference of the Institute of Systems, Control and Information Engineers (SCI'18)*, 143-2, Kyoto, Japan, May 2018 (in Japanese).